PHOTOCATALYTIC DEGRADATION OF METHYL VIOLET IN WATER USING TiO_2/CELLULOSE-N-MWCNTs

By

Xiluva Mathebula

A dissertation submitted in fulfillment of the requirements for the degree of **Master of Science in Chemistry** in the Faculty of Science School of Chemistry University of the Witwatersrand Private Bag X 03

WITS

2050

Supervisors: Dr Z.N. Tetana

Prof N. Moloto

DECLARATIONS

This dissertation is my own unaided work under the supervision of Dr Z.N Tetana and Prof N. Moloto. It is being submitted for the degree of Master of Science at the University of the Witwatersrand, Johannesburg.

Candidate — Date: 04/06/2018

(Xiluva Mathebula – 1592929)

Supervisor — Date: 04/06/2018

(DR Z.N Tetana)

Co-supervisor — Date: 04/06/2018

(Prof N. Moloto)

ABSTRACT

TiO_2-carbon based composites are of great significance in a wide range of applications including photocatalytic degradation. This is attributed to the high photodecomposition efficiency of the composites as compared to independent TiO_2. Carbon materials such as cellulose polymer and multiwalled carbon nanotubes (MWCNTs) are considered as good supports for TiO_2 owing to their unique properties such as lightweight, large surface area and high aspect ratio. Lately, the study of cellulose-MWCNTs composite has been an area of academic interest due to its large mass fraction, and prowess to facilitate toughening mechanisms in fiber bridging. However, a cost-effective method that can improve the dispersion and interfacial adhesion of the MWCNTs in the polymer is still required. Thus different modification methods of MWCNTs have been explored to increase the binding sites of the material. In this study, it was hypothesized that the cellulose's potential as a TiO_2 support can be improved by hybridizing it with MWCNTs resulting in high TiO_2-C photocatalytic activity through synergistic effect.

A catalytic decomposition of Fe-Co/$CaCO_3$ was used over C_2H_2 to fabricate the MWCNTs. Thereafter, the MWCNTs were functionalized by (1) acid-treatment (referred to as fMWCNTs), (2) nitrogen doping by *in situ* and *ex situ* methods (referred to as *in situ* N-MWCNTs and *ex situ* N-MWCNTs, respectively) and (3) both acid treatment and nitrogen doping (referred to as *in situ* fN-MWCNTs and *ex situ* fN-MWCNTs). Moreover, cellulose-N-MWCNTs (C@fN-MWCNTs) hybrid was prepared by electrospinning a solution of cellulose acetate/*in situ* fN-MWCNTs (11/0.115) in DMAc at 25 kv and 1 mL/h. The prepared MWCNTs and cellulosic materials were further used as support materials of TiO_2 in the photodegradation of methyl violet (MV 6B). The supported TiO_2 catalysts were prepared by a sol-gel method and then analyzed using various techniques, such as transmission electron microscopy (TEM), X-ray diffraction (XRD), thermogravimetric analysis (TGA), and Raman spectroscopy.

TGA results revealed that *in situ* N-MWCNTs contained high impurities inclusive of as Fe, Co, Ca, and amorphous carbon which were identified by XRD analysis. Nevertheless, TGA, BET and TEM, showed that acid treatment of MWCNTs improves their purity, surface area and anchoring sites for the TiO_2, respectively. Furthermore, SEM results showed that C@fN-MWCNTs hybrid interacts with TiO_2 better than cellulose fibers. This was in accord with the PL results which showed a reduction in the electron/hole recombination. However, the surface area of C@fN-MWCNTs was very low compared to cellulose fibers which resulted in low dye adsorption capacity by C@fN-MWCNTs.

The photocatalytic degradation activity commercial TiO_2 was enhanced by 3.7% and 5.6% after being supported on cellulose and C@fN-MWCNTs, respectively. Thus, incorporating *in situ* fN-MWCNTs with cellulose did improve the cellulose's potential as a TiO_2 support. However, the overall photocatalytic degradation performance of TiO_2/C@fN-MWCNTs was less than that of *in situ* TiO_2/fN-MWCNTs. This may be due to the reduction in the surface area, which resulted in reduced adsorption and thus lowers degradation efficiency.

To my best friend Clifford Mabunda and amazing family

ACKNOWLEDGEMENTS

First and foremost I would like to praise the **omnipotent GOD** for capacitating this work and for graciously carrying me through this journey to the end.

I would also like to present my gratefulness to the following people for their effort into making this work a success:

- **My wonderful supervisors**: Prof N. Moloto and Dr. Z.N Tetana, thank you for your support, patience, guidance, ideas and constant advices accompanied with motherly love.

- **Quantum dots** and **Catalysis-Organometallic-Materials (CATOMAT)** research members, many thanks for teaching me everything I know in this field and for continuously offering assistance willingly. You made this experience illustrious!

- The **Microscopy and Microanalysis Unit (MMU)**, I appreciate your training and the prerogative to use your facilities.

- My **mentors** Dr. F. Muganza and Dr. Michael KAB, I treasure your constant motivation, support and the assistance you offered for some characterizations presented in this work.

- **Center of Excellence in strong materials (CoE-SM)** thank you for funding this work.
- Many thanks to the **School of Chemistry** and the **University Of The Witwatersrand** for giving me the edge.

- My **family**, I have become, because of my true blessing “mom and dad”. Sincere thanks to my siblings and my babies Mixo, Masungulo, Mihla, and Risima, you are my motivation.

- Finally, to **my best friend**, Clifford Mabunda, your support throughout the course of my studies has landed this great achievement. Thank you for your contribution to this work, for always believing in me and for your amazing love.

PRESENTATIONS

- Oral presentation: Catalysis-Organometallic-Materials (CATOMAT) research group at the University of the Witwatersrand (03/2016): The photocatalytic degradation of methyl orange in water using TiO_2 supported on cellulose-N-MWCNTs.

- Paper presentation: Catalysis-Organometallic-Materials (CATOMAT) research group at the University of the Witwatersrand (07/2016): Adsorption of pollutants using marula seed husks.

- Poster presentation: Centre of excellence in strong materials (CoE-SM) seminar at the University of the Witwatersrand (05/2017): Photocatalytic degradation of methyl violet using TiO_2/N-MWCNTs.

- Paper presentation: Catalysis-Organometallic-Materials (CATOMAT) research group at the University of the Witwatersrand (09/2016): Membraneless water filtration using CO_2

- Poster presentation: South African Chemical Institute (SACI) conference at Western Cape (06/2017): Photocatalytic degradation of methyl violet using TiO_2 supported N-MWCNTs.

- Poster presentation: Frontiers of Electron Microscopy in materials Science (FEMMS) at Gauteng, Johannesburg (09/2017): Photocatalytic degradation of methyl violet using TiO_2 supported N-MWCNTs.

Table of Contents

List of figures

List of Tables

List of Abbreviations

arb. units	Arbitrary units
BET	Brunauer-Emmett-Teller
C_2H_2	Acetylene
CH_3CN	Acetonitrile
CVD	Chemical Vapor Deposition
C@N-MWCNTs	Cellulose coupled with nitrogen doped multiwalled carbon nanotubes
fMWCNTs	MWCNTs functionalized with acid treatment
fN-MWCNTs	Acid-treated Nitrogen doped MWCNTs
FT-IR	Fourier transform infrared Internal
ID/IG	The intensity ratio of D to G band
mL/min	Millilitre per minute
MV	Methyl violet
MWCNTs	Multiwalled carbon nanotubes
N-MWCNTs	Nitrogen-doped multiwalled carbon nanotubes
r.t	Room temperature
SEM	Scanning electron microscopy
TEM	Transmission electron microscopy
TGA	Thermogravimetric analysis
UV-Vis	Ultra-Violet visible

1

Chapter one

Background to the study

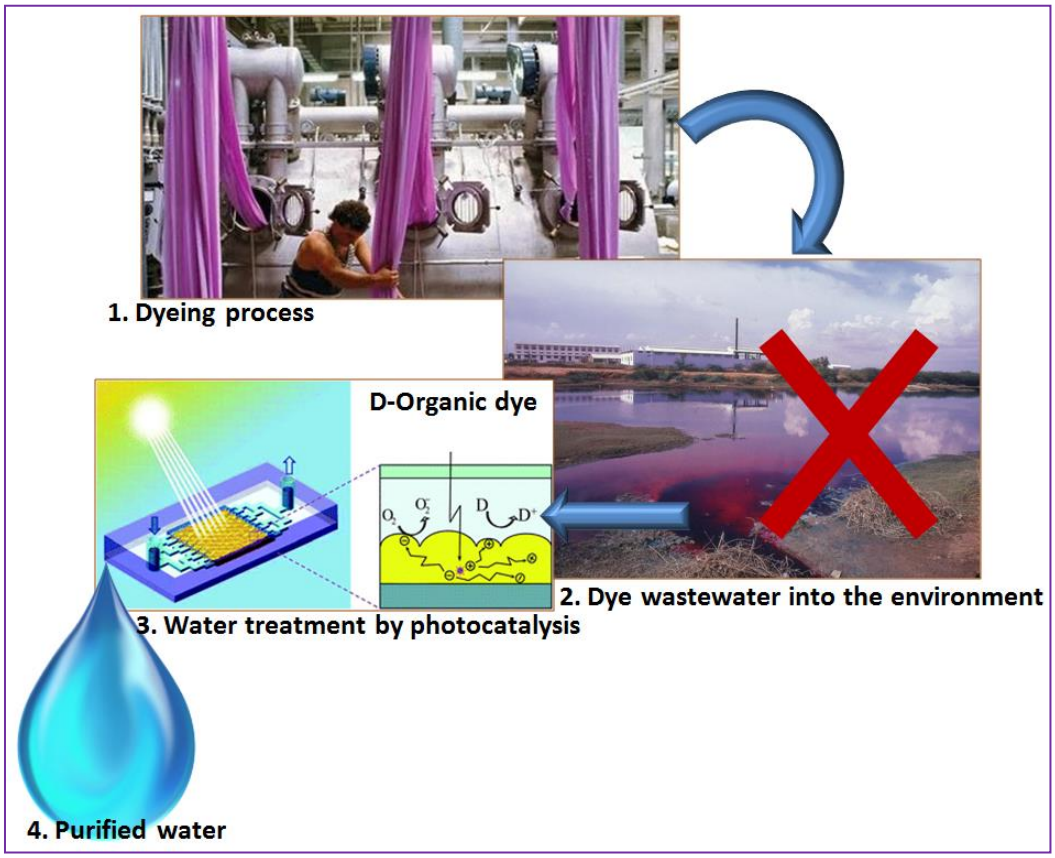

1.1 Introduction

A global water crisis has been identified as a top risk facing humanity for the next decade [1]. There are many reasons that attribute to the growth of water crisis which include the continuous increase of population, urbanization, and climate change. South Africa is currently one of the most water stressed countries globally. This is largely influenced by the low rainfall and poor sanitation. Consequently, the threat of water borne diseases in the country's rural areas keeps escalating by virtue of the escalating water pollution. In May 2017, the eNCA news broadcasted that Cape Town, the most popular tourist city has currently reached a very critical point that the city is left with only 12.3% of usable dam water. This tragedy affects the wildlife, aquatic life, business sector, agriculture and the economy of the country. With such a wounded economy, it is indisputable that manufacturing companies such as the textile industry are of great significance for the country's economic growth and employment creation. However, industrialization is a large contributing factor to air and water pollution, and textile industry in particular, is water-intensive and contribute enormously to the pollution leading to environmental and health problems [2].

Textile industries use toxic chemicals that are persistent in the environment. Among many other chemicals in textile wastewater, dyes are the most common cause of enormous amount of environmental degradation and human illness. Thus, untreated or incompletely treated textile effluent can be harmful to both aquatic and terrestrial life by adversely affecting the natural ecosystem and causing long-term health effects [3], [4]. However, treating textile wastewater is costly and time consuming [5], [6]. Thus, many researchers have focused on the development of qualifying methods which can be used to recycle textile wastewater to prevent discharging the dye-contaminated water into the environment [7]. The explored methods thus far include physical processes (such as filtration, distillation, etc.), biological processes (such as slow sand filters), and chemical processes (such as flocculation and chlorination) [8], [9]. However, most of these conventional treatment methods have difficulty in handling organic dye-contaminated wastewater due to the strong electron-withdrawing groups characterizing the chemical structure of the dyes that protect them from the bacterial oxygenases [10], [11]. It was found that

photocatalytic degradation may be an interdisciplinary method that provides a satisfactory and economically viable solution in the removal of organic dyes and harmful bacteria in the aqueous medium [12]–[15]. In general, the photocatalytic degradation process involves several steps such as adsorption-desorption of pollutants on the catalyst, electron-hole pair production, and a chemical reaction, as explained thoroughly in literature [9]–[11]. Anatase TiO_2 has shown great potential as an ideal and powerful photocatalyst among many other photocatalysts such as ZnO, Fe_2O_3, ZnS, SnO_2, WO_3, SiO_2, Nb_2O_3, and CdS [16]. The preference of TiO_2 is justified by its excellent photocatalytic properties, direct band gap (3.2 eV), chemical stability, non-toxicity, high reactivity, porosity and abundance [17]. However TiO_2-based photocatalytic processes have some limitations which include the following: (i) TiO_2 has poor affinity towards organic pollutants which resulting in low adsorption of organic pollutants to the surface of the TiO_2 and leading to mass transfer limitation (ii) The tiny particle sizes of TiO_2 result in high aggregation tendencies and higher light scattering which can reduce their photocatalytic activity [18], [19] (iii) Recovering TiO_2 from treated water is very difficult due to its small sizes [20] and (iv) The kinetics of the electron-to-hole recombination tends to be faster than surface redox reaction and thus greatly reduces the quantum efficiency of photocatalysis [13], [19].

TiO_2 may be modified by doping with metals, non-metals, carbon-based materials or by immobilizing the TiO_2 particles on a support structure. The supporting materials that have been studied include silica-based material [20]**,** alumina [21]**,** zeolites [22], carbon materials [26]–[29], etc. The role of a support material is to reduce the fast recombination of charges, thus favoring surface redox reaction [27]. The study of carbon nanotubes (CNTs) is still escalating, due to their valuable characteristics including their high surface area, high aspect ratio, and flexibility [31],[33]. Lately, various studies have been focused on the reinforcement of multiwalled carbon nanotubes (MWCNTs) in polymer fibers for a number of applications such as scaffolds in tissue engineering, artificial blood vessels, fine filtration, drug delivery systems, catalyst and enzyme carrier, and protective clothing [30]. The MWCNTs can be used as fillers in order to maximize the surface area, crystallinity, aspect ratio, and the fractional interface area in the design of stronger polymer composites. Wei *et al.* explained that the industrial CVD synthesis of MWCNTs uses coal, a non-renewable resource, thus it is essential to use minimal

amount of MWCNTs by blending them with natural polymers [31]. However, the major problems in such fabrications include the inertness, hydrophobic nature and the aggregation tendency of the MWCNTs due to Van der Waals forces which prevents their ability to disperse and form the C-O-C interphase with the cellulose polymers. Thus, the surface of the MWCNTs is normally modified through oxidation of CNTs by air [36], ozone [32], and acid oxidation (e.g. HNO_3 and H_2SO_4) to covalently attach chemical groups such as alcohols and acids [33]. Oxidation of CNTs through strong acids such as HNO_3 is usually preferred because it oxidizes the CNTs and simultaneously purifies the material [34]. This type of functionalization occurs by reducing the conductance of the MWCNTs base through refluxing in concentrated acids where the π conjugations are destroyed [35], [36].

Modification of CNTs can also be done by plasma treatment where the CNTs surface is decorated with foreign atoms at elevated temperatures [15], [37]. This type of modification incorporates heteroatoms such as, nitrogen, boron, sulphur, or phosphorus in the CNTs lattice [38], [39]. Boron and nitrogen, among the other dopants, are the mostly studied because they are neighboring atoms of carbon and thus have small atomic sizes compatible to that of the carbon atom [40]. Thus B and N atoms have a reasonable probability of incorporating into a nanotube lattice [40], [41]. N doping introduces lone pairs of electrons with respect to the delocalized π-electrons of the CNTs [40]. This further induces more positive charge on the adjacent carbon atoms which then enhances the electronic properties and chemical reactivity of the side-walls of CNTs resulting in better dispersion of noble metals and facilitate the oxygen dissociation [48]–[50]. The incorporation of nitrogen atoms into the CNTs can be done using two approaches; *in situ* doping [45] and *ex situ* doping [46]. Because the former incorporates the nitrogen atoms as the carbon lattice grows, the nitrogen may be homogeneously distributed from the inner shells to the outer layers of the CNTs. However, the latter incorporates the N atoms on a fully grown carbon lattice; hence the incorporation starts from the surface of the lattice. The N atoms first attach at the edges and the defective sites of the nanotubes [47]. Thus it is advisable to first create more defects on the nanotubes if the goal is to achieve high N content through *ex situ* doping. Hence, most studies reported on the oxidation of the nanotubes prior to *ex situ* N doping [36], [46]. However, *ex situ* N-doping requires the nanotubes to be treated at high temperatures

(700 – 950 ^{o}C) under inert conditions to distort the lattice and allow the formation of new N to C bonds. This may result in a loss of the oxygen-containing functional groups during the heating process [48]. Consequently, functionalization of CNTs through *in situ* and *ex situ* N doping may result in different N content, N configurations, and completely different structural forms leading to different reactivity of the nanotubes. This study examines the properties of N-MWCNTs that emerge from *in situ* and *ex situ* doping methods in order to determine the most effective method for a TiO_2 support in photocatalytic degradation of organic dyes. Thereafter, the competent method will be used on the MWCNTs reinforced with cellulose polymer fibers to examine its effect on the morphology, crystallinity, and surface area of cellulose-MWCNTs composite nanofibers [50]. Cellulose is an abundant polymer that is hygroscopic, polar with a large surface area and high affinity for water [50]. Cellulose-MWCNTs hybrid was discovered to have good mechanical properties, large surface area, high porosity and thermal stability[50]. This was attributed to the fascinating properties of MWCNTs coupled with those of cellulose. Because of these qualities, it was anticipated that this hybrid may be an ideal support of TiO_2 in photocatalysis. In this study, cellulose-N-MWCNTs hybrid was studied as TiO_2 support in the photocatalytic degradation of methyl violet owing to the remarkable properties of cellulose and N-MWCNTs.

The research questions that influenced this project were:

1. Does the method of nitrogen doping of MWCNTs affect the properties of TiO_2/N-MWCNTs catalyst?
2. How is the photocatalytic degradation efficiency of TiO_2/N-MWCNTs affected by the method of nitrogen doping?
3. Can N-MWCNTs improve the adsorption capacity and other properties of cellulose fibers in the composite?
4. What effect will cellulose coupled with N-MWCNTs (C@fN-MWCNTs) have on the photocatalytic efficiency of TiO_2?

1.2 Aim and objectives

The aim of this study was two-fold: To investigate the feasible method of nitrogen doping of MWCNTs as support of TiO_2 in photocatalytic degradation of methyl violet and to investigate the effect of cellulose-N-MWCNTs (C@fN-MWCNTs) on the photocatalytic degradation capacity of TiO_2.

The objectives were:

- Synthesis of multiwalled carbon nanotubes (MWCNTs) by catalytic vapor decomposition of Fe-Co/$CaCO_3$ over acetylene (C_2H_2). This was followed by the modification of the MWCNTs by (i) acid-treatment [referred to as fMWCNTs] (ii) nitrogen-doping by *in situ* and *ex situ* [referred to as *in situ* N-MWCNTs and *ex situ* N-MWCNTs] (iii) acid-treatment and nitrogen doping [referred to as *in situ* fN-MWCNTs and *ex situ* fN-MWCNTs]. The nitrogen doping was done using CVD method whilst acid-treatment was done by refluxing the materials in 55% HNO_3.
- Characterization of the modified MWCNTs followed by the preparation and characterization of their respective catalysts (*in situ* TiO_2/N-MWCNTs, *ex situ* TiO_2/N-MWCNTs, TiO_2/fMWCNTs, *in situ* TiO_2/fN-MWCNTs, and *ex situ* TiO_2/fN-MWCNTs) by sol-gel method.
- The properties of *in situ* N-MWCNTs will be compared with the *ex situ* N-MWCNTs. The photocatalytic efficiency of *in situ* TiO_2/fN-MWCNTs and *ex situ* TiO_2/fN-MWCNTs will be evaluated in the photocatalytic degradation of methyl violet.
- Synthesis and characterization of cellulose fibrils and cellulose-N-MWCNTs (C@fN-MWCNTs) hybrid by electrospinning.
- The effect of *in situ* fN-MWCNTs on cellulose polymer's properties as TiO_2 support will be assessed. The effectiveness of TiO_2/cellulose and TiO_2/C@fN-MWCNTs will be ascertained in the photocatalytic degradation of methyl violet.

1.3 Outline of Dissertation

Chapter 1 confers the elementary research background, aim and objectives of the study.

Chapter 2 elucidates a detailed review pertaining to TiO_2-based photocatalytic degradation method in the removal of organic dyes and the mechanisms involved in the process. Furthermore, the properties, synthesis methods, and applications of carbon nanotubes, cellulose and cellulose-MWCNTs composites as TiO_2 supports have been expounded with reference to previous studies.

Chapter 3 delineates the experimental procedures of the synthesis methods and the characterization techniques used for the analyses of the materials studied.

Chapter 4 presents the results and discussion of the work done on the "study of functionalized MWCNTs" where the properties of functionalized MWCNTs are investigated.

Chapter 5 examines the supporting role of functionalized MWCNTs in the TiO_2-carbon composites. This chapter is titled "Study of TiO_2-based composites". The effect of *in situ* versus *ex situ* doping methods on the TiO_2 catalyst was divulged.

Chapter 6 enunciates about the application of the prepared catalysts in the photocatalytic degradation of methyl violet. The effect of method of nitrogen doping on the photocatalytic degradation efficiency of TiO_2/fN-MWCNTs was established in this chapter. Furthermore, the optimal parameters were determined to be used in further studies.

Chapter 7 reports on the characterization and application of cellulose, and cellulose-N-MWCNTs (C@fN-MWCNTs) as TiO_2 supports. The effect of C@fN-MWCNTs on the photocatalytic efficiency of TiO_2 was investigated by degrading methyl violet under optimal parameters reported in the previous chapter.

Chapter 8 confers conclusions and recommendations of this study.

1.4 References

[1] G. H. Brundtland, "The Global Water Crisis: Addressing an urgent security Issue," *Papers for the InterAction Council*, vol. 92, no. 1, 2012.

[2] D. Pimentel, B. Berger, and D. Filiberto, "Water resources: agricultural and environmental issues," vol. 54, no. 10, pp. 909–918, 2004.

[3] K. V. Wong and B. Bachelier, "Carbon nanotubes used for renewable energy applications and environmental protection/remediation: A Review," *Journal of energy resources technology*, vol. 136, no. 2, p. 21601, 2013.

[4] N. Mathur and A. Kumar, "Physico-chemical characterization of industrial effluents contaminated soil of sanganer," vol. 4, no. 2, pp. 226–228, 2013.

[5] C. J. Ogugbue and T. Sawidis, "Bioremediation and detoxification of synthetic wastewater containing triarylmethane dyes by aeromonas hydrophila isolated from industrial Effluent," *Biotechnology research international*, vol. 11,no. 1, pp. 967–985, 2011.

[6] F. Ahmed, T. S. Tofa, and B. N. Saha, "Applicability of chemical process in textile dye wastewater treatment," vol. 42, no. 2, pp. 233–247, 2014.

[7] G. Sudarjanto, B. Keller-Lehmann, and J. Keller, "Optimization of integrated chemical-biological degradation of a reactive azo dye using response surface methodology," *Journal of Hazardous Materials*, vol. 138, no. 1, pp. 160–168, 2006.

[8] K. M. Reza, A. S. W. Kurny, and F. Gulshan, "Parameters affecting the photocatalytic degradation of dyes using TiO_2: a review," *Applied Water Science*, pp. 1–10, 2015.

[9] S. Zhezhova, S. Risteski, and G. Saska, "Methods for waste waters treatment in textile industry," *International Scientific Conference*, vol. 17, no. 2, pp. 248–252, 2014.

[10] N. Jafari, R. Kasra-Kermanshahi, M. R. Soudi, A. H. Mahvi, and S. Gharavi, "Degradation of a textile reactive azo dye by a combined biological-photocatalytic process: Candida tropicalis -TiO_2/UV.," *Iranian Journal of Environmental Health Science & Engineering*, vol. 9, no. 1, pp. 33–45, 2012.

[11] A. A. Dias, M. S. Lucas, A. Sampaio, J. A. Peres, and R. M. F. F. Bezerra, "Decolorization of azo dyes by yeasts", vol. 9, no. 1, pp. 1–16, 2010.

[12] R. J. Tayade, P. K. Surolia, R. G. Kulkarni, and R. V. Jasra, "Photocatalytic degradation of dyes and organic contaminants in water using nanocrystalline anatase and rutile TiO_2," *Science and Technology of Advanced Materials*, vol. 8, no. 6, pp. 455–462, 2007.

[13] J. Šíma and P. Hasal, "Photocatalytic Degradation of textile dyes in aTiO_2 / UV System," *Journal of chemical engineering transactions*, vol. 32, no. 19, pp. 79–84, 2013.

[14] H. Hassena, "Photocatalytic degradation of methylene blue by using Al_2O_3/Fe_2O_3 nano composite under Visible Light," *Modern chemistry & applications*, vol. 4, no. 1, pp. 3–7, 2016.

[15] L. Wang, L. Shen, Y. Li, L. Zhu, J. Shen, and L. Wang, "Enhancement of photocatalytic activity on TiO_2-nitrogen-doped carbon nanotubes nanocomposites," *International journal of photoenergy*, vol. 2013, no. July, pp. 1–7, 2013.

[16] R. Su, N. Dimitratos, J. Liu, E. Carter, S. Althahban, X. Wang, S. Xueqin, W. Yanbin, W. Stefan, N. Xiaodong, "Mechanistic Insight into the Interaction between a Titanium Dioxide Photocatalyst and Pd Cocatalyst for Improved Photocatalytic Performance," *ACS Catalysis*, vol. 6, no. 7, pp. 4239–4247, 2016.

[17] J. Schneider, M. Matsuoka, M. Takeuchi, J.Zhang, Y. Horiuchi, M. Anpo, D. W. Bahnemann, "Understanding TiO_2 photocatalysis : Mechanisms and Materials," *Chem. Rev.*, vol. 114, pp. 9919–9986, 2014.

[18] W. Q. Betancourt and J. B. Rose, "Drinking water treatment processes for removal of Cryptosporidium and Giardia," *Veterinary Parasitology*, vol. 126, no. 1–2 SPEC.ISS., pp. 219–234, 2004.

[19] H. Dong, G. Zeng, L. Tang, C. Fan, C. Zhang, X. He, Y. He, "An overview on limitations of TiO_2-based particles for photocatalytic degradation of organic pollutants and the corresponding countermeasures," *Water Research*, vol. 79, pp. 128–146, 2015.

[20] N. O. Ramoraswi and P. G. Ndungu, "Photocatalytic Properties of TiO_2 Supported on MWCNTs, SBA-15 and Silica-Coated MWCNTs Nanocomposites," *Nanoscale Research Letters*, vol. 10, no. 1, p. 427, 2015.

[21] B. E. Solsona, J.K Edwards, Jennifer, K. P. Landon, A. F. Carley, A. Herzing, C. J. Kiely, G. J. Hutchings, Graham J, "Direct Synthesis of Hydrogen Peroxide from H_2 and O_2 Using Al_2O_3 Supported Au−Pd Catalysts," *Chemistry of Materials*, vol. 18, no. 11, pp. 2689–2695, 2006.

[22] K. Guesh, Á. Mayoral, C. Márquez-Álvarez, Y. Chebude, and I. Díaz, "Enhanced photocatalytic activity of TiO_2 supported on zeolites tested in real wastewaters from the textile industry of Ethiopia," *Microporous and Mesoporous Materials*, vol. 225, pp. 88–97, 2016.

[23] V. O. Nyamori, S. D. Mhlanga, and N. J. Coville, "The use of organometallic transition metal complexes in the synthesis of shaped carbon nanomaterials," *Journal of Organometallic Chemistry*, vol. 693, no. 13, pp. 2205–2222, 2008.

[24] Z. N. Tetana, "Boron and nitrogen doped carbons for photochemical degradation reactions" pp. 1–235, 2013.

[25] A. Q. Zhao, J. Masa, and W. Xia, "Very low amount of TiO_2 on N-doped carbon nanotubes significantly improves oxygen reduction activity and stability of supported Pt nanoparticles," *Physical Chemistry Chemical Physics*, vol. 17, no. 16, pp. 10767–10773, 2015.

[26] Y. Yao, G. Li, S. Ciston, R. M. Lueptow, and K. A. Gray, "Photoreactive TiO_2 /carbon nanotube composites: Synthesis and Reactivity," *Environmental science & technology*, vol. 42, no. 13, pp. 4952–4957, 2008.

[27] A. Peigney, C. Laurent, E. Flahaut, R. R. Bacsa, and A. Rousset, "Specific surface area of carbon nanotubes and bundles of carbon nanotubes," *Carbon*, vol. 39, no. 4, pp. 507–514, 2001.

[28] M. S. Maubane, M. A. Mamo, E. N. Nxumalo, W. A. L. Van Otterlo, and N. J. Coville, "Tubular shaped composites made from polythiophene covalently linked to Prato functionalized N-doped carbon nanotubes," *Synthetic Metals*, vol. 162, no. 24, pp. 2307–2315, 2012.

[29] O. Saligheh, M. Forouharshad, and R. Arasteh, "The effect of multi-walled carbon nanotubes on morphology , crystallinity and mechanical properties of PBT / MWCNTs composite nanofibers," vol. 56, no. 1, pp. 4–9, 2013.

[30] C. Wei, "Adhesion and reinforcement in carbon nanotube polymer composite," *Applied physics letters*, vol. 88, no. 1, pp. 1–4, 2006.

[31] J. M. Simmons, B.M Nichols, S. E Baker, M. S. Marcus, O. M. Castellini, C. Lee, R. J. Hamers, M. A. Eriksson, "Effect of ozone oxidation on singlewalled carbon nanotubes," *Materials*, vol. 12, no. 1, pp. 7113–7118, 2006.

[32] M. A. M. Motchelaho, H. Xiong, M. Moyo, L. L. Jewell, and N. J. Coville, "Effect of acid treatment on the surface of multiwalled carbon nanotubes prepared from Fe-Co supported on $CaCO_3$: Correlation with Fischer-Tropsch catalyst activity," *Journal of Molecular Catalysis A: Chemical*, vol. 335, no. 1–2, pp. 189–198, 2011.

[33] S. D. Mhlanga, . M. K, Witcomb, M. J. Carter, and N.J. Coville. "The effect of synthesis parameters on the catalytic synthesis of multiwalled carbon nanotubes using Fe-Co/ $CaCO_3$ catalysts," *S. Afr. J. Chem.*, vol. 62, no. 1, pp. 67–76, 2009.

[34] J. Bhattacharjee, "Activation of graphenic carbon due to substitutional doping by nitrogen: Mechanistic understanding from first principles," *Journal of Physical Chemistry Letters*, vol. 6, no. 9, pp. 1653–1660, 2015.

[35] M. A. M. Motchelaho, "Iron and cobalt catalysts supported on carbon nanotubes for use in the Fischer-Tropsch synthesis," *Thesis*, pp.1–289, 2011.

[36] O. Y. Podyacheva and Z. R. Ismagilov, "Nitrogen-doped carbon nanomaterials: To the mechanism of growth, electrical conductivity and application in catalysis," *Catalysis Today*, vol. 249, no. 1,pp. 12–22, 2015.

[37] M. A. Mamo, A. O. Sustaita, Z. N. Tetana, N. J. Coville, and I. A. Hümmelgen, "Undoped, nitrogen-doped and boron-doped multiwalled carbon nanotube/poly(vinyl alcohol) composite as active layer in simple hydrostatic pressure sensors," *Journal of Materials Science: Materials in Electronics*, vol. 24, no. 10, pp. 3995–4000, 2013.

[38] K. C. Mondal, A. M. Strydom, R. M. Erasmus, J. M. Keartland, and N. J. Coville, "Physical properties of CVD boron-doped multiwalled carbon nanotubes," *Materials Chemistry and Physics*, vol. 111, no. 3, pp. 386–390, 2008.

[39] L. F. Mabena, "Synthesis , characterisation and activity of Ruthenium/N-doped multiwalled Carbon nanotubes" *Thesis*, pp. 1–214, 2013.

[40] E. N. Nxumalo and N. J. Coville, "Nitrogen doped carbon nanotubes from organometallic compounds: A review," *Materials*, vol. 3, no. 3, pp. 2141–2171, 2010.

[41] H. Liu, Y. Zhang, Yong, R. Li, X. Ruying, S. Xueliang, S. Désilets, H. Rachid, M. Jaidann, L. Mounir, "Structural and morphological control of aligned nitrogen-doped carbon nanotubes," *Carbon*, vol. 48, no. 5, pp. 1498–1507, 2010.

[42] Q. Wei, X. Tong, G. Zhang, J. Qiao, Q. Gong, and S. Sun, "Nitrogen-doped carbon nanotube and graphene materials for oxygen reduction reactions," *Catalysts*, vol. 5, no. 3, pp. 1574–1602, 2015.

[43] G. Bepete, Z. N. Tetana, S. Lindner, M. H. Rümmeli, Z. Chiguvare, and N. J. Coville, "The use of aliphatic alcohol chain length to control the nitrogen type and content in nitrogen doped carbon nanotubes," *Carbon*, vol. 52, pp. 316–325, 2013.

[44] S. D. Mhlanga, E. N. Nxumalo, N. J. Coville, and V. V. Srinivasu, "Nitrogen doping of CVD multiwalled carbon nanotubes: Observation of a large g-factor shift," *Materials Chemistry and Physics*, vol. 130, no. 3, pp. 1182–1186, 2011.

[45] C. Tang, Y. Bando, D. Golberg, and F. Xu, "Structure and nitrogen incorporation of carbon nanotubes synthesized by catalytic pyrolysis of dimethylformamide," *Carbon*, vol. 42, no. 12–13, pp. 2625–2633, 2004.

[46] B. J. Matsoso, K. Ranganathan, B. K. Mutuma, T. Lerotholi, G. Jones, and N. J. Coville, "Time-dependent evolution of the nitrogen configurations in N-doped graphene films," *RSC Adv.*, vol. 6, no. 108, pp. 106914–106920, 2016.

[47] H. Xiong, M. A. M. Motchelaho, M. Moyo, L. L. Jewell, and N. J. Coville, "Cobalt catalysts supported on a micro-coil carbon in Fischer-Tropsch synthesis: A comparison with CNTs and CNFs," *Catalysis Today*, vol. 214, pp. 50–60, 2013.

[48] S. Yun and J. Kim, "Multi-walled carbon nanotubes-cellulose paper for a chemical vapor sensor," *Sensors and Actuators, B: Chemical*, vol. 150, no. 1, pp. 308–313, 2010.

[49] B. Ghorani, S. J. Russell, and P. Goswami, "Controlled morphology and mechanical characterisation of electrospun cellulose acetate fibre webs," *International Journal of Polymer Science*, 2013.

[50] S. Mun, Y. Chen, and J. Kim, "Cellulose-titanium dioxide-multiwalled carbon nanotube hybrid nanocomposite and its ammonia gas sensing properties at room temperature," *Sensors and Actuators, B: Chemical*, vol. 171–172, pp. 1186–1191, 2012.

2

Chapter two

Literature review

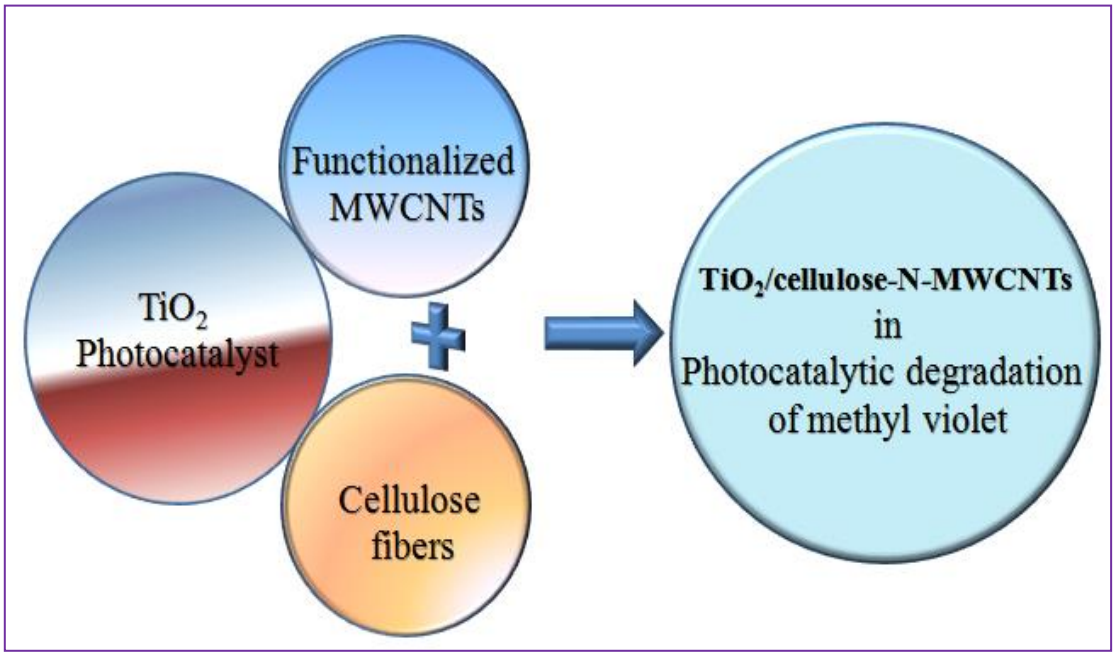

2.1 Introduction

Water scarcity keeps escalating due to the continuous increase of populations; urbanization; and climate change. South Africa is currently facing drought on account of low rainfall which goes further to affect the economy, human health, the environment and civil society. The low rainfall, coupled with the increasing population density and the potential impact of climate change only exacerbate the water-stress [1]. Hence every input in saving water and ways to improve its quality are essential [2]. Organic dyes are one of the major concerns because dye-industries consume substantial amount of water and generates highly polluted water which negatively impacts the quality of the receiving streams [3]. Dye-contaminated water enormously affects the aesthetic quality, food chain organisms and the aquatic life. In addition, dye contaminants are inhibitory towards conventional wastewater treatment systems, thus costly treatment processes are being used to achieve complete removal of these dyes from wastewater [4]. Nevertheless, TiO_2-based photocatalysis has proved to be an efficient, destructive and cost-effective method under optimal conditions [2], [3]. However, the application of TiO_2 photocatalysis is limited by the poor affinity of TiO_2 towards organic dyes/mass transfer limitation, recombination of charges, and low turnover number [5].

Previous studies have attempted various countermeasures to overcome these limitations [5], [6]. Immobilizing TiO_2 on a large surface area support where pollutants can be condensed is one of the most preferred approaches [7]. Cellulose and multiwalled carbon nanotubes (MWCNTs) are carbon materials with large surface area and high porosity, hence they have been widely studied as TiO_2 supports [6], [8]. The study of cellulose has gained a lot of attention because of its abundance, low cost, UV light resistance, mechanical strength, biocompatibility, biodegradability and its functional groups that may be employed in various activation processes [9]–[11]. More interestingly, the reactivity of cellulose may be increased by converting the bulk cellulose into nanocellulose. This is ascribed to more hydroxyl groups being exposed to the surface of the materials [12]. On the other hand, MWCNTs have fascinating properties which can be tuned suitably for a specific application [13]. In 2008, Yun and Kim developed a method of creating more reactive sites on the surface of cellulose by decorating the material with multiwalled carbon nanotubes (MWCNTs) [13]. This study has ever since gained a lot of

attention in various applications. The hybrid of cellulose and MWCNTs exhibited remarkable enhancement of elastic modulus, strength and surface area with addition of very small amounts of MWCNTs [14]. Besides cellulose, other polymers such as polyacrylonitrile (PAN), polyethylene oxide (PEO) have been used to investigate the influence of MWCNTs on these polymers in various fields. However, there still exist research gaps in obtaining a homogeneous dispersion of MWCNTs in their host polymer matrices and enhancing interfacial adhesion of the MWCNTs to the polymer. A typical approach thus far to bridge these gaps is by functionalizing the MWCNTs either by heteroatom doping, or by treating them in basic or acidic conditions [15], [16]. Functionalization introduces defects on the MWCNTs by incorporating new functional groups in the lattice [17]. The introduced defects are typically evaluated using Raman spectroscopy [17]. Mhlanga *et al.* reported that treating MWCNTs with HNO_3, in particular, introduces functional groups such as OH, COOH and simultaneously reduce impurities [18].

Functionalization through heteroatom doping is usually done with nitrogen as a dopant owing to its small size which is similar to that of carbon, and its relatively higher electronegativity which induce a net positive charge in the carbon lattice [19], [20]. Nitrogen dopants can be incorporated into MWCNTs in several ways resulting in several bonding configurations [21]. Two approaches of incorporating N namely "*in situ*" and "*ex situ*" syntheses are used. These methods may result in different N configurations and N level, hence affect the photocatalytic activity of the anchored TiO_2 differently [22]–[24]. For instance, *in situ* N-MWCNTs may be homogeneously doped since the doping occurs during the lattice growth [24]. On the other hand, *ex situ* N-MWCNTs is surface functionalization which may result in limited N incorporation since doping occurs mostly at the defect sites and the edges of a fully formed lattice [24], [25]. Thus, acid treatment is normally done prior to *ex situ* N doping to improve incorporation sites. Notably, Ayala *et al.* highlighted that the final objective should not only be to reach the maximum possible amount of N but to keep in mind the final use of these N-MWCNTs as well as type of N configurations required for the application of interest [26].

This study investigates the ideal method of synthesizing N-MWCNTs in order to achieve mandatory properties for higher photocatalytic degradation capacity of the TiO_2 nanocomposites.

These properties will be endowed into cellulose by fabricating cellulose-N-MWCNTs (C@fN-MWCNTs) composites. The C@fN-MWCNTs composite will be studied as TiO_2 support in photodegradation of methyl violet.

2.2 TiO_2 photocatalyst

Titanium dioxide (TiO_2) is a natural n-type semiconductor with a band gap of approximately 3 eV. However its particle size and crystalline phase have a great influence in its n- or p-type behavior and band gap, respectively. Although TiO_2 is known as an intrinsic n-type semiconductor in bulk, the behavior of nanostructured-TiO_2 cannot be predicted. Additionally, TiO_2 exists in three crystalline phases namely brookite, anatase, and rutile. In photocatalysis anatase usually shows a higher photocatalytic activity than rutile and brookite as illustrated in Figure 2.1 [27]. This is influenced by the higher charge-carrier mobility of 80 $cm^2.v^{-1}s^{-1}$ in anatase, which is 8 times faster than that of rutile [28]. Furthermore, anatase has high redox potential corresponding to its wide band gap (3.2 eV) compared to rutile (3.0 eV) [29], [30]. Besides water purification photocatalysis, TiO_2 has shown potential in many other applications such as air purification [31], deodorization [32], and self-cleaning materials [33]. This is attributed to its non-toxicity, non-corrosiveness, high reactivity, photocatalytic stability, cost-effectiveness, strong oxidizing power and tenable properties which can be modified by size reduction, doping and sensitization [29], [34], [35]. Thus in analogy with many other semiconductors such as ZnO, ZnS, CdS, and Fe_3O_2, TiO_2 is highly advantageous because the metal sulphides undergo photoanodic corrosion in aqueous medium, while Fe and Zn oxides undergo photocathodic corrosion [32].

Nonetheless, studies have been developed with an aim to maximize the photocatalytic capacity of anatase TiO_2. These studies have been motivated by the drawbacks that TiO_2 exhibits such as (i) its high aggregation tendencies leading to a loss of active sites as well as catalytic efficiency [36], [37], (ii) its low adsorption ability due to its low affinity and porosity [36], [38] and (iii) the electron-hole recombination which causes low quantum yield of excitons [5], [8], [36]. A number of proposed elucidations to these drawbacks involve doping TiO_2 with some transitional

metals [39], [40], or adding a moderate amount of co-sorbent as a support of TiO_2 [9]. Immobilizing TiO_2 on various supports including carbon [5], [41], glass fibers [42], montmorillonite clay [38], [43], organic materials [7], [27] and zeolites [7] may increase the photochemical stability and recyclability of TiO_2 [44], [45]. Carbon-based supports are mostly preferred simply because of the versatility nature of carbon, stability, flexible electronic configuration and abundance.

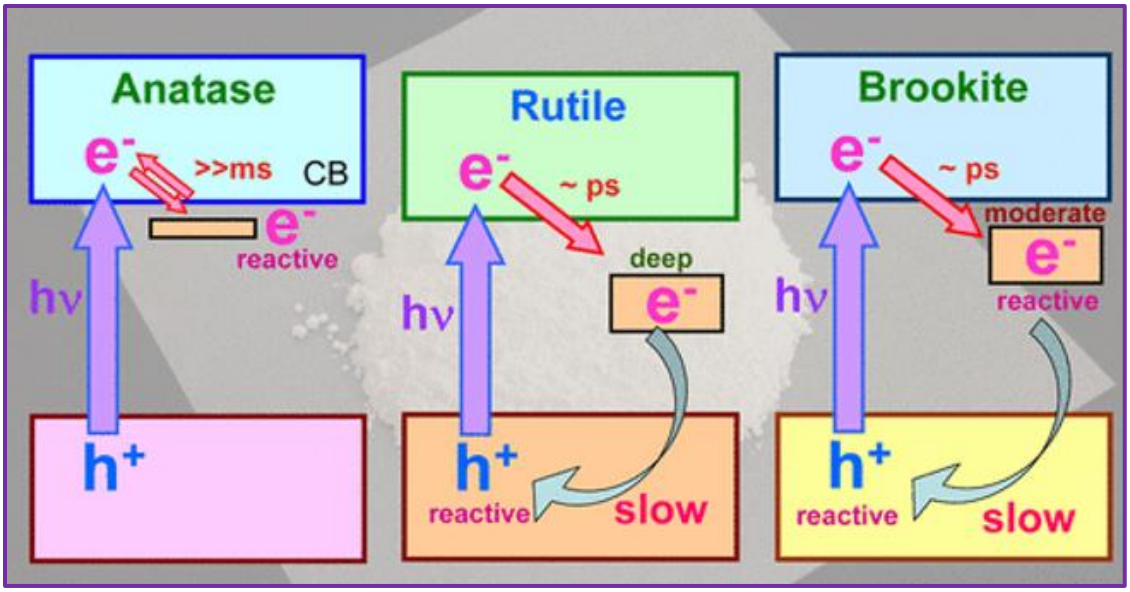

Figure 2.1: Schematic diagram comparing the reaction rates of anatase, rutile and brookite TiO_2.

2.3 Properties of carbon nanotubes

Carbon nanotubes (CNTs) can be construed as rolled up graphene in a well-defined direction along the nanotube axis [46]. Depending on the rolling direction of the graphene sheet, CNTs can be zigzag, chiral or armchair [47]. Figure 2.2 illustrates the different molecular structures of zigzag, chiral and armchair nanotubes [47]. The orientation is indicated by the circumferential vector C which delineates the circumference of a specific tube as $\mathbf{C = n_1a_1 + n_2a_2}$, where a_1 and a_2 are the lattice vectors of graphene, while n_1 and n_2 are the chiral indices. It is noteworthy that

armchair CNTs have equal chiral indices, such that $n_1=n_2$, hence they are always metallic. The metallic nature of armchair CNTs is endorsed by their immutable properties even with different intrinsic symmetry and curvature [48]. The conductivity of armchair CNTs is 103 times higher than copper. Zigzag CNTs have at least one zero chiral indices; such that n_1 or n_2 equals 0, thus they can be metallic when each chiral index is a multiple of 3, otherwise it is a semiconductor. Moreover, chiral indices with other values indicate chiral CNTs, which are CNTs are semiconductor or metallic when n_1 or n_2 = (2n+m)/3 is an integer. The correlation between the CNTs "chirality" has brought more interest in the study of compliant electronic properties of CNTs [49]. Notably, the band gaps of zigzag and chiral CNTs can be assorted upon chiral pitch and diameter to obtain an ideal semiconductor [49]. The diameter (d) of the nanotube can be estimated using the equation:

$$\mathbf{d} = |\mathbf{C}|/\boldsymbol{\pi} = \frac{\boldsymbol{x}}{\boldsymbol{\pi}}\sqrt{(\boldsymbol{n_1}^2)\mathbf{n_2}+\mathbf{n_2}^2} \qquad \text{eq (2.1)}$$

where x is the lattice constant of the honeycomb network, defined by $\mathbf{x} = \sqrt{\mathbf{3}}\mathbf{(bond\text{-}length)}$. Although a lot of research has been done on CNTs, it is still a challenge to synthesize uniform molecular structure (or CNTs chirality) of CNTs [48], [49].

The properties of CNTs can also vary based on the physical design of the nanotubes. For instance, CNTs can be branched through X-, Y-, T- junction [50], or they can have buckled shapes [51] resulting in different reactivities and characters. This motivates more studies on CNTs.

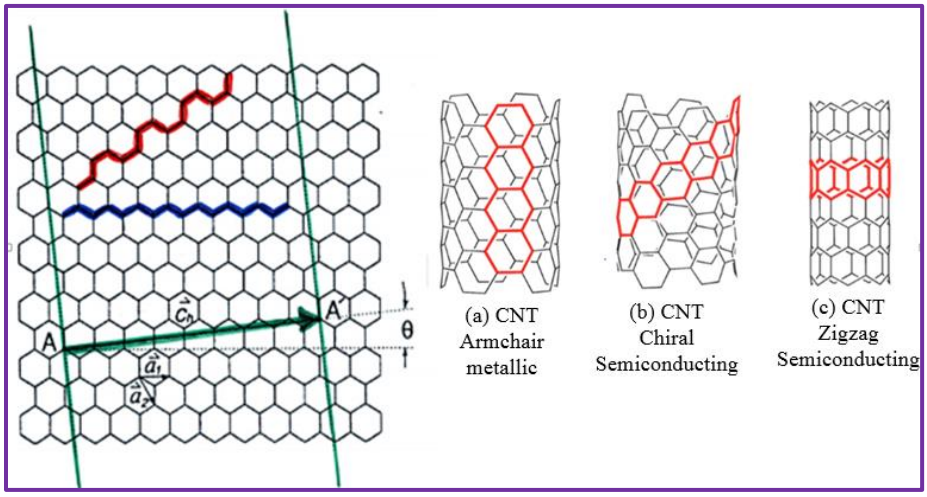

Figure 2.2: Schematic view of graphene honeycomb network illustrating possibilities of wrapping into three CNTs chiralities. (a) Zigzag, (b) Chiral and (c) Armchair CNTs: The dashed arrows show the circumferential vector C (indicates the rolling direction for CNTs) [52].

CNTs can consist of either one (SWCNTs) or more (MWCNTs) rolled up graphene sheets (see Figure 2.3). The structures of MWCNTs may be described using the Russian Doll model or the Parchment model [52]. The former describes MWCNTs as the coordinated cylinders of graphene whilst the latter describes them as a single sheet of graphene wrapped around resembling a rolled paper [52]. A few studies have focused on identifying properties that distinguish MWCNTs from SWCNTs in order to make economic and engineering judgments, and also for conformity with probable environment, health and safety requirements [23], [53]. The studies concluded that diameters of SWCNTs are typically in a range of 0.4–3 nm, and the length can be up to several microns [54], whereas MWCNTs may have inner diameters of 1–30 nm with outer diameters of up to 100 nm [55]. Thus SWCNTs typically exhibit on A1g symmetry radial breathing mode (RBM) peaks in the low frequencies of their Raman spectrum [17], [55]. These vibrations usually respond to diameter of <2 nm, hence they are not expected in MWCNTs Raman spectrum [55]. Nonetheless, Jantoljak and co-workers observed similar peaks from their MWCNTs Raman spectrum [56]. Lehman *et al.* suggested that MWCNTs exhibit the RBM's peaks provided their innermost tube has a diameter of <2 nm [57].

However, when Donato and co-workers observed similar peaks, they assigned them to the presence of defects and impurities which may include SWCNTs [58]. It is noteworthy that SWCNTs can form during MWCNTs synthesis depending on the amount of catalyst fed during the synthesis [59]. Thus Donato's observation may be valid. Hence there is still a need to further understanding of Raman spectroscopy in characterization of MWCNTs. MWCNTs are the most studied than SWCNTs because they are easy to make, and relatively cheaper [60], [61].

MWCNTs also have fascinating properties such as high electrical conductivity, high elasticity and high thermal conductivity, high aspect ratio and good field emission properties [62]. Consequently, they have been intensively studied by many researchers for various applications which include but not limited to thermal conductivity [63], field emission [64],energy storage [21], [65], molecular electronics [66], air and water purification [67], [68], and in polymers to control or enhance conductivity [62]. In almost all of the applications, the graphitic properties of the MWCNTs play an important role. Hence researchers have developed a way to estimate the graphitization degree of the MWCNTs using X-ray diffraction technique.

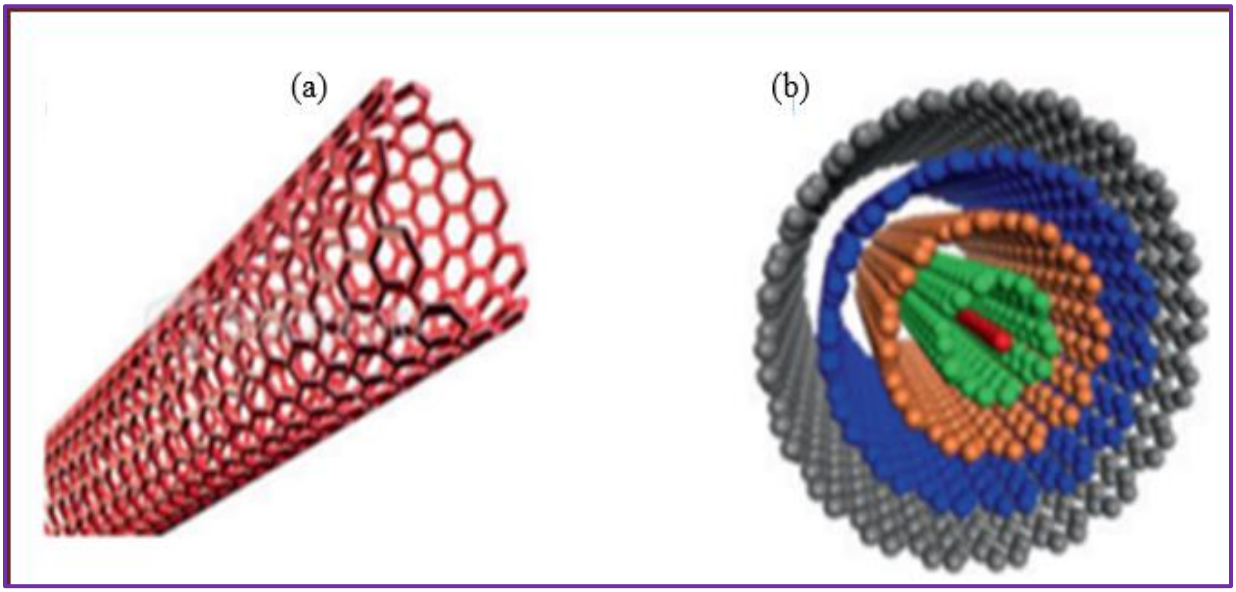

Figure 2.3: Schematic diagram illustrating types of CNTs ascertained by the number of their layers (a) SWCNTs (b) MWCNTs [12].

2.3.1 Synthesis and growth of MWCNTs

The well known methods used for CNTs synthesis include laser ablation, arc discharge, and chemical vapor deposition (CVD), and more recently autoclave method [69], [70]. CVD is a widely used method as it is the only method that can produce high yields of MWCNTs [71]**,** and can be carried out in a continuous mode at a relatively low temperature compared with the other methods [72]. The CVD synthesis of MWCNTs requires a catalyst which is normally a metal (e.g.: Fe, Co) supported catalyst [18], [73]. It has been reported that the activity of these different metals rate in this order: Fe-Co/$CaCO_3$ > Fe/$CaCO_3$>>> Co/$CaCO_3$ [18], [74] but the explanation behind this is still not fully understood.

There are two accepted mechanisms used to explain the catalytic growth of MWCNTs as shown in Figure 2.4. The two methods are (a) the tip-growth mechanism (where the catalyst particle is located at the tip of a growing tube) which is induced by a weak catalyst-support interaction and (b) the root-growth mechanism (where the catalyst particle is found at the bottom of the tube) which is induced by a strong catalyst–support interaction [75]–[77]. The former starts from the interaction of the hydrocarbon gas (e.g. C_2H_2) and the metal catalyst in a raised temperature resulting in a decomposition of the gas to generate hydrogen and elementary carbon atoms [78]. The generated carbon atoms may further dissolve in the metal to generate pseudoliquid metastable carbide until a saturation of the metal catalyst with solid carbon is reached at the rear side of the catalyst allowing a formation of the carbon lattice with a hollow core [76]. However, the tip-growth mechanism is not ideal because the growth of CNTs is limited to the availability of the metal tip for new interaction with the hydrocarbon gas [79]. In case of the latter, the elementary carbon atoms are initiated from the metal catalyst in a form of a hemispherical dome and the growth is controlled by surface carbon diffusion rather than through the bulk of the catalyst nanoparticles [79]. In summary growth of CNTs is strongly dependent on the synthesis parameters (i.e. synthesis temperature, pressure of gases, carbon source, particle size of catalyst, and chemical nature of the catalyst).

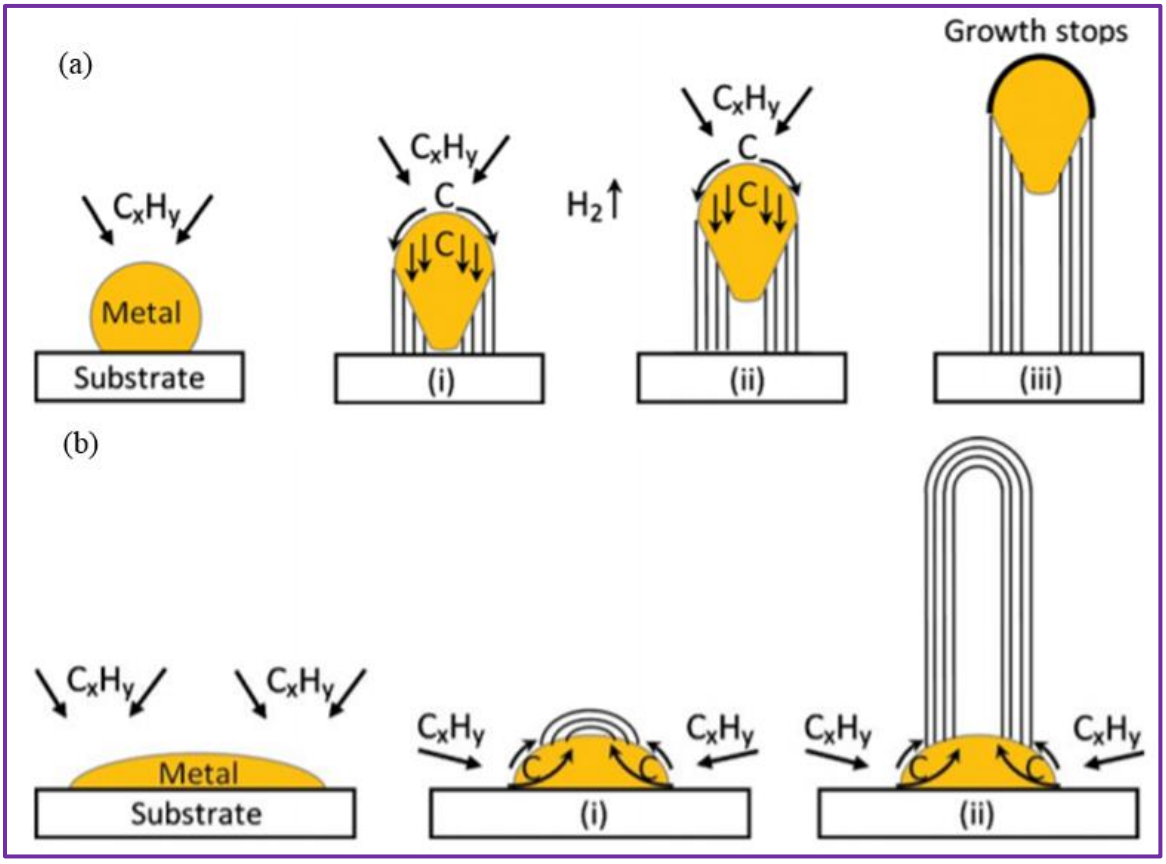

Figure 2.4: Accepted carbon nanotube mechanistic models (a) Tip-growth mechanism (b) Root-growth mechanism [5].

2.3.2 Functionalization of MWCNTs

Recently, MWCNTs are at the forefront of today's research and heterogeneous catalysis is among the potential applications of these fascinating nanostructures [80]. However, MWCNTs are naturally inert and usually hydrophobic after synthesis, thus modification of their surface through functionalization to create charged points on their surface and make them reactive is required [53]. MWCNTs can be effectively functionalized with $KMnO_4$, H_2SO_4, HNO_3, or a mixture of HNO_3 and H_2SO_4 to introduce functional groups such as carboxyl, carboxylic anhydride, phenol groups, carbonyl groups (demonstrated in Figure 2.5) [68], [81] or by doping a heteroatom [69], [82]. However, in a process of functionalizing the MWCNTs, certain properties such as the thermal stability, graphitization degree, and the interlayer spacing can be affected.

Graphitization degree refers to the probability of neighboring layers in the MWCNTs structure to be parallel. Thus, highly graphitized MWCNTs are expected to exhibit highly ordered lattice which correlates to smaller layer distances. The correspondence between the graphitization degree with the interlayer spacing is presented by the Maire and Mering formula in equation 2.2.

$$d = 3.354 + 0.086(1 - g) \qquad \text{eq. (2.2)}$$

where d is the interlayer spacing and g refers to the graphitization degree. Ideal graphite exhibit the graphitization degree of 1 (g=1), while amorphous carbon have zero graphitization degree (g=0). This is calculated from the Gaussian peak (002) that is typically exhibited in the X-ray diffraction (XRD) pattern of carbon materials. On the other hand, the thermal stability of the MWCNTs is ascertained using thermal gravimetric analysis (TGA).

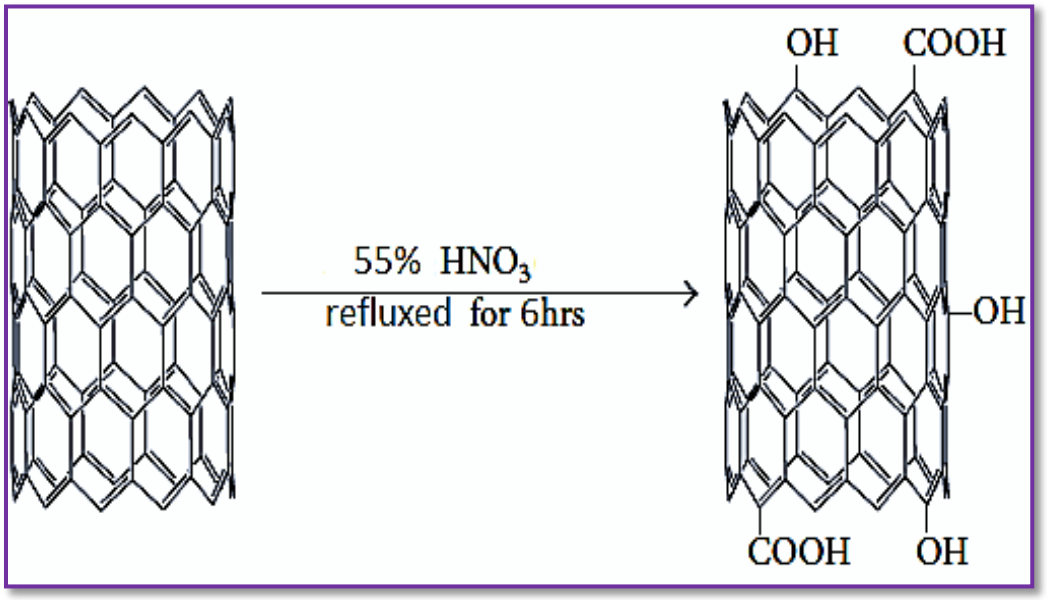

Figure 2.5: A schematic diagram showing typical functionalization of MWCNTs through acid treatment [25].

Nonetheless, the presence of oxygen and hydrogen within the surface groups comes with benefits of improving the adsorption properties of the MWCNTs mainly due to the p-p bond interaction, hydrophobic and electrostatic interactions [82]. Thus functionalized MWCNTs interact strongly

with the benzene ring of aromatic compounds which are also found in organic dyes, and hence influence their degradation positively by improving the mass transfer effect [53], [82]. On the other hand, doping is a process of creating reactive sites on the walls of MWCNTs with heteroatoms leading to the formation of electron-rich n-type (e.g. nitrogen-doped CNTs) or electron-deficient p-type (e.g. boron-doped CNTs) semiconducting nanotubes [80].

Heteroatom dopants, such as nitrogen, phosphorus, boron, and sulfur, in carbon materials endow them with improved and controllable electronic features as well as rich surface chemistry [19]. The most effective dopants used to modify the behavior of CNTs are nitrogen and boron atoms because of their small atomic size that is similar to that of the carbon atom [83]. Therefore, they have a reasonable probability of entering the nanotubes lattice [21], [60]. However, boron is less electronegative compared to carbon, hence it donates electrons to carbon resulting in a partially negative carbon whereas nitrogen tends to receive electrons from carbon, thus generating a partial positive charge on its neighboring carbon atoms. Thus the capability of N atoms to draw electrons towards itself from carbon expedite the oxygen dissociation [71], [84]. In this work, N-doped MWCNTs were studied.

2.3.3. Properties of N-MWCNTs

Since Terrones *et al.* reported on the synthesis of nitrogen doped carbon nanotubes, (N-CNTs) in 1997 [85], N-CNTs have been extensively studied owing to their special physical, electronic, catalytic and conductivity properties [86]. For instance, Wong *et al.* [65] reported that the nitrogen atom in CNTs increases its conductivity due to the rise in of the Fermi-level towards the conduction band. Jiang and Gao reported that basic N-containing groups in CNTs can generate hydrophilic properties leading to more dispersible CNTs in aqueous medium [87]. The incorporation of nitrogen atoms introduces defects on the benzene rings of MWCNTs by forming, sp^3 carbons, pyridine, pentagons and heptagons, resulting in a higher degree of disorder in N-MWCNTs relative to MWCNTs [88], [89]. This may increase the reactivity of the neighboring carbon atoms, and it can be confirmed using Raman spectroscopy, where the N-MWCNTs have high I_D/I_G ratios which are associated with high defects relative to MWCNTs.

The insertion of N atoms into a CNTs lattice changes the overall structure; thus far, the common structure observed on N-CNTs synthesized by *in situ* method is the bamboo-like structure, although this feature is not unique for N-CNTs [90], [91]. The bamboo-like structure is usually not observed from *ex situ* synthesized N-CNTs because this method affects the surface of the CNTs. Nxumalo *et al.* reported that the distance between the bamboo compartments decreases with increasing nitrogen content in the CNTs structure. They further received a general agreement with Tao *et al.* [53] that nitrogen doping result in narrower inner diameter of the tubes (i.e. the numbers of walls decrease with N inclusion). Housseinou pointed out that bamboo-like structures are not observed when the pristine N-CNTs contain very low concentrations of N, or when Co and Ni are used as growth catalyst instead of Fe [49]. However, a few studies observed the bamboo compartments from the N-CNTs grown from Co catalyst [54].

N doping can enhance the reactivity and selectivity of the CNTs, especially in catalytic applications [57]. This may be attributed to the shorter bond length of C-N compared to the C-C bond, which may result to a distortion of the CNTs lattice into a different shape of the graphene layers with different selectivity. This was also supported by Serp *et al.* who reported that different curvature of the surfaces of the carbon materials result in different available binding sites, thus different selectivity and reactivity [58]. The nitrogen configurations also play an important role in the electronic nature of the N-CNTs. Many studies have reported the N-doping in three main bonding configurations: (i) pyridine-like: where the N atom is two-fold coordinated, (ii) pyrrole-like: where the N sits substitutionally in a five-membered ring and (iii) graphitic/substitutional: where N replaces a graphitic C atom in the CNT lattice [22], [32], [34]. Figure 2.6 shows the type of N species which can be incorporated in N-CNTs. N-CNTs with a high pyridinic type N content exhibit catalytic activity in oxygen reduction reactions [22].

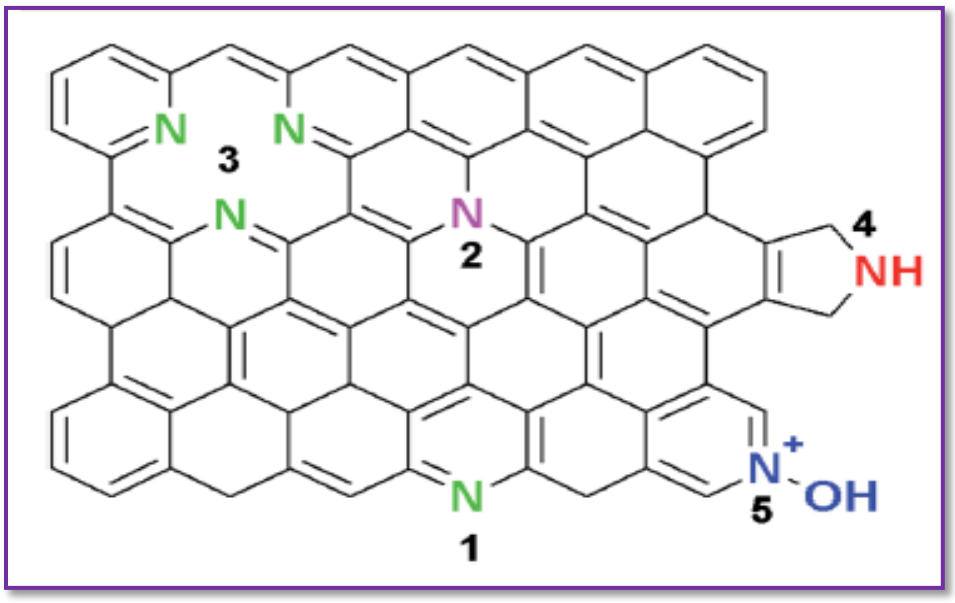

Figure 2.6: Nitrogen configurations the MWCNTs (1) pyridinic N, (2) substitutional or graphitic N, (3) triple vacancy pyridinic N, (4) pyrrolic N, and (5) oxidized pyridinic-N (NOx).

2.3.4 Synthesis and growth of N-MWCNTs

Although the mechanistic model of the formation of the distinct morphology of N-CNTs is still not fully understood, a few studies proposed plausible mechanism models of the formation of the bamboo-like structures observed on N-CNTs. Ayala *et al.* reported that the bamboo structure is due to the surface strain resulting from the presence of N in the carbon deposit which causes the carbon or nitrogen surface atoms to detach from the metal particles intermittently [26]. Reyes-Reyes *et al.* suggested that the bamboo structure result from the differences in precipitation rates of the C/N species [91]. Slow precipitation of the carbon atoms that are deposited on the metal catalyst may lead to insufficient material to maintain inner N-CNTs growth, thus the layers suddenly close leading to the formation of periodically bamboo-like structure [91]. Generally, nitrogen-doping of carbon nanostructures is divided into two: (i) *in situ* doping which is doping directly during the growth of porous nanostructure materials; and (ii) *ex situ* (also known as post-doping) which is the post-treatment of pre-synthesized carbon nanostructure material [22], [92].

The *in situ* doping method has been adopted in many studies [75], [84], as compared to *ex situ* doping method. This is because in *ex situ* doping, N incorporation occurs mostly at the defect sites and the edges of graphene, thus the N concentration is typically low. To lessen this drawback, the MWCNTs are first functionalized to create more defects allowing more N atoms to be incorporated in the lattice [22]. Although *in situ* doping method is highly preferred, it carries its own drawbacks such as low yield due to excessive by-products, which as a result, also requires complicated purification, which is usually done through the process of functionalization [24]. Recently, a lot of studies have been focused on controlling the level of nitrogen doping and the nitrogen configuration as they are important in modulating the properties of N-CNTs [75]. Bebete *et al.* suggested that the level of nitrogen doping is influenced by the flow rate of the carrier gas bubbled through the nitrogen-containing source relative to that of the carbon containing source which can be a gas or a liquid [88]. Thus, for a controlled growth of N-MWCNTs, there are a number of experimental parameters that should be studied.

2.3.4.1 The influence of synthesis parameters on the CVD-growth of N-MWCNTs

2.3.4.1.1 Effect of carbon and nitrogen precursor

A wide range of compounds, gaseous or volatiles in particular, have been used in the synthesis of N-CNT as carbon and nitrogen sources. This includes pyridine [93], acetonitrile [84], benzylamine [91], ammonia [87], etc. These precursors may result in different N levels, configurations or the number of layers of the nanotubes. For *in situ* method small hydrocarbon precursors are mostly preferred because they give out high yield owing to their selective decomposition on the metal catalyst surface and increase the carbon yield percentage. On the other hand, harsh conditions and precursors such as ammonia are usually used during *ex situ* doping if the goal is to achieve high N level. This is because precursors like ammonia are highly volatile, hence they can be easily incorporated in the matrix of the CNTs [22], [87].

2.3.4.1.2 Effect of Temperature

According to Kooset *et al.*, an increase in the reaction temperature from 800 ^{o}C to 900 ^{o}C result in a decrease of the N content with relatively longer distances between the bamboo compartment separations [94]. In 2013, Tetana and co-workers studied the synthesis of N-MWCNTs using *in situ* doping under different temperatures (700-850 ^{o}C). They concluded that high quality N-MWCNTs in good yields may be obtained at synthesis temperature of 800 ^{o}C, and 26 ^{o}C CH_3CN vaporization temperature [68]. With the *ex situ* method, temperature plays a significant role on the formation of wall defects on the MWCNTs because they tend to decompose at temperatures around 600 ^{o}C while N-MWCNTs decompose at slightly lower temperatures than that in the presence of oxygen. The low decomposition temperature of N-MWCNTs is attributed to the lower bond strength of C-N compared to C-C. Thus is it crucial to ensure the absence of oxygen by conducting the synthesis strictly under inert gas such as N_2 to maintain the wall structure of the MWCNTs. Nonetheless, the pyrolysis of the MWCNTs under N_2 atmosphere has been studied by Motchelaho *et al.* (2011).

It was indicated that the actual decomposition of MWCNTs in inert atmosphere begins at 779 ^{o}C. However, the acid-treated MWCNTs tend to lose the OH groups in a form of H_2O at 60 ^{o}C, and the acid groups (COOH) are lost in a form of CO_2 at 260 ^{o}C [15]. This confirms that increasing temperature introduces defects (e.g. dangling bonds on the tube's edges, pentagonal rings, etc.) on the wall structure of the MWCNTs either through the lattice distortion or through desorption of the functional groups. This may be advantageous in *ex situ* synthesis if the goal is to achieve high content of nitrogen because N incorporation occurs at the edges of the lattice and at the defect sites [24].

2.3.4.1.3 Effect of reaction time

This is the fundamental parameter that concerns every reaction. Shorter reaction times using *in situ* method may result in highly impure N-MWCNTs due to a high amount of unreacted metal catalyst. On the contrary, holding the reaction for longer periods may result in a loss of N

contents in a form of NH_3. Furthermore, the time period of *ex situ* synthesis must be chosen such that the lattice has enough time to distort the lattice, incorporate the N atoms, and further reform or stabilize the N-containing lattice.

2.4 Properties of cellulose and cellulose-N-MWCNTs composites

Cellulose is an abundant polymer that occurs naturally. Unlike carbon nanotubes, cellulose does not require complicated purification and functionalization as it naturally contains OH functional groups. The enormous amount of research on cellulose is motivated by it versatile uses in various industries such as wood and paper, cosmetic and pharmaceutical, as well as fibers and clothes. Ghorani *et al.* suggested that cellulose nanofibers can be a replacement of MWCNTs in the industries on account of their high level of purity, high crystallinity, and ultrafine network [95]. However, cellulose has low surface area, thermal stability, and aspect ratio relative to MWCNTs. Thus, Yun and Kim pointed out that the electronic, mechanical, and thermal properties of MWCNTs are unique and cannot be replaced [108]. Subsequently, studies to conglomerate the fascinating properties of the MWCNTs with those of cellulose polymer have been developed [96]. According to Wei *et al.*, cellulose nanofibers blended with a small amount of CNTs exhibits a remarkable enhancement of elastic modulus and strength [97].

Previous studies have explored the reinforcement of MWCNTs on polymer matrices. Reports have been made that the inclusion of MWCNTs on a polymer matrix can enhance the polymer's electrical conductivity, thermal stability, surface area, and tensile strength. Mantena *et al.* pointed out that the compatibility of cellulose and MWCNTs with regard to their light weight and high aspect ratio enhances the electrical and mechanical properties at low MWCNTs loadings and improves the corrosion resistant and mechanical strength of the MWCNTs-cellulose composite. However, the study of MWCNTs on cellulose polymer in particular has been circumscribed by the insolubility of the cellulose in many solvents. Thus, the use of cellulose derivatives in the fabrication of cellulose-MWCNTs has been explored. Subsequently, the study of cellulose-MWCNTs is increasing in various applications, such as electrical conductivity [94], electro-active paper (EAPap) [13] and gas sensors [14]. There is a great need

of a cost-effective method that can be used to fabricate the cellulose-MWCNTs composite, adjustments of manufacturing processes in order to obtain highly dispersed MWCNTs on the cellulose polymer, and a means to improve the interaction between the MWCNTs and the cellulose polymer. Thus, this study has hypothesized that reinforcing N-MWCNTs on cellulose fibers may result in good dispersion and a strong C-O-C interphase between the N-MWCNTs and cellulose, and may therefore improve the properties of cellulose. This was attributed to the fact that the hydroxyl groups on the MWCNTs surface are the main participants in the anchoring of the cellulose to the MWCNTs. Thus, the oxidation of N-MWCNTs endows them with higher interactive sites compared to pristine MWCNTs.

2.4.1 Synthesis of cellulose fibers and cellulose-N-MWCNTs composites

It has been the researchers' most interest to convert cellulose into nanofibers in order to enhance its surface area, thermal strength, and aspect ratio. Various techniques inclusive of wet spinning [96], viscose process [95], dry-jet wet spinning [98], and electrospinning [99] have been used to synthesize cellulose nanofibers. However, wet spinning processes produce nanocellulose with high modulus and orientation but low elongation [106]. Viscose process produce highly impure nanofibers from side reaction included in the process, hence it requires extra purification steps [107]. On the other hand, electrospinning process is straightforward and it produces pure nanofibers with very large surface area and high aspect ratio through electrostatic forces [107].

Electrospinning has gained intensive attention in the nanofibers technology because it can produce ultrafine polymer fibers exhibiting high surface area-to-volume and length-to-diameter ratios [98]. Notably, the preparation of cellulose nanofibers requires the cellulose to be dissolved in a solvent. The cellulose solution will then be charged by the high voltage source and then accelerated toward a collector of opposite charge. However, cellulose has limited solubility in most solvents due to its numerous intermolecular and intramolecular hydrogen bonding. Hence cellulose derivatives are preferably used in spinning solutions to obtain ultrafine nanofibers [98], [99]. Cellulose acetate (CA) is the commonly used derivative to obtain a homogeneous solution with very low absorption characteristics and high flow rates [100]. In addition to the solute used,

it is crucial to also find the most suitable solvent system for preparing the CA solutions. Wrong choice of solvent may result in electro-spraying, highly dense, bigger fibers, or nanofibers with beads [95]. Thus the effect of solvents on electrospun fibers has been one of the main areas of research recently [95]. Son *et al.* reported that acetone could not be efficiently used as a solvent because it constantly blocks the tip of a needle due to its rapid evaporation [101]. Liu and Hsieh conducted a similar study and reported that acetone could be diluted with dimethyl acetamide (DMac) [acetone/DMac (2:1 v/v)] to obtain pure electrospun fibers with average diameters close to 100 nm [102]. After a similar study, Schueren *et al.* showed that binary solvent system can be used ideally to achieve finer fiber diameter using electrospinning. Nevertheless, this brought a question of optimum ratio of the binary solvent to achieve high productivity and reduction of cross sectional area of the electrospun fibers, and it is still an ongoing research topic. However, solvent selection is not the only factor that affects the quality and quantity of the electrospun fibers. Other parameters which are inclusive of flow rate, power, syringe diameter, concentration of the solution, distance between the collector and the syringe tip, and the collection method also play an important role in the preparation of electrospun fibers.

2.5 TiO_2-based nanocomposites

MWCNTs and cellulose nanofibers make remarkable catalyst supports particularly due to their high surface area and high aspect ratio. TiO_2/MWCNTs, TiO_2/N-MWCNTs, TiO_2/cellulose and MWCNTs-TiO_2-cellulose have been fabricated following various methods such as mechanical mixing, sol gel method, electrospinning methods, and chemical vapor deposition [103]. These nanocomposites have not only been useful in water purification but have also attracted attention in hydrogen evolution, CO_2 photo-reduction, dye sensitized solar cells, and sensors devices [34]. One fundamental requirement in all these applications is a strong Ti-O-C interaction of the TiO_2 and the support-material which may be verified using photoluminescence (PL) technique [8], [104]. The PL confirms the electron flow from Ti to C atoms by the reduction of the emission peak, which corresponds to the reduction of charge recombination [5], [8]. In photocatalytic degradation, strong interaction of MWCNTs with TiO_2 remarkably improves the photocatalytic efficiency of TiO_2 as explained below:

(1) Photocatalytic degradation occurs on the surface of TiO_2, however TiO_2 has poor affinity towards organic pollutants thus catalyst support gives an adsorption synergistic effect to minimize mass transfer limitations.

(2) The supports (i.e. MWCNTs and cellulose) have large electron-storage capacity (one e^- for every 32 carbon atoms), and therefore may accept photon-exited electrons in mixtures or nanocomposites with titania, thus hindering the excitons recombination [105].

(3) Ideally, the large surface area of the support allows a uniform dispersion of TiO_2, preventing its aggregation tendencies which may hamper the light incidence on the active centers of TiO_2

(4) Immobilization on a support is highly essential to prevent light scattering (in tiny particles of TiO_2), and make recovering of the TiO_2 much easier resulting in high turnover number.

(5) TiO_2 is an n-type semiconductor; however, in the presence of MWCNTs the photogenerated electrons may move freely towards the CNT surface, which provides a lower Fermi level, leaving an excess of valence band holes in the TiO_2 to migrate to the surface and react. Under such circumstances, the TiO_2 effectively behaves as a p-type semiconductor, which is highly photoactive.

The mechanisms on the efficiency enhancement of TiO_2 by the carbon-support are illustrated in Figure 2.7 below.

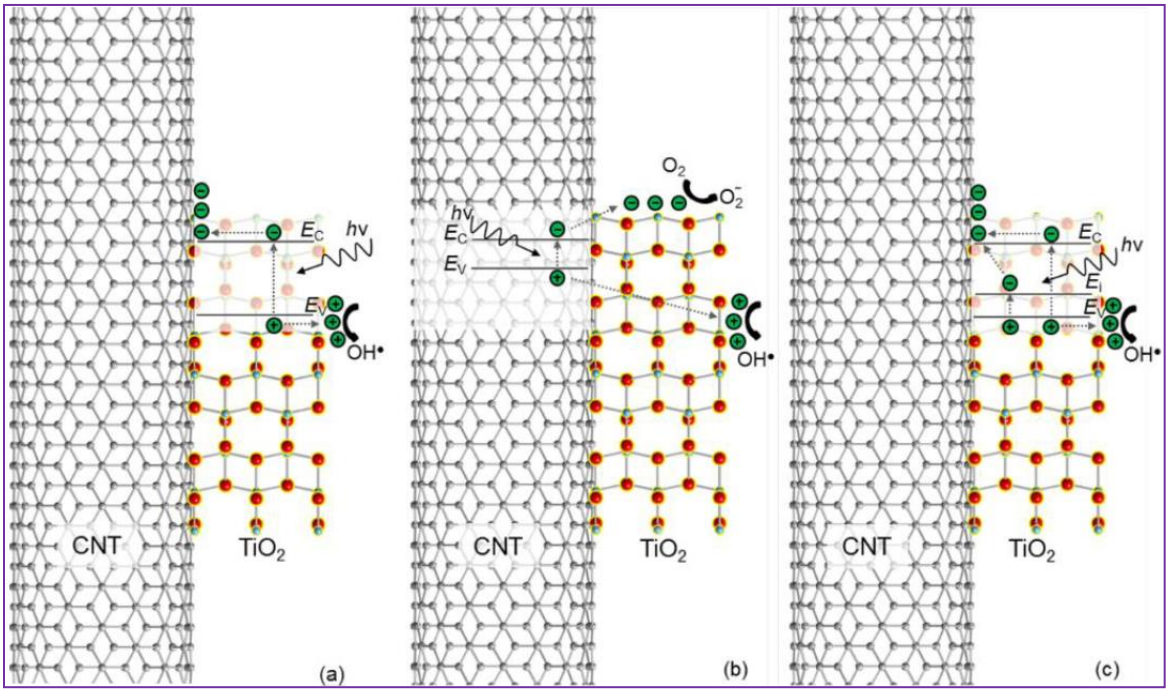

Figure 2.7: Schematic diagram showing the enhancement mechanisms of the photocatalytic efficiency in carbon supported TiO_2 composites. (a) The CNT capture the photogenerated electrons from TiO_2 allowing excessive holes to eventuate on the catalyst surface for redox reactions. (b) The electrons and holes are photogenerated from the CNT functions into TiO_2 for redox reactions. (c) CNT modifies the band gap of TiO2 by introducing new energy states which can transform long wavelength photons to electrons and holes [105], [106].

2.6 Photocatalytic degradation of dyes

Photocatalysis refers to the acceleration of a chemical transformation by the presence of a catalyst and light [107], [108]. This is a promising method because it is more economically and environmentally viable as compared to chemical, physical and biological techniques that have been employed for dye removal [108]–[110]. The physical techniques such as adsorption (activated carbon as an adsorbent), reverse osmosis, ultrafiltration simply transfer the pollutants from one form to another medium causing secondary pollution; this generally requires further treatment of solid-wastes and regeneration of the adsorbent, which adds more cost to the process

[111]–[113]. Biological techniques which include microbiological or enzymatic decomposition and biodegradation are generally cheap, simple and easy to apply to remove organic compounds from the textile wastewater [2], [111]. However, the refractory pollutants present in the textile wastewater cannot easily be degraded by traditional biological process with microorganisms [111].

Furthermore, chemical techniques are expensive and have a disadvantage of the accumulation of the concentrated sludge during disposal [108]. However, the recent developments of chemical treatment of wastewater gave birth to improved methods to completely degrade organic compounds in aqueous media. Among the developed chemical treatments, heterogeneous photocatalysis has emerged as a destructive technology leading to the total mineralization of most of organic pollutants [38]. Heterogeneous photocatalysis is initiated by the illumination of light with greater energy than that of the band gap on the semiconductor (e.g. TiO_2). An electron is promoted from the valence band (VB) to the conduction band (CB) leaving a positive hole behind in the VB as illustrated in Figure 2.8. If charge separation is maintained, the electron and hole may migrate to the catalyst surface where they participate in redox reactions with adsorbed species.

In summary the photodegradation mechanism may be illustrated as equations (2.3) - (2.7):

Absorption of photons by titania ($h\nu \geq Eg = 3.2$ ev): $TiO_2 + h\nu \rightarrow e^-_{cb} + h^+_{vb}$ eq. (2.3)

Formation of superoxide radical anion: $O_2 + e^-_{cb} \rightarrow O_2\bullet^-$ eq. (2.4)

Formation of OH• radicals from OH^-/H_2O: $(H_2O \Leftrightarrow H^+ + OH^-)_{ads} + h^+_{vb} \rightarrow OH\bullet + H\bullet$ eq. (2.5)

The hydroxyl radical (OH•) and superoxide radical anions ($O_2\bullet^-$) are the primary oxidizing species in the photocatalytic oxidation processes. Thus, they initiate the degradation of the organic dyes as summarized in the following equations (2.5)-(2.6). The entire process is illustrated in Figure 2.8.

Oxidation of the organic dye pollutants (D): $D + OH\bullet \rightarrow D\bullet' + H_2O$ eq. (2.6)

$D + h^+ \rightarrow D\bullet^+ \rightarrow$ degradation products eq. (2.7)

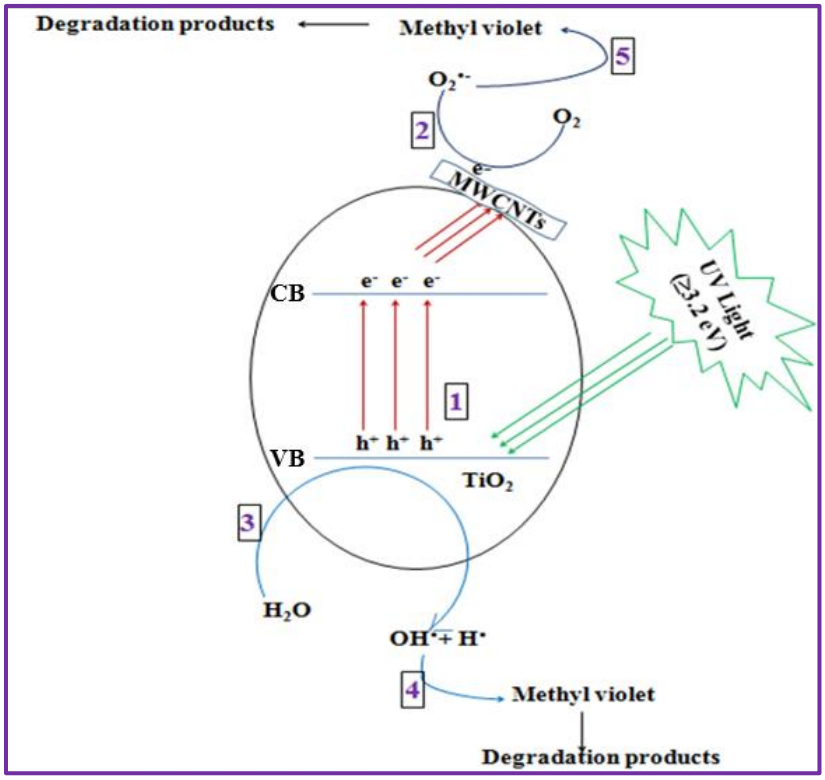

Figure 2.8: Schematic diagram demonstrating the photocatalytic degradation process

2.7 Evaluation of degradation products

Because hydroxyl radicals react non-selectively, the formation of by-products may be unavoidable in this process [39]. Previous studies have used various techniques such as high performance liquid chromatography (HPLC), gas chromatography–mass spectrometry (GC–MS), liquid chromatography–mass spectrometry (LC–MS), 1H NMR, diffuse reflectance FT-IR, etc to investigate the by-products in order to maximize the overall process efficiency [114], [115]. The initial steps of methyl violet decomposition are presented in Figure 2.9 and also summarized by equations (2.8) – (2.15):

Ionization of H_2O: $H_2O \rightarrow H\bullet + OH\bullet$ eq. (2.8)

Demethylation from $-N(CH_3)_2$: $C_{24}H_{28}N_3Cl + 5H\bullet \rightarrow 5CH_3\bullet + C_{19}H_{18}N_3Cl$ eq. (2.9)

Formation of methanol: $CH_3\bullet + OH\bullet \rightarrow CH_3OH$ eq. (2.10)

Formation of formic acid: (i) $CH_3OH+OH\bullet \rightarrow H_2O+CH_2OH\bullet$ eq. (2.11)

(ii) $CH_2OH\bullet \rightarrow CH_2O+H\bullet$ eq. (2.12)

(iii) $CH_2O+OH\bullet \rightarrow CHO\bullet + H_2O$ eq. (2.13)

(iv) $H–CO^{\bullet}+OH^{\bullet} \rightarrow CH_2O_2$ eq. (2.14)

Decarboxylation of formic acid: $CH_2O_2 + h^+ \rightarrow CO_2 + H^{\bullet} + H^+$ eq. (2.15)

Furthermore, the nitrogen atoms in the newly formed amino-groups are desorbed in a form of NH_4^+ ions by successive attacks by $H^{\bullet}$ atoms. The decomposition of the remaining benzyl groups are illustrated by Figure 2.10. The degradation may follow the photo-kolbe reaction by the generation of ammonium ions. The mass fragments reported by Bhattacharjee *et al.* are shown below:

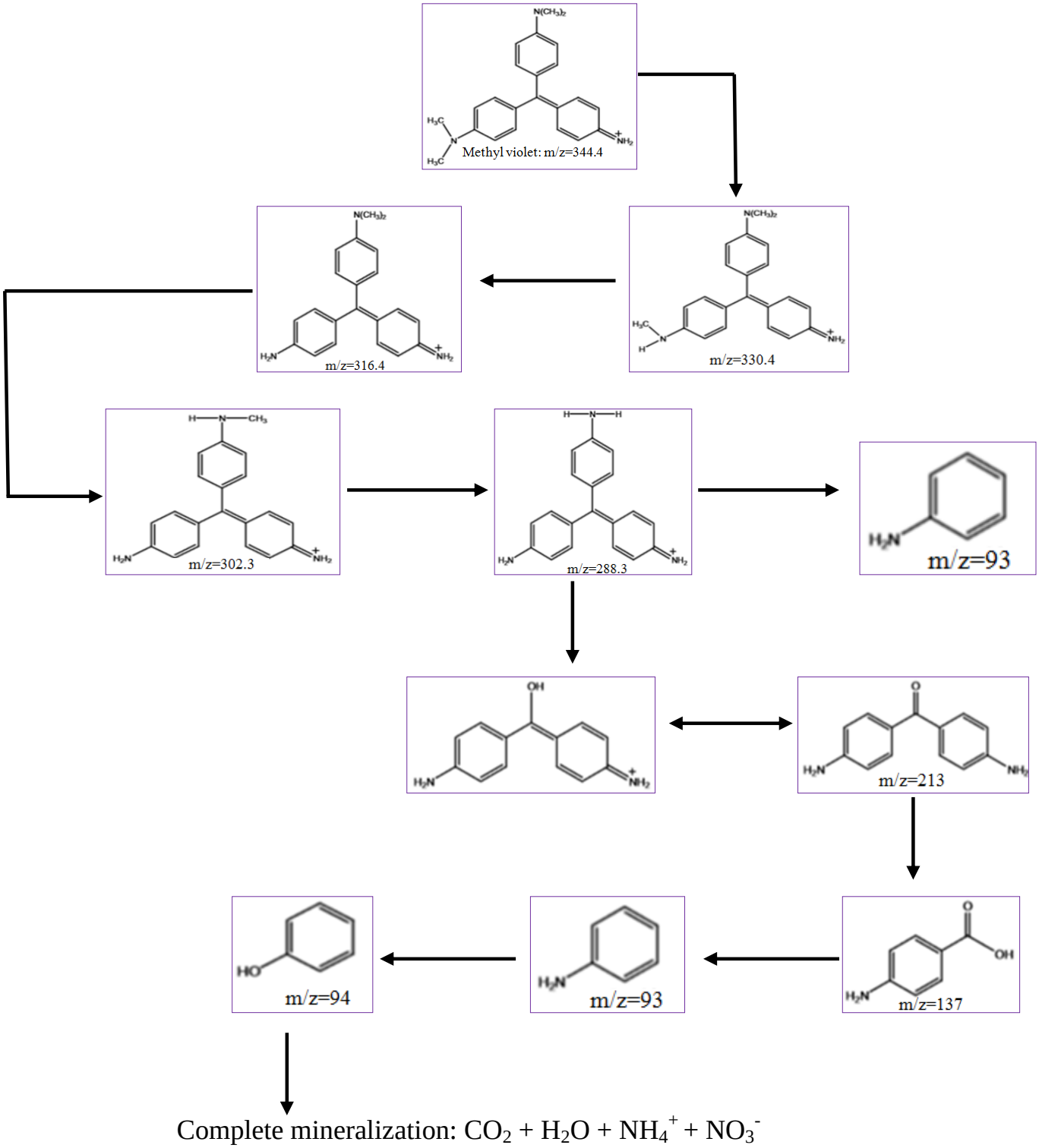

Figure 2.9: Schematic diagram illustrating the mineralization of methyl violet in water [37].

2.8 Method application of TiO_2-based catalysts

It is highly essential to report the optimal parameters and conditions required for economic, environmental and health safety purposes. Parameters such as catalyst dosage, pH value, time, temperature, initial dye concentrations and the interaction between TiO_2 and the support material need to be optimized as they strongly affect the photocatalytic rate of TiO_2 catalyst. Several studies concerned, in particular, the photocatalytic degradation of organic dyes, either single or multiple dyes and showed very encouraging results. For instance, Charkrabarti and Dutta studied the effects of catalyst loading, initial dye concentration, airflow rate, pH, and UV radiation intensity on the rate of organic dye degradation. They reported that the degradation rate tends to increase with increase in catalyst loading up to a limiting value, decrease in initial concentration, increase in airflow rate, pH, and UV light intensity [117].

In addition, Lei *et al.* reported that immobilizing TiO_2 on polymers such as PVA dramatically improves its photocatalytic activity and turnover number, where the PVA/TiO_2 hybrid showed a potential for high photoactivity even after 25 cycles of photodegradation of MO in aqueous solution [118]. In addition, Djaoued and co-workers pointed out that the photoactivity of TiO_2/C composites strongly depends on the optical properties which are influenced by the phase, crystallite size, and the porosity of the coatings [119]. Thus, multitudes of works has been done on various support materials of TiO_2 to obtain a more crystalline, small crystallite sizes, and a thin layer of TiO_2 coating as means of achieving enhanced photocatalytic activity of the catalyst.

It is also important to keep in mind that real wastewater that is aimed to be purified contains other species such as organic, inorganic, and metallic ions which may affect the entire process. For instance, Sudarjanto *et al.* studied this method in real wastewater where they monitored the end-products using biological oxygen demand [116]. They observed that total mineralization is obtained at longer irradiation time in real wastewaters than in dye-contaminated deionized water. This was attributed to the presence of additional species in real wastewater which increase the competition to the reactive sites of the catalyst. Lachheb *et al.* studied the activity of TiO_2 for various organic dyes [3]. They observed that photodegradation favors dyes with smaller

molecular weight, less substituents, and positively charged surface [3]. This observation was in correspondence with Charkrabarti et al. who reported that Methylene Blue degraded faster as compared to Eosin Y under the same photocatalytic conditions.

2.8 References

[1] K. M. Reza, A. S. W. Kurny, and F. Gulshan, "Parameters affecting the photocatalytic degradation of dyes using TiO_2: a review," *Applied water science*, pp. 1–10, 2015.

[2] A. Ajmal, I. Majeed, R. N. Malik, H. Idriss, and M. A. Nadeem, "Principles and mechanisms of photocatalytic dye degradation on TiO_2 based photocatalysts: a comparative overview," *RSC Advances*, vol. 4, no. 70, pp. 37003–37026, 2014.

[3] H. Lachheb, E. Puzenat, A. Houas, M. Ksibi, E. Elaloui, C. Guillard, "Photocatalytic degradation of various types of dyes (Alizarin S, Crocein Orange G, Methyl Red, Congo Red, Methylene Blue) in water by UV-irradiated titania," *Applied Catalysis B: Environmental*, vol. 39, no. 1, pp. 75–90, 2002.

[4] N. Jafari, R. Kasra-Kermanshahi, M. R. Soudi, A. H. Mahvi, and S. Gharavi, "Degradation of a textile reactive azo dye by a combined biological-photocatalytic process: Candida tropicalis Jks2 -TiO_2/UV," *Iranian Journal of Environmental Health Science & Engineering*, vol. 9, no. 1, p. 33, 2012.

[5] N. O. Ramoraswi and P. G. Ndungu, "Photocatalytic properties of TiO_2 supported on MWCNTs, SBA-15 and silica-coated MWCNTs nanocomposites," *Nanoscale research letters*, vol. 10, no. 1, p. 427, 2015.

[6] M. J. Uddin, Cesano, F. Bonino, S. Bordiga, G. Spoto, D. Scarano, and A. Zecchina, "Photoactive TiO_2 films on cellulose fibres : synthesis and characterization," *Catalysis*, vol. 189, pp. 286–294, 2007.

[7] K. Guesh, Á. Mayoral, C. Márquez-Álvarez, Y. Chebude, and I. Díaz, "Enhanced photocatalytic activity of TiO_2 supported on zeolites tested in real wastewaters from the textile industry of Ethiopia," *Microporous and mesoporous materials*, vol. 225, pp. 88–97, 2016.

[8] Y. Yao, G. Li, S. Ciston, R. M. Lueptow, and K. A. Gray, "Photoreactive TiO_2/Carbon nanotube composites: Synthesis and Reactivity," *Environmental science & technology*, vol. 42, no. 13, pp. 4952–4957, 2008.

[9] W. A. Daoud, J. H. Xin, and Y. Zhang, "Surface functionalization of cellulose fibers with titanium dioxide nanoparticles and their combined bactericidal activities," vol. 599, pp. 69–75, 2005.

[10] C. Y. Yan, P. G. Ren, Z. P. Zhang, H. Wang, and Z. M. Li, "*in situ* preparation and characterization of highly oriented graphene oxide/cellulose-poly(butylene succinate) ternary composite films," *Polymer material science*, vol. 22, no. 2, pp. 1243–1251, 2015.

[11] T. S. Anirudhan, S. R. Rejeena, "Photocatalytic degradation of eosin yellow using Poly (pyrrole-co-aniline)-coated TiO2/nanocellulose composite under solar light irradiation," Journal of Materials, vol. 2015, pp. 512-876, 2015.

[12] Z. Pang, X. Sun, X. Wu, Y. Nie, Z. Liu, and L. Yue, "Fabrication and application of carbon nanotubes/cellulose composite paper," *Vacuum*, vol. 122, pp. 135–142, 2015.

[13] S. Yun and J. Kim, "Characteristics and performance of functionalized MWNT blended cellulose electro-active paper actuator," *Synthetic Metals*, vol. 158, no. 13, pp. 521–526, 2008.

[14] S. Mun, Y. Chen, and J. Kim, "Cellulose-titanium dioxide-multiwalled carbon nanotube hybrid nanocomposite and its ammonia gas sensing properties at room temperature," *Sensors and Actuators, B: Chemical*, vol. 171–172, pp. 1186–1191, 2012.

[15] M. A. M. Motchelaho, H. Xiong, M. Moyo, L. L. Jewell, and N. J. Coville, "Effect of acid treatment on the surface of multiwalled carbon nanotubes prepared from Fe-Co supported on $CaCO_3$: Correlation with Fischer-Tropsch catalyst activity," *Journal of Molecular Catalysis A: Chemical*, vol. 335, no. 1–2, pp. 189–198, 2011.

[16] N. Phao, E. N. Nxumalo, B. B. Mamba, and S. D. Mhlanga, "A nitrogen-doped carbon nanotube enhanced polyethersulfone membrane system for water treatment," *Physics and chemistry of the Earth*, vol. 66, pp. 148–156, 2013.

[17] M. S. Dresselhaus, G. Dresselhaus, R. Saito, and A. Jorio, "Raman spectroscopy of carbon nanotubes," *Physics reports*, vol. 409, no. 2, p. 47, 2005.

[18] S. D. Mhlanga, M. J. Witcomb, R. Carter, and N. J. Coville, "The effect of synthesis

parameters on the catalytic synthesis of multiwalled carbon nanotubes using Fe-Co/$CaCO_3$ catalysts," *S. Afr. J. Chem.*, vol. 62, pp. 67–76, 2009.

[19] C. Shan, Zhao, X. L. Lu, D. J. O'Brien, Y. Li, and Z. Cao, A. Elias, R. Cruz-Silva, M. Terrones, B. Wei, J. Suhr, "Three-dimensional nitrogen-doped multiwall carbon nanotube sponges with tunable properties," Nano Letters, vol. 13, no. 11, pp. 5514–5520, 2013.

[20] O. Y. Podyacheva and Z. R. Ismagilov, "Nitrogen-doped carbon nanomaterials: To the mechanism of growth, electrical conductivity and application in catalysis," *Catalysis Today*, vol. 249, pp. 12–22, 2015.

[21] H. B. Wang, T. Maiyalagan, and X. Wang, "Review on recent progress in nitrogen-doped graphene: synthesis, characterization, and its ootential applications," *Acs Catalysis*, vol. 2, no. 5, pp. 781–794, 2012.

[22] C. Tang, Y. Bando, D. Golberg, and F. Xu, "Structure and nitrogen incorporation of carbon nanotubes synthesized by catalytic pyrolysis of dimethylformamide," *Carbon*, vol. 42, no. 12–13, pp. 2625–2633, 2004.

[23] H. Cheng, C. Lu, J. Liu, Y. Jingjing, , X. Yongke, X. Han, H. Jin, Y. Huiming, Y. Wang, C. Wu, "Synchrotron radiation X-ray powder diffraction techniques applied in hydrogen storage materials - A review," *Progress in Natural Science: Materials International*, vol. 27, no. 1, pp. 66–73, 2017.

[24] B. J. Matsoso, K. Ranganathan, B. K. Mutuma, T. Lerotholi, G. Jones, and N. J. Coville, "Time-dependent evolution of the nitrogen configurations in N-doped graphene films," *RSC Adv.*, vol. 6, no. 108, pp. 106914–106920, 2016.

[25] A. Snyder, Z. Bo, R. Moon, J. Rochet, and L. Stanciu, "Reusable photocatalytic titanium dioxide – cellulose nanofiber films," *Journal of colloid and interface science*, vol. 399, pp. 92–98, 2013.

[26] P. Ayala, R. Arenal, M. Rümmeli, A. Rubio, and T. Pichler, "The doping of carbon nanotubes with nitrogen and their potential applications," *Carbon*, vol. 48, no. 3, pp. 575–586, 2010.

[27] R. J. Tayade, P. K. Surolia, R. G. Kulkarni, and R. V. Jasra, "Photocatalytic degradation of dyes and organic contaminants in water using nanocrystalline anatase and rutile TiO_2," *Science and technology of advanced materials*, vol. 8, no. 6, pp. 455–462, 2007.

[28] T. Luttrell, S. Halpegamage, J. Tao, A. Kramer, E. Sutter, and M. Batzill, "Why is anatase a better photocatalyst than rutile-Model studies on epitaxial TiO_2 films.," *Scientific reports*, vol. 4, p. 4043, 2014.

[29] H. Wang, H. Li, J. Wang, W. Junshu, D. Li, M. Liu, P. Su, "Nitrogen-doped TiO_2 nanoparticles better TiO_2 nanotube array photo-anodes for dye sensitized solar cells," *Electrochimica Acta*, vol. 137, pp. 744–750, 2014.

[30] T. Luttrell, S. Halpegamage, J. Tao, A. Kramer, E. Sutter, and M. Batzill, "Why is anatase a better photocatalyst than rutile-Model studies on epitaxial TiO_2 films.," *Scientific reports*, vol. 4, p. 4043, 2014.

[31] C. H. Ao and S. C. Lee, "Indoor air purification by photocatalyst TiO_2 immobilized on an activated carbon filter installed in an air cleaner," *Scientific and purification tecnology*, vol. 60, pp. 103–109, 2005.

[32] F. Maria, D. Chequer, G. Augusto, R. Oliveira, R. E. Raquel, "World's largest Science, technology & medicine open Access book publisher textile dyes : dyeing process and environmental impact," *h waste 31/31*, vol.10, pp. 778-954, 2010.

[33] S. Ortelli, M. Blosi, S. Albonetti, A. Vaccari, M. Dondi, and A. L. Costa, "Chemistry TiO_2 based nano-photocatalysis immobilized on cellulose substrates," *Journal of photochemistry and photobiology: Chemistry*, vol. 276, pp. 58–64, 2014.

[34] J. Jiménez Reinosa, P. Leret, C. M. Álvarez-Docio, A. Del Campo, and J. F. Fernández, "Enhancement of UV absorption behavior in ZnO-TiO_2 composites," *Boletin de la Sociedad Espanola de Ceramica y Vidrio*, vol. 55, no. 2, pp. 55–62, 2016.

[35] B. E. Solsona, P. Landon, A. F Carley, A. Herzing, C. J Kiely, G. J. Hutchings, "Direct synthesis of hydrogen peroxide from H_2 and O_2 Using Al_2O_3 supported Au−Pd Catalysts," *Chemistry of materials*, vol. 18, no. 11, pp. 2689–2695, 2006.

[36] L. T. S. Thao, T. T. T. Dang, W. Khanitchaidecha, D. Channei, and A. Nakaruk, "Photocatalytic degradation of organic dye under UV-A irradiation using TiO_2-vetiver multifunctional nano particles," *Materials*, vol. 10, no. 2, pp. 1–12, 2017.

[37] S. Bagheri, N. Muhd Julkapli, and S. Hamid, "Titanium dioxide as a catalyst support in heterogeneous catalysis," *ScientificWorld Journal*, vol. 2014, p. 727-496, 2014.

[38] G. Li, X. S. Zhao, and M. B. Ray, "Advanced oxidation of orange II using TiO_2 supported on porous adsorbents: The role of pH, H_2O_2 and O_3," *Separation and Purification Technology*, vol. 55, no. 1, pp. 91–97, 2007.

[39] K. Saeed, I. Khan, T. Gul, and M. Sadiq, "Efficient photodegradation of methyl violet dye using TiO_2/Pt and TiO_2/Pd photocatalysts," *Applied water science*, vol. 1007, no. 18, pp. 3352–3447, 2017.

[40] X. Gao, J. Zhang, N. Chen, Q. Ma, S. Fan, and T. Zhao, "Effects of zinc on Fe-based catalysts during the synthesis of light olefins from the Fischer-Tropsch process," vol. 37, no. 4, pp. 510–516, 2016.

[41] B. Gao, G. Z. Chen, and G. Li Puma, "Carbon nanotubes/titanium dioxide (CNTs/TiO_2) nanocomposites prepared by conventional and novel surfactant wrapping sol-gel methods exhibiting enhanced photocatalytic activity," *Applied catalysis B: Environmental*, vol. 89, no. 3–4, pp. 503–509, 2009.

[42] T. D. Pham and B. K. Lee, "Feasibility of silver doped TiO_2/glass fiber photocatalyst under visible irradiation as an indoor air germicide," *International Journal of Environmental research and public Health*, vol. 11, no. 3, pp. 3271–3288, 2014.

[43] T. S. Wu, K. X. Wang, G. D. Li, S. Y. Sun, J. Sun, and J. S. Chen, "Montmorillonite-Supported Ag/TiO_2 nanoparticles: An efficient visible-Light bacteria photodegradation material," *ACS Applied materials and interfaces*, vol. 2, no. 2, pp. 544–550, 2010.

[44] T. A. Egerton, "UV-absorption-the primary process in photocatalysis and some practical consequences," *Molecules*, vol. 19, no. 11, pp. 18192–18214, 2014.

[45] I. Chauhan and P. Mohanty, "RSC Advances immobilization of titania nanoparticles on the surface of cellulose fibres by a facile single step hydrothermal method" *RSC Advances*, vol. 4, pp. 57885–57890, 2014.

[46] V. O. Nyamori, S. D. Mhlanga, and N. J. Coville, "The use of organometallic transition metal complexes in the synthesis of shaped carbon nanomaterials," *Journal of organometallic Chemistry*, vol. 693, no. 13, pp. 2205–2222, 2008.

[47] J. Bhattacharjee, "Activation of graphenic carbon due to substitutional doping by nitrogen: Mechanistic understanding from first principles," *Journal of Physical chemistry Letters*, vol. 6, no. 9, pp. 1653–1660, 2015.

[48] M. Scarselli, P. Castrucci, and M. De Crescenzi, "Electronic and optoelectronic nano-devices based on carbon nanotubes," *Journal of Physics: Condensed matter*, vol. 24, no. 31, p. 313202, 2012.

[49] T. J. Sisto, L. N. Zakharov, B. M. White, and R. Jasti, "Towards pi-extended cycloparaphenylenes as seeds for CNT growth: investigating strain relieving ring-openings and rearrangements," *Chemical. Science*, vol. 7, p. 1, 2016.

[50] S. Darbari, Y. Abdi, F. Haghighi, S. Mohajerzadeh, and N. Haghighi, "Investigating the antifungal activity of TiO_2 nanoparticles deposited on branched carbon nanotube arrays," *Journal of Physics D: Applied physics*, vol. 44, no. 24, p. 245401, 2011.

[51] Y. Ohsumi, "World's largest Science, technology & medicine open access book publisher," *Mechatronic systems in engineering*, vol.33, no. 7, pp. 135–152, 2017.

[52] M. Kumar, "Carbon Nanotube Synthesis and Growth Mechanism,"Journal of *Material Science*, vol. 2, no. 1, pp. 147–170, 1999.

[53] C. Lamprecht, A. Ebner, F. Kienberger, and P. Hinterdorfer, "Exploring carbon nanotubes and their interaction with cells using Atomic Force Microscopy," *Biomedical science*, vol. 3, no. 5, pp. 1–16, 2011.

[54] D. Christofilos, J. Arvanitidis, X. Zhao, Y. Ando, T. Takenobu, Y. Iwasa, H. Kataura, S. Ves, and G. Kourouklis,"High pressure Raman studies of carbon nanotube materials," *Journal of Physics: Conference Series*, vol. 121, no. 16, pp. 162–1003, 2008.

[55] P. Lu, and H. You-Lo Hsieh, "Multiwalled carbon nanotube (MWCNT) reinforced cellulose fibers by electrospinning," *fiber and polymer science,* vol. 2, no. 8, pp. 2413-2420, 2010.

[56] H. Jantoljak, J.-P. Salvetat, L. Forr, and C. Thomsen, "Low-energy Raman-active phonons of multiwalled carbon nanotubes," *Applied physics A: Materials science & processing*, vol. 67, pp. 113–116, 1998.

[57] J. H. Lehman, M. Terrones, E. Mansfield, K. E. Hurst, and V. Meunier, "Evaluating the characteristics of multiwall carbon nanotubes," *Carbon*, vol. 49, no. 8, pp. 2581–2602, 2011.

[58] M. G. Donato, G. Messina, S. Santangelo, S. Galvagno, C. Milone, and A. Pistone, "Aid of Raman spectroscopy in diagnostics of MWCNTs synthesised by Fe-catalysed CVD," *Journal of Physics: Conference series*, vol. 61, no. 1, pp. 931–935, 2007.

[59] M. A. Mamo, A. O. Sustaita, Z. N. Tetana, N. J. Coville, and I. A. Hümmelgen, "Undoped, nitrogen-doped and boron-doped multiwalled carbon nanotube/poly(vinyl alcohol) composite as active layer in simple hydrostatic pressure sensors," *Journal of materials science: Materials in electronics*, vol. 24, no. 10, pp. 3995–4000, 2013.

[60] A. M. Kamil, F. H. Hussein, A. F. Halbus, and D. W. Bahnemann, "Applications of MWCNTs /TiO_2 composite," vol. 2014, 2014.

[61] N. El-Badawi, A. R. Ramadan, A. M. K. Esawi, and M. El-Morsi, "Novel carbon nanotube-cellulose acetate nanocomposite membranes for water filtration applications," *Desalination*, vol. 344, no. 19, pp. 79–85, 2014.

[62] R. Jin, X. Zhou, D. Mandrus, I. N Ivanov, G. Eres, J. Y. Howe, "The effect of annealing on the electrical and thermal transport properties of macroscopic bundles of long multi-wall carbon nanotubes," Physica B: Condensed matter, vol. 388, no. 1–2, pp. 326–330,

2007.

[63] Y. T. Lee, N. S. Kim, Bae, J. Park, S. C. Yu, and S. H. Ryu, "Growth of vertically aligned nitrogen-doped carbon nanotubes: Control of the nitrogen content over the temperature range 900-1100 degrees C," *Journal of Physical chemistry B*, vol. 107, no. 47, pp. 12958–12963, 2003.

[64] K. V. Wong and B. Bachelier, "Carbon Nanotubes used for renewable energy applications and environmental protection/remediation: A Review," *Journal of energy resources technology*, vol. 136, no. 2, p. 21601, 2013.

[65] V. Agarwal, P. J. Dauenhauer, G. W. Huber, and S. M. Auerbach, "Ab initio dynamics of cellulose pyrolysis: Nascent decomposition pathways at 327 and 600 ^{o}C," *Journal of the american chemical society*, vol. 134, no. 36, pp. 14958–14972, 2012.

[66] A. T. Kuvarega, R. W. M. Krause, and B. B. Mamba, "Multiwalled carbon nanotubes decorated with nitrogen , palladium co-doped TiO_2 (MWCNTs/N, Pd co-doped TiO_2) for visible light photocatalytic degradation of eosin yellow in water," vol. 2, no. 17, pp. 35-89, 2012.

[67] Z. N. Tetana, "Boron and nitrogen doped carbons for photochemical degradation reactions," *Thesis*, pp. 1–235, 2013.

[68] K. C. Mondal, A. M. Strydomc, Z. Tetana, S. D. Mhlanga, M. J. Witcombb, J. Havel, R. M. Erasmus, N. J. Coville, "Boron-doped carbon microspheres," *Materials chemistry and physics*, vol. 114, no. 2–3, pp. 973–977, 2009.

[69] K. Koziol, B. O. Boskovic, and N. Yahya, "Synthesis of carbon nanostructures by CVD method," vol. 20, no. 1, pp. 4222–5876, 2010.

[70] S. D. Mhlanga, E. N. Nxumalo, N. J. Coville, and V. V. Srinivasu, "Nitrogen doping of CVD multiwalled carbon nanotubes: Observation of a large g-factor shift," *Materials chemistry and physics*, vol. 130, no. 3, pp. 1182–1186, 2011.

[71] D. V. Cuong, L. Truong-Phuoc, T. Tran-Thanh, J. M. Nhut, L. Nguyen-Dinh, I. Janowska,

D. Begin, and C. Pham-Huu, "Nitrogen-doped carbon nanotubes decorated silicon carbide as a metal-free catalyst for partial oxidation of H2S," Applied catalysis A: General, vol. 482, 2014.

[72] W. K. Maboya, N. J. Coville, and S. D. Mhlanga, "The Synthesis of carbon nanomaterials using chlorinated hydrocarbons over a Fe-Co/$CaCO_3$ catalyst," vol. 69, no. 3, pp. 15–26, 2016.

[73] M. A. M. Motchelaho, "Iron and cobalt catalysts supported on carbon nanotubes for use in the Fischer-Tropsch synthesis," *Thesis*, pp. 1-289, 2011.

[74] E. N. Nxumalo, V. O. Nyamori, and N. J. Coville, "CVD synthesis of nitrogen doped carbon nanotubes using ferrocene/aniline mixtures," *Journal of organometallic chemistry*, vol. 693, no. 17, pp. 2942–2948, 2008.

[76] T. N. Phaahlamohlaka, "Synthesis of carbon nanofibers and their subsequent use as catalyst supports for Fischer- Tropsch synthesis," *Thesis*, pp. 1–293, 2013.

[77] S. D. Mhlanga and N. J. Coville, "Iron-cobalt catalysts synthesized by a reverse micelle impregnation method for controlled growth of carbon nanotubes," *Diamond and related materials*, vol. 17, no. 7–10, pp. 1489–1493, 2008.

[78] S. Bhoware, M. S. Maubane, T. Phaahlamohlaka, A. Shaikjee, and N. J. Coville, "Cu grown carbon nanofibers - Variation of their chemical and physical properties," *Chemical physics Letters*, vol. 577, pp. 71–75, 2013.

[79] M. Kumar and Y. Ando, "Chemical vapor deposition of carbon nanotubes: a review on growth mechanism and mass production.," *Journal of nanoscience and nanotechnology*, vol. 10, no. 6, pp. 3739–3758, 2010.

[80] L. Mabena, S. Sinha Ray, S. Mhlanga, and N. Coville, "Nitrogen-doped carbon nanotubes as a metal catalyst support," *Applied nanoscience*, vol. 1, no. 2, pp. 67–77, 2011.

[81] F. Avile, "Evaluation of mild acid oxidation treatments for MWCNTs functionalization," vol. 7, pp. 5–10, 2009.

[82] K. Mphahlele, M. S. Onyango, and S. D. Mhlanga, "Efficient preparation of greener N-

doped carbon nanotube composites for water treatment by the microwave polyol method," *Environmental chemistry letters*, vol. 11, no. 4, pp. 353–358, 2013.

[83] A. N. Suboch, S. V. Cherepanova, L. S. Kibis, D. A. Svintsitskiy, O. A. Stonkus, A. I. Boronin, V. V. Chesnokov, A. I. Romanenko, Z. R. Ismagilov, and O. Y. Podyacheva, "Observation of the superstructural diffraction peak in the nitrogen doped carbon nanotubes: simulation of the structure," *Fullerenes, nanotubes and carbon nanostructures*, vol. 24, no. 8, pp. 00–00, 2016.

[84] Z. N. Tetana, S. D. Mhlanga, G. Bepete, R. W. M. Krause, and N. J. Coville, "The synthesis of nitrogen-doped multiwalled carbon nanotubes using an Fe-Co/$CaCO_3$ catalyst," *South african journal of chemistry*, vol. 65, pp. 39–49, 2012.

[85] N. Chiwaye, L. L. Jewell, D. G. Billing, D. Naidoo, M. Ncube, and N. J. Coville, "*In situ* powder XRD and Mössbauer study of Fe-Co supported on $CaCO_3$," *Materials research bulletin*, vol. 56, no. 9, pp. 98–106, 2014.

[86] L. Hlekelele, P. Tripathi, P. J. Franklyn, and S. H. Durbach, "Morphological and crystallinity differences in nitrogen-doped carbon nanotubes grown by Chemical Vapour decomposition of melamine over Coal Fly Ash," *RSC Adv.*, vol. 6, pp. 76773–76779, 2016.

[87] X. Li, K. Lian, L. Liu, Y. Wu, Q. Qiu, J. Jiang, M. Deng, and Y. Luo, "Unraveling the formation mechanism of graphitic nitrogen-doping in thermally treated graphene with ammonia," *Scientific reports*, vol. 6, no.1, pp. 23–495, 2016.

[88] S. D. Mhlanga, G. Bepete, R. W. M. Krause, and N. J. Coville, "The Synthesis of Nitrogen-doped multiwalled carbon nanotubes using an Fe-Co/$CaCO_3$ catalyst," vol. 65, no. 2, pp. 39–49, 2012.

[89] L. Wang, L. Shen, Y. Li, L. Zhu, J. Shen, and L. Wang, "Enhancement of photocatalytic activity on TiO_2-nitrogen-doped carbon nanotubes nanocomposites enhancement of photocatalytic activity on TiO_2-nitrogen-doped carbon nanotubes nanocomposites," *International journal of photoenergy*, vol. 2013, no. July, pp. 1–7, 2013.

[90] Y. Xiong, Z. Li, Q. Guo, and Y. Xie, "Synthesis of multiwalled and bamboo-like well-

crystalline CNx," *Society*, vol. 44, no. 19, pp. 6506–6508, 2005.

[91] M. Reyes-Reyes, N. Grobert, R. Kamalakaran, T. Seeger, D. Golberg, M. Ruhle, Y. Bando, H. Terrones, and M. Terrones, "Efficient encapsulation of gaseous nitrogen inside carbon nanotubes with bamboo-like structure using aerosol thermolysis," *Chemical physics letters*, vol. 396, no. 3, pp. 167–173, 2004.

[92] H. Xiong, M. Moyo, M. A. Motchelaho, Z. N. Tetana, S. M. A. Dubea, L. L. Jewell, and N. J. Coville "Fischer-Tropsch synthesis: Iron catalysts supported on N-doped carbon spheres prepared by chemical vapor deposition and hydrothermal approaches," *Journal of catalysis*, vol. 311, pp. 80–87, 2014.

[93] D. C. Higgins, D. Meza, and Z. Chen, "Nitrogen-doped carbon nanotubes as platinum catalyst supports for oxygen reduction reaction in proton exchange membrane fuel cells," *Journal of physical chemistry C*, vol. 114, no. 50, pp. 21982–21988, 2010.

[94] S. H. Yoon, H. Jin, M. Kook, and Y. R. Pyun, "Electrically conductive bacterial cellulose by incorporation of carbon nanotubes," vol. 10, no. 32, pp. 1280–1284, 2006.

[95] B. Ghorani, S. J. Russell, and P. Goswami, "Controlled morphology and mechanical characterisation of electrospun cellulose acetate fibre webs," *International journal of polymer science*, vol. 25, no. 6, pp. 1–12, 2013.

[96] S. Yun and J. Kim, "Multi-walled carbon nanotubes-cellulose paper for a chemical vapor sensor," *Sensors and actuators, B: chemical*, vol. 150, no. 1, pp. 308–313, 2010.

[97] C. Wei, "Adhesion and reinforcement in carbon nanotube polymer composite," *Applied physics*, vol. 88, no. 1, pp. 1–4, 2006.

[98] K. Ohkawa, "Nanofibers of cellulose and its derivatives fabricated using direct electrospinning," *Molecules*, vol. 20, no. 5, pp. 9139–9154, 2015.

[99] M. W. Frey and M. W. Frey, "Electrospinning cellulose and cellulose derivatives," *Polymer Reviews*, vol. 3724, no. 23, pp. 378-391, 2016.

[100] L. N. Nthunya, L. N. Nthunya, M. L. Masheane, S. P. Malinga, E. N. Nxumalo, T. G. Barnard, M. Kao, Z. N. Tetana, and S. D. Mhlanga "Greener approach to prepare

electrospun antibacterial β-Cyclodextrin/cellulose acetate nanofibers for removal of bacteria from water," *ACS sustainable chemistry and engineering*, vol. 5, no. 1, pp. 153–160, 2017.

[101] H. Fan, G. Li, F. Yang, L. Yang, and S. Zhang, "Photodegradation of cellulose under UV light catalysed by TiO_2," no. January, pp. 1107–1112, 2011.

[102] P.-Y. Du, H. Li, X. Fu, W. Gu, and X. Liu, "A 1D anionic lanthanide coordination polymer as an adsorbent material for the selective uptake of cationic dyes from aqueous solutions," *RSC Dalton Transaction home*, vol. 44, no. 30, pp. 13752–13759, 2015.

[103] C. Papo, Z. N. Tetana, P. Franklyn, and S. D Mhlanga, "Synthesis and study of carbon/TiO_2 and carbon/TiO_2 core–shell micro-/nanospheres with increased density," *Journal of materials research*, vol. 28, no. 3, pp. 440–448, 2012.

[104] R. Su, N. Dimitratos, J. Liu, E. Carter, S. Althahban, X. Wang, Y. Shen, S. Wendt, X. Wen, J. W. Niemantsverdriet, B. Iversen, C. J. Kiely, G. J. Hutchings, F. Besenbacher, "Mechanistic insight into the interaction between a Titanium Dioxide photocatalyst and Pd co-catalyst for improved photocatalytic performance," *ACS catalysis*, vol. 6, no. 7, pp. 4239–4247, 2016.

[105] H. Dong, G. Zeng, L. Tang, C. Fan, C.Zhang, X. He, and Y. He "An overview on limitations of TiO_2-based particles for photocatalytic degradation of organic pollutants and the corresponding countermeasures," *Water research*, vol. 79, pp. 128–146, 2015.

[106] K. Woan, G. Pyrgiotakis, and W. Sigmund, "Photocatalytic carbon-nanotube-TiO_2 composites," *Advanced materials*, pp. 2233–2239, 2009.

[107] A. Ibhadon and P. Fitzpatrick, "Heterogeneous Photocatalysis: Recent advances and applications," *Catalysts*, vol. 3, no. 1, pp. 189–218, 2013.

[108] J. Schneider, "Understanding TiO_2 photocatalysis : Mechanisms and Materials," *ACS Chemical Reviews*, vol. 114, pp. 9919–9986, 2014.

[109] T. L. Hathway, "Titanium dioxide photocatalysis : studies of the degradation of organic

molecules and characterization of photocatalysts using mechanistic organic chemistry," *Thesis*, pp. 1–164, 2009.

[110] M. Umar and H. A. Aziz, "Photocatalytic Degradation of organic pollutants in Water," *Organic Pollutants - Monitoring, Risk and Treatment*, vol. 6, no. 9, pp. 195–208, 2013.

[111] A. R. Khataee and M. B. Kasiri, "Photocatalytic degradation of organic dyes in the presence of nanostructured titanium dioxide : Influence of the chemical structure of dyes," *"Journal of molecular catalysis. A, chemical,"* vol. 328, no. 2, pp. 8–26, 2010.

[112] M. M. Haque, D. Bahnemann, and M. Muneer, "Photocatalytic degradation of organic pollutants : Mechanisms and Kinetics," *Photocatalysis*, vol. 3, pp. 294–326, 2012.

[113] C. Baiocchi, M. C. Brussino, E. Pramauro, A. B. Prevot, L. Palmisano, and G. Marci, "Characterization of methyl orange and its photocatalytic degradation products by HPLC/UV-Vis diode array and atmospheric pressure ionization quadrupole ion trap Mass Spectrometry," *International Journal of Mass spectrom.*, vol. 214, no. 2, pp. 247–256, 2002.

[115] G. Favaro, D. Confortin, P. Pastore, and M. Brustolon, "Application of LC-MS and LC-MS-MS to the analysis of photo-decomposed crystal violet in the investigation of cultural heritage materials aging," *Journal of mass spectrometry*, vol. 47, no. 12, pp. 1660–1670, 2012.

[116] G. Sudarjanto, B. Keller-Lehmann, and J. Keller, "Optimization of integrated chemical-biological degradation of a reactive azo dye using response surface methodology," *Journal of hazardous materials*, vol. 138, no. 1, pp. 160–168, 2006.

[117] S. Chakrabarti, and B. K. Dutta, "Photocatalytic degradation of model textile dyes in wastewater using ZnO as semiconductor catalyst," *Journal of Hazardous Materials*,vol. 112, no. 10, pp. 269-278, 2004.

[118] P. Lei, F. Wang, X. Gao, Y. Dinga, S. Zhanga, J. Zhaob, S. Liuc, M. Yanga, "Immobilization of TiO_2 nanoparticles in polymeric substrates by chemical bonding for multi-cycle photodegradation of organic pollutants, " *Journal of Hazardous Materials*, vol. 10, no. 5, pp. 185– 194, 2007.

[119] Y. Djaoued, S. Badilescu, P.V. Ashrit, D. Bersani, P.P. Lottici R. Bruning, "Sol-gel syntheis of TiO_2 coatings," *Scientific technology*, vol. 24, no. 1, pp. 247-254, 2012

3

Chapter three

Experimental

3.1 Chemicals and materials

Various chemicals and gases were used for the syntheses, purification, characterization and evaluation of the materials used in this project.

Chemicals: $CaCO_3$, NaOH, $Fe(NO_3)_3.9H_2O$, $Co(NO_3)_2.6H_2O$, CH_3CN, 55% HNO_3, Cellulose acetate, Dimethylacetamide, TiO_2 (Anatase), methyl violet, methyl orange, ethanol, titanium (IV) butoxide, isopropanol, acetone. The chemicals were purchased from Sigma-Aldrich or Merck chemicals. All chemicals used were of analytical reagent grade and required no further treatment.

Gases: Acetylene and nitrogen gases were supplied by African Oxygen (AFROX).

3.2. Synthesis of carbon nanotubes

3.2.1 Preparation of Fe-Co/$CaCO_3$ catalyst

The Fe-Co/$CaCO_3$ catalyst was prepared using the wet impregnation method which has been elucidated in most of the citations below [1]–[3]. Two metal nitrates, $Fe(NO_3)_3.9H_2O$ and $Co(NO_3)_2.6H_2O$, were mixed, ground and dissolved in 25 mL distilled water to obtain 0.3 M Fe-Co (1:1) precursor solution. The precursor solution was then added dropwise to a stirred $CaCO_3$ (9.0 g) which was then stirred for 30 minutes. The resulting mixture was further agitated for 1 h while heating at 90 $^{\circ}$C until semi dry. The semi-dried Fe-Co/$CaCO_3$ catalyst was dried completely for 18 h in an oven at 120 $^{\circ}$C and thereafter cooled to room temperature, ground and sieved using a 150 µm mesh sieve. The resulting bimetal-supported catalyst was then calcined in air at 400 $^{\circ}$C for 6 h.

3.2.2 Fabrication of multiwalled carbon nanotubes (MWCNTs)

Multiwalled carbon nanotubes (MWCNTs) were contrived using a chemical vapor deposition (CVD) under operational experimental conditions reported in literature [1]–[4]. Figure 3.1 shows the CVD set-up that was used for this synthesis. 1g of Fe-Co/$CaCO_3$ catalyst was spread into a quartz boat (120 mm length and 15 mm width) which was placed in the centre of quartz tube with an internal diameter of 19 mm. The quartz tube was then inserted inside a furnace and the

temperature was raised to 700 ^{o}C at 10 ^{o}C/min under flowing N_2 gas (240 mL/min) which was used as a carrier gas. After the temperature reached 700 ^{o}C, the flow of the carbon source (C_2H_2) along with the carrier gas was initiated at 100 mL/min flow rate. To preserve a constant flow of the gases without any leakage, an inlet and outlet adaptor connectors were used. The heating rate was guided by a thermocouple which was located inside the furnace from the temperature controller. The reaction was held at 700 ^{o}C for 1 h after which the C_2H_2 was switched off, and the reactor was allowed to cool down to room temperature under N_2 gas. The quartz boat was then pulled out from the reactor and the product was transferred into a dessicator.

3.2.3 Functionalization of MWCNTs

3.2.3.1 Nitrogen doping of MWCNTs

The two main methods of nitrogen doping (*in situ*doping and *ex situ*doping method) were enunciated. The MWCNTs were *in situ*doped over a decomposition of Fe-Co/$CaCO_3$ with C_2H_2 as a carbon source and CH_3CN as nitrogen and carbon source. In this method, the bimetallic catalyst was spread in a quartz boat, inside a quartz tube, and then positioned at the center of the furnace. The furnace temperature was raised to 800 ^{o}C at 10 ^{o}C/min under N_2 gas (240 mL/min), and then it was held for 1 hour while both N_2 and C_2H_2 (100 mL/min) were bubbled through CH_3CN. After an hour, the furnace was cooled to room temperature and the functionalized MWCNTs were denoted as *in situ*N-MWCNTs.

On the other hand, *ex situ*doping was compassed by placing the prepared MWCNTs in a quartz boat, inside a quartz tube which was put inside a furnace. The temperature of the furnace temperature was raised to 800 ^{o}C at the same ramping rate as in *in situ*doping. It was crucial for this reaction to be conducted under flowing N_2 to prevent a complete decomposition of the MWCNTs. After 800 ^{o}C was reached, N_2 was bubbled through CH_3CN for 1 hour. Thereafter, the furnace was cooled down to room temperature and the resulting material was denoted as *ex situ*N-MWCNTs. Notably, both *in situ*and *ex situ*doping methods used a similar set-up that is shown in Figure 3.1.

3.2.3.2 Functionalization through acid-treatment

Acid treatment was used to remove the residual catalyst as well as the amorphous carbon and to add oxygenated functional groups on the layers of the MWCNTs and N-MWCNTs. A weighed amount of MWCNTs or N-MWCNTs was treated with 50 ml of 55% HNO_3 under reflux in an oil bath held at 110 ^oC for 6 h. The acid-treated materials were filtered and washed with large volumes of deionized water to remove the residual HNO_3 until the pH of the filtrate was neutral. The acid-treated MWCNTs were dried at 120 ^oC for 12 h. The MWCNTs functionalized by acid-treatment were denoted as fMWCNTs, and the acid-treated *in situ*N-MWCNTs and *ex situ*N-MWCNTs were denoted as *in situ*fN-MWCNTs and *ex situ*fN-MWCNTs, respectively.

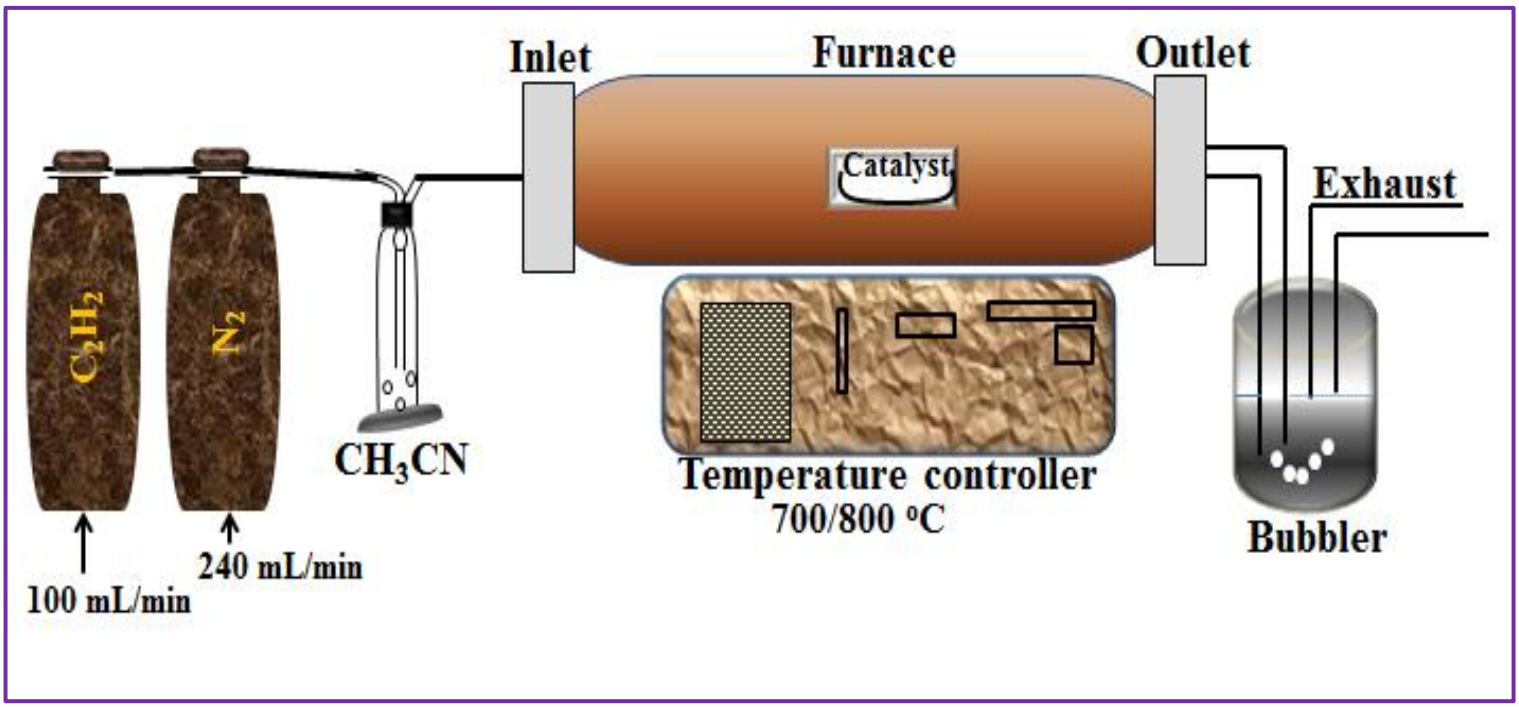

Figure 3.1 Schematic diagram of a horizontal CVD set-up used for the syntheses of MWCNTs, *in situ*N-MWCNTs and *ex situ*N-MWCNTs.

3.3 Synthesis of cellulose-N-MWCNTs nanofibers

The functionalized MWCNTs that exhibited adequate catalyst-supporting capabilities were used in the synthesis of cellulose-N-MWCNTs hybrid using electrospinning. A solution of 15 wt% N-MWCNTs/cellulose acetate (CA) (0.05/15) in 2:1 w:w acetone/Dimethylacetamide (DMAc) was prepared under ultra sonication for 1 h, followed by constant agitation for 12 h. The N-MWCNTs loaded cellulose acetate solution was transferred into a standard 5 ml syringe fitted with a blunt gauge-20 stainless steel needle with an outer diameter of 1.2 mm. The N-MWCNTs and cellulose mixture was then electrospun by applying a 15 kV voltage using a DC power supply at 1 mL/h with a syringe pump. The fibers were collected on a rotar that was covered with aluminum foil, at a distance of 25 cm. The obtained N-MWCNTs-CA nanofibers were then deacetylated in 0.05M aqueous NaOH solution at ambient temperature for 4 days to generate cellulose-N-MWCNTs (C@N-MWCNTs). The solution was then filtered, and washed with deionized water until the pH was neutral.

3.4 Fabrication of TiO_2/MWCNTs composites

TiO_2 was immobilized on carbonaceous materials by a conventional sol-gel method [3]. The procedure for the preparation of TiO_2-based nanocomposites is shown in Figure 3.2 below. For the preparation of TiO_2/N-MWCNTs (both *in situ*and *ex situ*), TiO_2/fMWCNTs, TiO_2/fN-MWCNTs (*in situ*and *ex situ*), the functionalized MWCNTs (0.1 g) were dispersed into a solution containing 2.7 mL water and 27.3 mL isopropanol, under ultra-sonication which lasted for 1 h. Then titanium (IV) butoxide used as a TiO_2 precursor was dispersed in isopropanol to provide a ratio of 3.41:18 (TiO_2:$C_4H_{10}O$) and was ultra sonicated for 1 h. After an hour, the TiO_2 slurry was carefully transferred dropwise into the MWCNTs suspension under vigorous stirring for 2 h to complete the hydrolysis reaction. The resulting solution was then filtered, washed with ethanol and water, and then dried at 100 $^{\circ}$C for 1.5 h. Thereafter, all the prepared catalysts were ground and annealed at 400 $^{\circ}$C for 2 h.

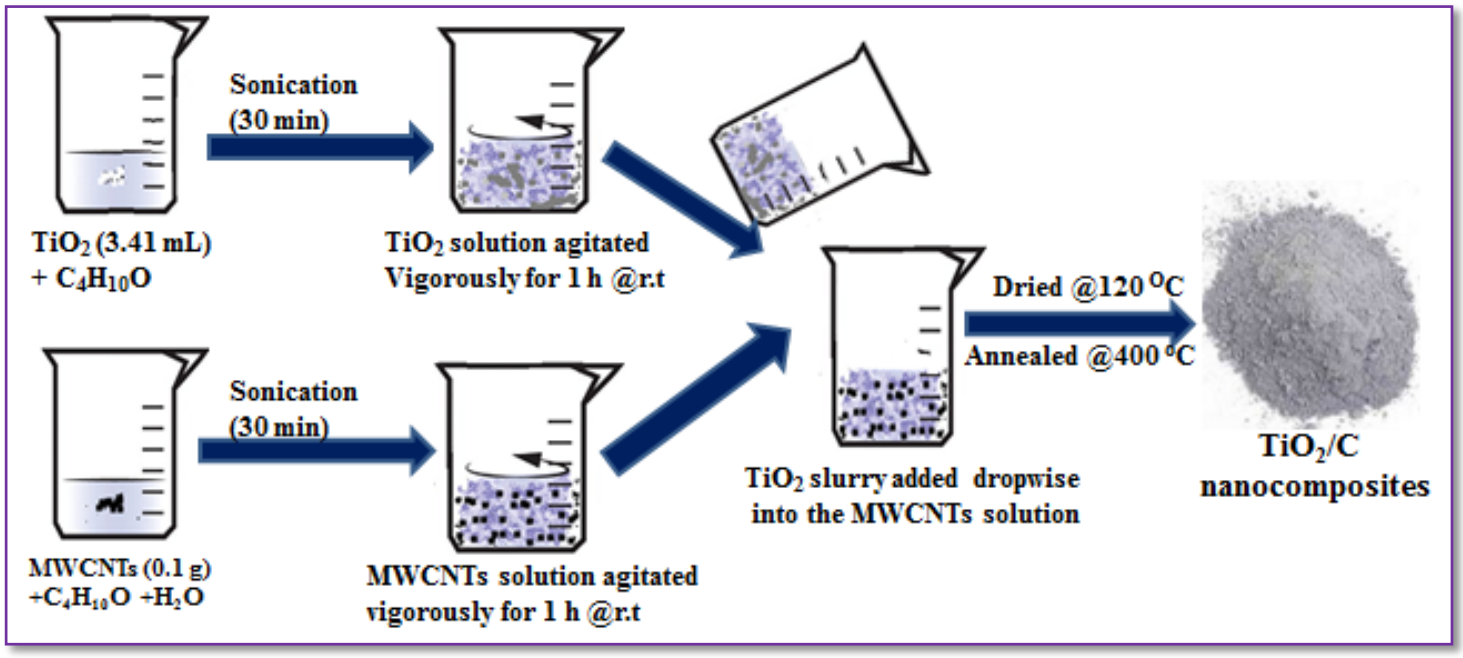

Figure 3.2: Schematic diagram showing the procedure for the preparation of TiO_2/MWCNTs composites.

3.5 Fabrication of TiO_2/C@fN-MWCNTs composites

A similar procedure was applied in the preparation of TiO_2/cellulose and TiO_2/C@fN-MWCNTs. 0.1 g of the cellulosic materials were separately dissolved into a 30 mL aqueous solution of isopropanol (27.3 mL) and distilled water (2.7 mL). A TiO_2 precursor solution was prepared by adding 3.41 mL of titanium (IV) butoxide in isopropanol (18 mL). The precursor solution was transferred dropwise into the cellulosic suspension under vigorous stirring for 2 h followed by filtering. The supported TiO_2 was then dried at 100 $^{\circ}$C for 1.5 h. Thereafter, the catalysts were ground and annealed at 300 $^{\circ}$C for 2 h under N_2 gas.

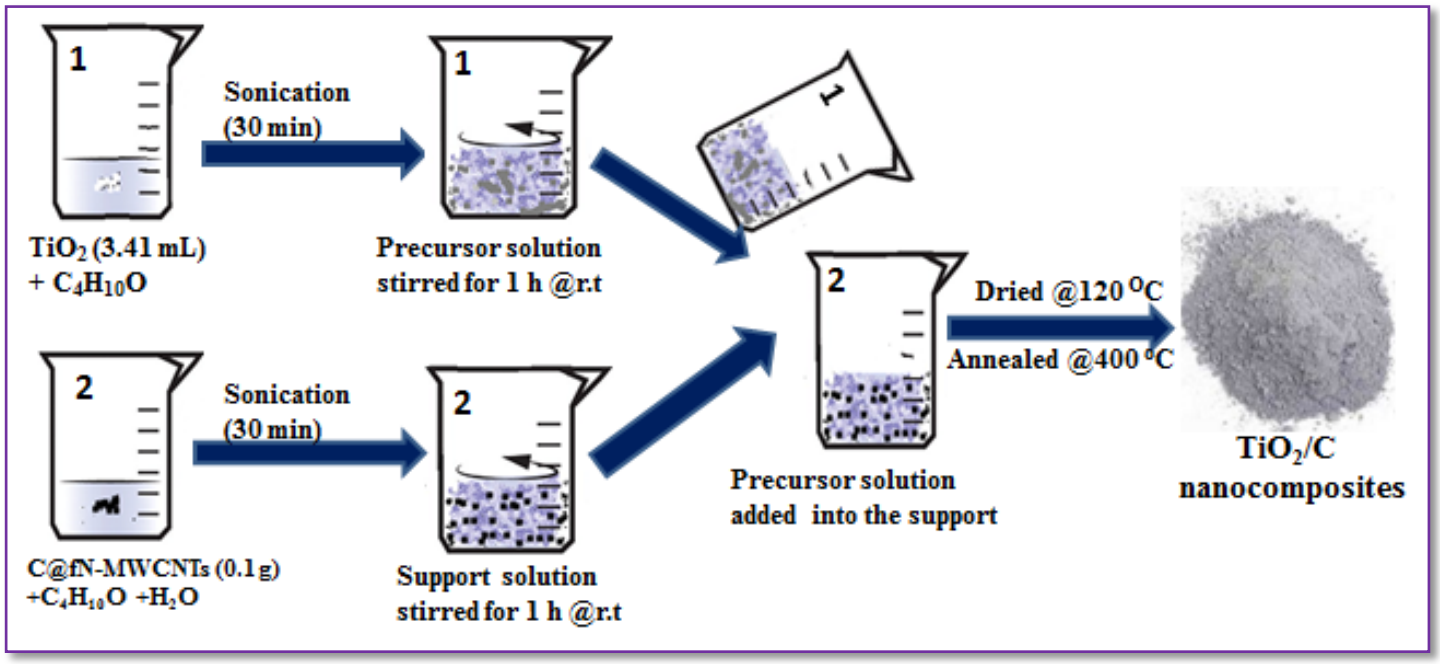

Figure 3.3: Schematic diagram showing the procedure for the preparation of TiO_2/C@fN-MWCNTs composites.

3.6 Photocatalytic degradation studies

The photocatalytic degradation of methyl violet (MV 6B) experiments were carried out to ascertain the photocatalytic degradation efficiency of the prepared catalysts. A weighed amount of the catalyst (150 mg) of interest was dispersed in 100 mL of 20 ppm aqueous solution of MV 6B dye and ultra-sonicated for 30 minutes in the dark. The catalyst-containing dye solution was then stirred in the dark for 1 h to reach adsorption-desorption equilibrium. After an hour, the first aliquot was withdrawn using a 5 mL syringe which was connected to a syringe filter of 0.45 µm. The absorbance was then measured to determine the initial concentration (Co) of the dye in the solution. Thereafter, the dye solution was irradiated by solar simulator (Sol 2A, Newport 94022A) emitting artificial solar light with a spectral distribution resembling the solar spectrum in which the power is around 180 W. More aliquots were periodically withdrawn at 30-minute intervals after light was impinged on the dye solution until the solution was clear with zero

absorbance. The decolorization of the dye solution was monitored by measuring the concentration of this dye solution by using UV-Vis absorption spectrometer (200-900 nm). Clean tap water was used as a reference/blank liquid to eliminate errors. All concentration values were obtained at the MV 6B maximum absorbance (464 nm) from the UV-Vis spectra. The photocatalytic activities and efficiencies of the catalysts were calculated using equation 3.1.

Furthermore, the operational parameters were optimized by varying the parameter being optimized under fixed conditions. The efficiency of *ex situ*TiO_2/fN-MWCNTs and *in situ*TiO_2/fN-MWCNTs catalysts were compared. Thereafter, the selectivity studies of the photodegradation were compassed using the catalyst which exhibited a high photocatalytic activity, whereby the degradation rate of methyl violet and methyl orange was compared. A similar procedure was then followed in the degradation of MV using TiO_2/cellulose and TiO_2/C@fN-MWCNTs where the optimal parameters were used. The effect of N-MWCNTs on the photocatalytic activity of TiO_2/cellulose was then evaluated.

$$(\eta) = \frac{Co - Ct}{Co} \text{ X } 100 \qquad \text{eq. (3.1)}$$

where η refers to the photocatalytic efficiency, Co is the initial concentration and Ct refers to the concentration after time, t.

Figure 3.4: Photograph of the solar simulator used as a UV light source in the photocatalytic degradation of dyes.

3.7 Characterization techniques

Various techniques were used to characterize the synthesized carbonaceous materials and the photocatalysts to obtain the optical, physical and chemical properties. The techniques employed in this study were chosen to probe the bulk and surface properties of the materials.

3.7.1 Thermogravimetric analysis (TGA)

Perkin Elmer STA 4000 analyzer (Figure 3.4) was used to ascertain the sample composition, thermal stability and the purity of the carbon-based materials in this study. The sample mass (10 mg) and flow rate (10 mL/min) were kept constant in every analysis to minimize instrumental error [5]. The sample of interest was transferred into a ceramic pan that was supported on an analytical balance located in the instrument's furnace where the temperature was increased to 900 ^{o}C at a rate of 10 ^{o}C/min, in controlled atmosphere. The sample composition, thermal

stability, and the purity of each sample were evaluated from the analysis. Analysis done in N_2 gas were used to investigate the pyrolysis of the functionalized MWCNTs [6]. The TGA profiles were accompanied by the derivative curves (DTG) which were used to determine the oxidation temperature and to depict the level of impurities [7].

Figure 3.5: Digital image of the Perkin Elmer STA 4000 thermogravimetric analyzer.

3.7.2 Raman spectroscopy

Raman spectroscopy is arguably the most powerful technique used in the evaluation of carbon materials' quality. In this study Raman spectroscopy was used to probe the quality of the functionalized MWCNTs and their respective catalysts. This analysis was performed using a Jobin-Yvon T64000 micro-Raman spectrometer as shown in Figure 3.5. This spectrometer is equipped with an argon ion laser source of 514.5 nm excitation wavelength and a charge coupled detector (CCD) which was cooled with liquid nitrogen. Using Raman spectroscopy, the phase of TiO_2 was evaluated. Furthermore, the ratio of sp^2 (graphite-like) to sp^3 (diamond-like) bonds was determined as means of depicting the graphitic property of the MWCNTs. This was also confirmed by the intensity ratios of the 2D to G band, whereby in both cases, lower ratios indicate more graphitized the MWCNTs, that is; ideal graphite has a zero intensity ratio [4], [8]. The Raman spectra were deconvulated using lorentzian function by using the Origin 8.50 software.

Figure 3.6: Digital image of the Jobin-Yvon T64000 micro-Raman spectrometer.

3.7.3 Powder X-ray diffraction

This analytical technique was rapidly used to ascertain the purity and the crystallinity of the bulk composition of the materials. Figure 3.6 shows the XRD instrument that was used (Bruker D2 phaser equipped with a Lynxeye detector). The radiation source was the Co-Kα at 30 kV (wavelength λ = 1.5406 Å**)** with variable slits at 45 kV/40 mA. The 2θ scan ranged from 10^o – 90^o in steps of 0.0260 with scan speed of 0.1^o/s. Prior to analysis, the sample of interest was first ground to fine powder and sieved using 150 µm sieves and then flatly packed on a sample holder using top packing method. All scans were done for 15 minutes and the phases of the materials were determined using the Xpert software. The peak widths from the diffractograms were used to estimate the crystallite size of supposedly spherical TiO_2 particles. Small crystallite structures were associated with broad peaks due to the shortage of planes to generate complete destructive interference in very small crystallite structure. Furthermore, various equations were used to ascertain important properties of the studied materials. The equations associated with the diffractograms are presented below:

Crystallite size: $D = \frac{k\lambda}{\beta cos\theta}$ eq. (3.2)

Where D is the crystallite size in Å, K is a shape factor equivalent to 0.9, β is instrumental broadening described by the full width half maximum (FWHM), and lambda λ is the wavelength of the X-ray used [9].

The drawback of using equation 3.2 is the fact that the value of the shape factor was over an assumption of spherical crystallites [10]. Thus, it was used to estimate TiO_2 crystallite sizes in the composites, presuming that they are complete spherical.

Graphitization degree: $d = 3.354 + 0.086(1 - g)$ eq. (3.3a)

Such that; $g = \frac{3.44-d}{0.086}$ eq. (3.3b)

Where g is the graphitization degree which is equivalent to 1(g=1) for an ideal graphite material, and d is the interplanar spacing in Å. The graphitization degree refers to the probability of parallel design for successive graphite layers [11]. In this study, the validity range of the Marie

and Mering formula (equation 3.2a and 3.2.b) could not hold due to the disorientated layers of the functionalized MWCNTs emerging from the harsh treatments. However, a comprehensive analysis was established with reference to the ideal graphite.

Specific surface area: $S = \frac{6\times10^3}{D_p\rho}$ eq. (3.4)

Where S is the specific surface area in g/cm^{-3}, D_p is the crystallite size and ρ is the density of TiO_2 equivalent to 4.23 g.cm^{-3}. The application of equation 3.3 is limited by confining to spherical shapes [11].

Crystalline index: $\%C.I = \frac{I200-Iam}{Iam} x\ 100$ eq. (3.5)

Where C.I is the crystalline index, I_{002} is the intensity attributed to the (002) peak at lattice diffraction of ~22^o, and I_{am} is the intensity of diffraction peak assigned to amorphous cellulose. Equation 3.4 is also known as the amorphous subtraction method [12], [13].

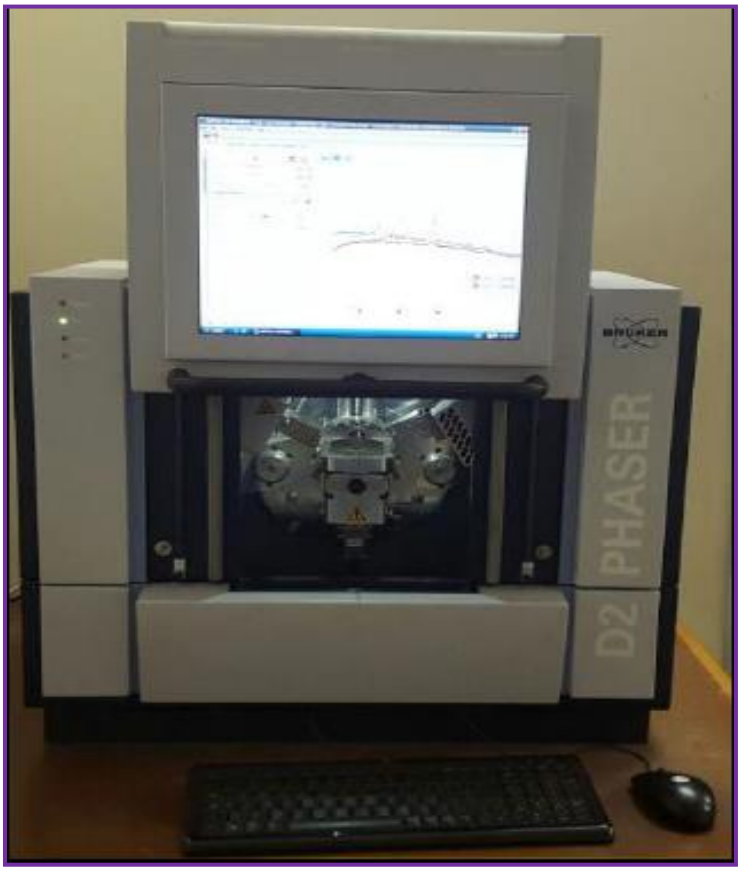

Figure 3.7: Digital image of the Power X-ray diffraction (Bruker D2 phaser)

3.7.4 Transmission Electron Microscopy

Transmission electron microscopy (TEM) was used to examine the morphological features (size, shape, diameter, length and the arrangement of particles in a specimen) of the materials using a FEI Technai G^2 Spirit electron microscope operated at 120 kV. The TEM instrument that was used is presented in Figure 3.7. Because TEM produces images through transmission of electrons, the sample preparation and beam alignment is very crucial. The sample was prepared by ultrasonic dispersion of the sample in ethanol to form a very dilute solution. A drop of the solution was then added onto an SPI-carbon coated copper grid and then dried in ambient air for 40 min before inserting it in the microscope. After inserting the copper grid in the microscope, the beam was aligned and then the sample images were photographed with a camera. The average sizes of the materials were determined using imageJ software where about 150-200 of particles' diameters were measured randomly.

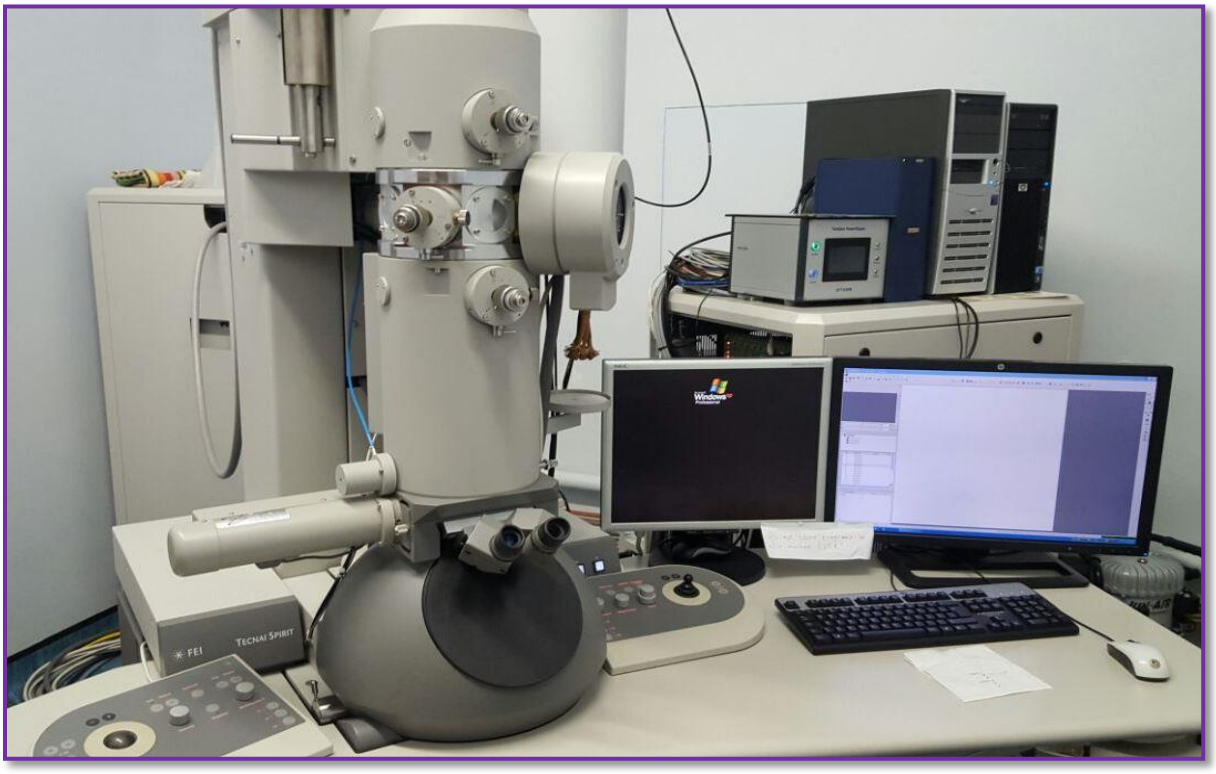

Figure 3.8: Digital image of the FEI Technai G^2 Spirit Transmission electron microscope.

3.7.5 Scanning electron microscopy (SEM)

FEI NOVA Nanolab 600 SEM (Figure 3.8) was used to investigate the morphologies of the materials as a complement of the findings from TEM. However, SEM showed only the surface details of the materials as it produce the images from scanning over the sample. Thus, it required neither complicated sample preparation nor any beam alignments. The solid samples were added on a carbon tape which was attached on a sample holder. Because all the materials used in this project were non-conductive, they were coated with Au to create a conductive layer on the sample. The coated layer was required to inhibit charging, reduce thermal damage and to enhance the secondary electron signal required for topographic examination in the SEM [14].

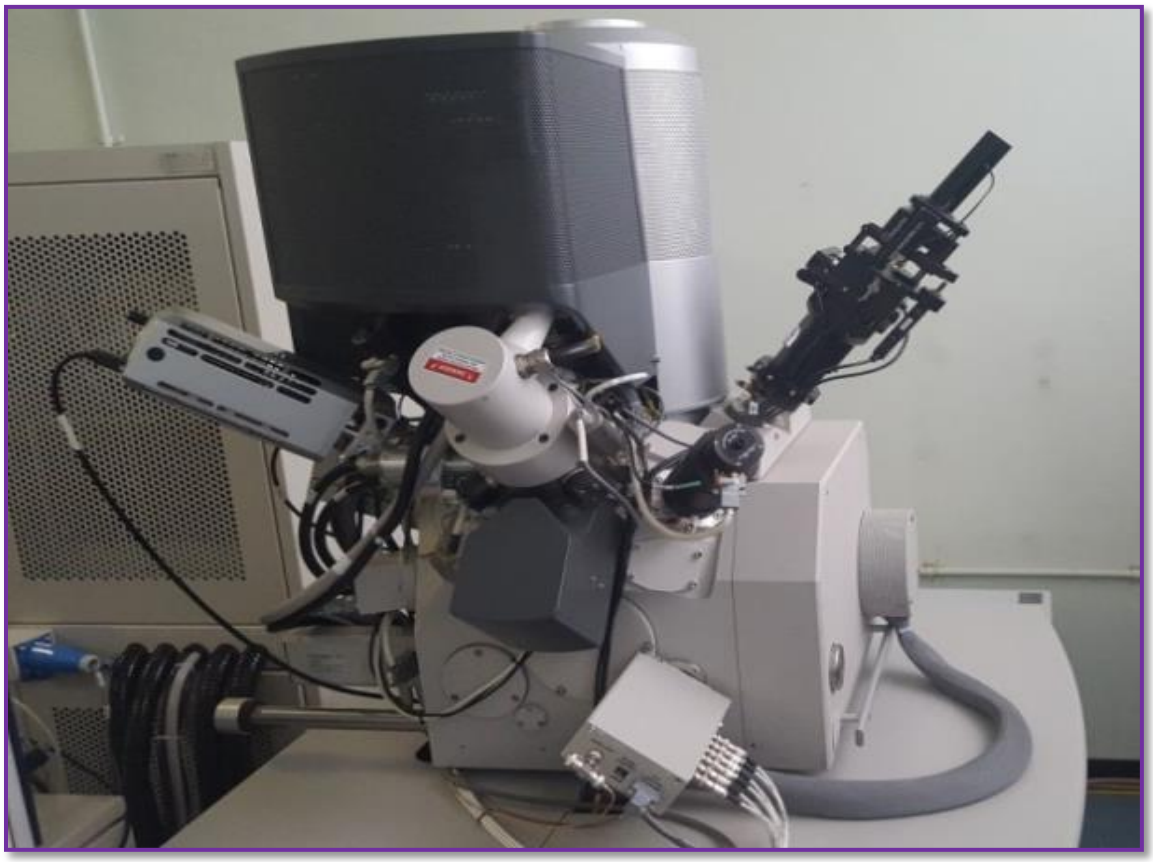

Figure 3.9: Digital image of Nova, scanning electron microscope (SEM)

3.7.6 Energy-dispersive X-ray Spectroscopy

For elemental composition analysis, Energy-dispersive X-ray (EDX) spectroscopy connected to FEI Nova Nanolab 600 SEM was used. The X-rays were captured using the INCA Microanalysis Suit version 4.08 software package. A spot size of roughly 30-40 µm was isolated for compositional analysis to be free foreign dirt or debris. However, monitoring the amount of carbon in the samples was nearly impossible due to the presence of foreign carbon atoms other than the sample. Also, it is worth to note that the EDX is notoriously unreliable in determining atoms with small atomic radii such as nitrogen due to its poor sensitivity to light elements.

3.7.7 Fourier Transform-Infrared Spectroscopy

Figure 3.9 shows the BRUKER TENSOR 27, FT-IR instrument that was used to record the absorption spectra of the cellulose-containing materials in a range of 4000-500 cm^{-1}. This was done by adding a dry sample of each the cellulosic composites on the KBr coated sample holder where the sample molecules selectively absorb radiation of specific wavelengths.

Figure 3.10: Digital image of Fourier-transform infrared spectroscopy, Tensor 27.

3.7.8 Brunauer-Emmet and Teller (BET) surface area measurement

N_2 Physisorption was used to determine the surface area (m^2/g) and pore volume of the materials using a Micromeritics TRISTAR 300 analyzer presented in Figure 3.10. Prior to the analysis, approximately 300 mg of each catalyst was degassed using Micromeritics Flow prep 060 sample degassing system (Figure 3.10(a)). The degassing of the samples is achieved through nitrogen purging at 120 ^oC for 3 hours. The analyte was then transferred into Micromeritics TriSta 3000 instrument where the surface area, pore volume and pore size of the sample was determined. The surface pores of the materials were measure with regard to the volume of N_2 gas adsorbed to the surface of the sample at the boiling point of nitrogen (-196 ^oC). This is in accordance to the (BET) theory as described by Fujita *et al.* [15]. All samples were analyzed using multi-point measurements.

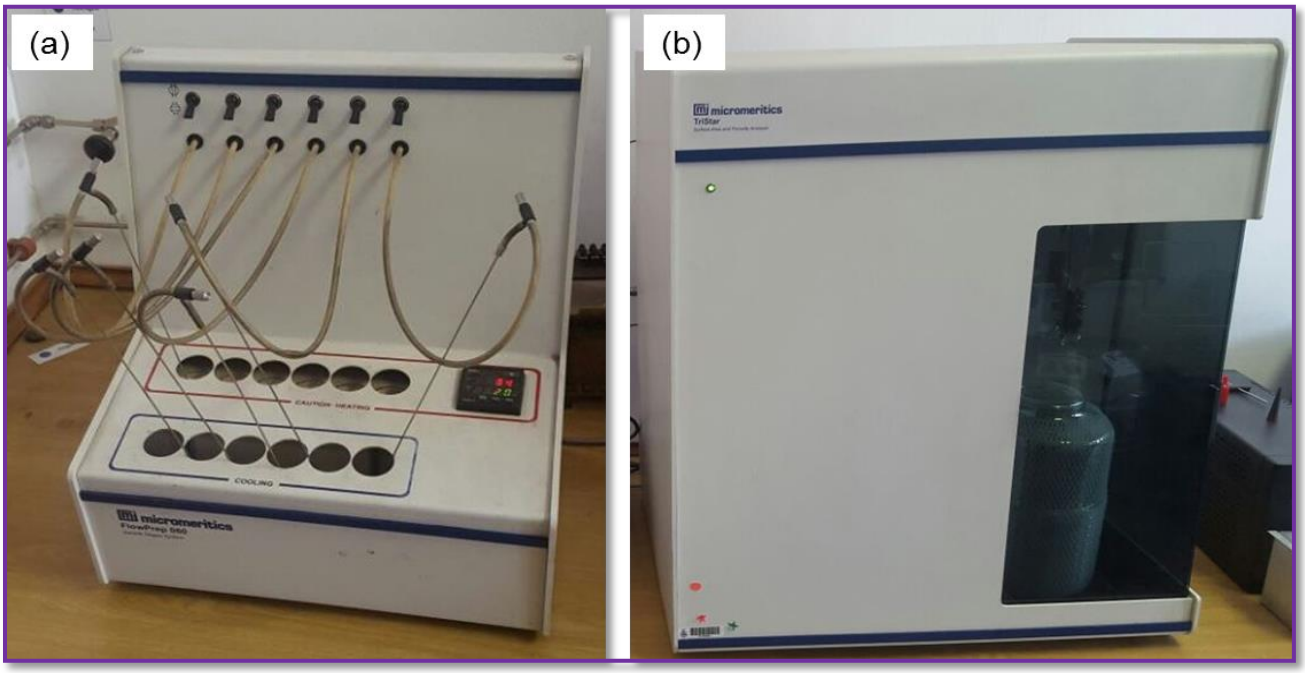

Figure 3.11: Digital image of the Brunner Emmett Teller (BET) (a) Micromeritics Flow prep 060 sample degassing system (b) Micrometrics TRISTAR 300 analyzer.

3.7.9 Ultraviolet–visible (UV-Vis) absorption Spectroscopy

Figure 3.11 shows an absorption spectrophotometer that was used to determine the absorption wavelengths of the catalysts and methyl violet in the ultraviolet-visible spectral region. From the excitation wavelength, the energy band gap of the material was determined using the equation $E=hc/\lambda$. For each analysis, a solution of 2 mg of the analyte was dispersed in 4 mL of ethanol under sonication for 5 minutes and then transferred into a cuvette. The cuvette used for this analysis was UV Quartz with a diameter of 1 mm. The UV-Vis technique was also used to measure the absorbance during the decolorization of the dye as explained above in section 3.5.

Figure 3.12: Digital image of the Ultraviolet-Visible absorption spectroscopy.

3.7.10 Photoluminescence (PL) Spectroscopy

Photoluminescence (PL) refers to the process of photon excitation followed by photon emission [16]. The PL spectrometer (Figure 3.12) was used to probe the electronic structure of the TiO_2-based composites and to assess the capability of the support materials to suppress the electron/hole recombination. For this analysis, a weighed amount of 2 mg of each sample was dispersed in ethanol using ultra sonication for 30 minutes to obtain a homogeneous solution. Then the solution was added in a quartz cuvette (1 mm) and analyzed at the excitation wavelength (344 nm) which was determined from the UV-Vis spectrometer. The background effect was subtracted by analyzing ethanol solvent before each run. All the analyses were done at an angle of 5 slit.

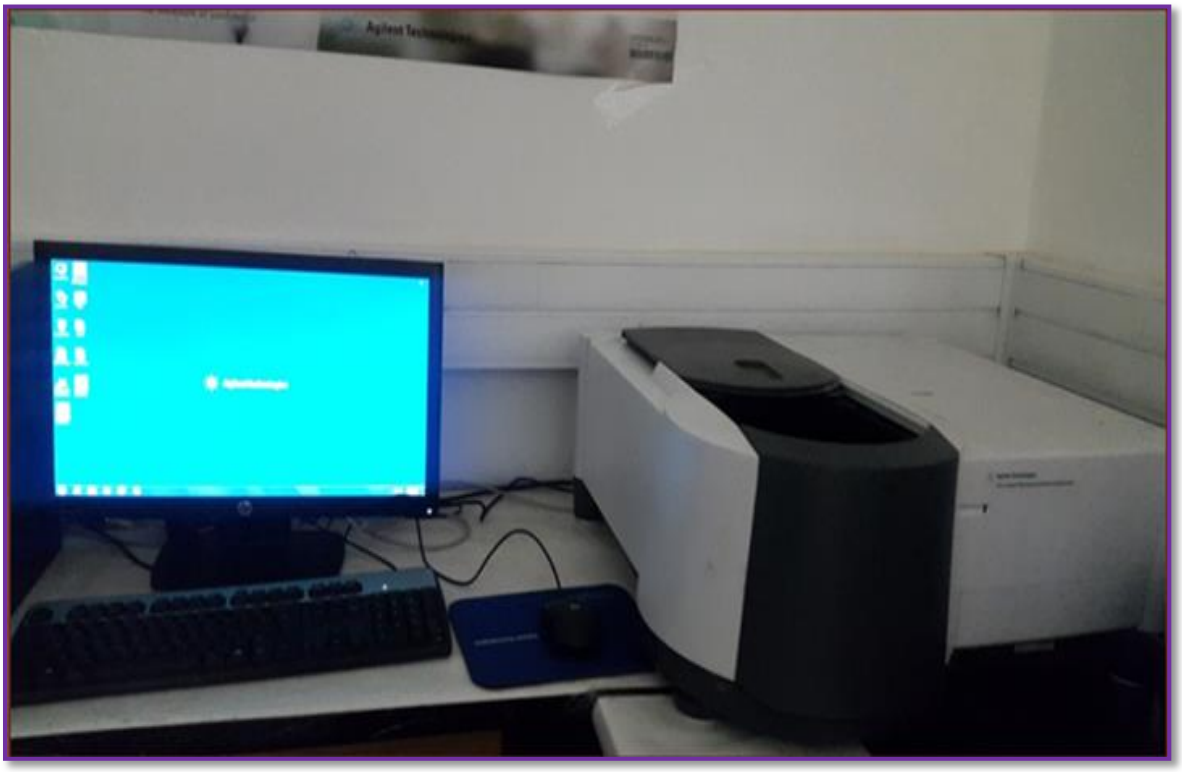

Figure 3.13: Digital image of the photoluminescence spectrometer.

3.8 References

[1] S. D. Mhlanga, K. C. Mondala, R. Carter, M. J. Witcomb, and N. J. Coville "The effect of synthesis parameters on the catalytic synthesis of multiwalled carbon nanotubes using Fe-Co/$CaCO_3$ catalysts," *South Afican. Journal of Chemicals,* vol. 62, pp. 67–76, 2009.

[2] M. A. M. Motchelaho, H. Xiong, M. Moyo, L. L. Jewell, and N. J. Coville, "Effect of acid treatment on the surface of multiwalled carbon nanotubes prepared from Fe-Co supported on $CaCO_3$: Correlation with Fischer-Tropsch catalyst activity," *Journal of molecular catalysis A: chemical,* vol. 335, no. 2, pp. 189–198, 2011.

[3] Z. N. Tetana, "Boron and nitrogen doped carbons for photochemical degradation reactions" *Thesis,* pp. 1–235, 2013.

[4] M. G. Donato, G. Messina, S. Santangelo, S. Galvagno, C. Milone, and A. Pistone, "Aid of Raman spectroscopy in diagnostics of MWCNT synthesised by Fe-catalysed CVD," *Journal of Physics: Conference series,* vol. 61, no. 1, pp. 931–935, 2007.

[5] D. Stawski, "The effect of sample weight in thermogravimetric analysis of low viscosity polypropylene in air atmosphere," *Polymer testing,* vol. 28, no. 2, pp. 223–225, 2009.

[6] N. A. Mansor, J. Tessonnier, M. G. Kutty, R. Schlögl, and S. B. A. Hamid, "Chemically Modified carbon nanotubes (CNTs) with oxygen and sulfur containing functional groups for adsorption of mercury," *Material science and engineering,* vol. 20, pp. 66–70, 2011.

[7] G. Widmann, "Interpreting TGA curves," *UserCom,* pp. 1–20, 2001.

[8] N. Mathur and A. Kumar, "Physico-chemical characterization of industrial effluents contaminated soil," *Journal of Material Sciences,* vol. 4, no. 2, pp. 226–228, 2013.

[9] H. Yang, S. Zhu, and N. Pan, "Studying the mechanisms of titanium dioxide as ultraviolet-blocking additive for films and fabrics by an improved scheme of fabrics," *Journal of applied polymer science,* vol. 92, no. 1, pp. 3201–3210, 2003.

[10] T. S. Wu, K. X. Wang, G. D. Li, S. Y. Sun, J. Sun, and J. S. Chen, "Montmorillonite-supported Ag/TiO_2 nanoparticles: An efficient visible-Light bacteria photodegradation material," *ACS applied materials and iInterfaces,* vol. 2, no. 2, pp. 544–550, 2010.

[11] J. Majewska and B. Michalkiewicz, "Low temperature one-step synthesis of cobalt nanowires encapsulated in carbon,"*Applied physics a material science and engineering*, pp. 1013–1016, 2013.

[12] K. Lefatshe, C. M. Muiva, and L. P. Kebaabetswe, "Extraction of nanocellulose and in-situ casting of ZnO/cellulose nanocomposite with enhanced photocatalytic and antibacterial activity," *Carbohydrate polymers*, vol. 164, pp. 301–308, 2017.

[13] S. Yun and J. Kim, "Characteristics and performance of functionalized MWNT blended cellulose electro-active paper actuator," *Synthetic metals*, vol. 158, no. 13, pp. 521–526, 2008.

[14] Leica microsystems, "EM Sample Preparation Coating Technology," *Living up to life*, pp.1–10 , 2013.

[15] Y. Fujita, "The Determination Method of Surface Area by the BET Method," *Shinku*, vol. 6, no. 5, pp. 169–176, 1963.

[16] D. K. Pallotti, L. Passoni, P. Maddalena, F. D. Fonzo, and S. Lettieri, "Photoluminescence mechanisms in anatase and rutile TiO_2," *ACS Journal of Physical Chemistry*, vol. 102, no. 10, pp. 9011–9021, 2017.

4

Chapter four

Study of functionalized multiwalled carbon nanotubes (MWCNTs)

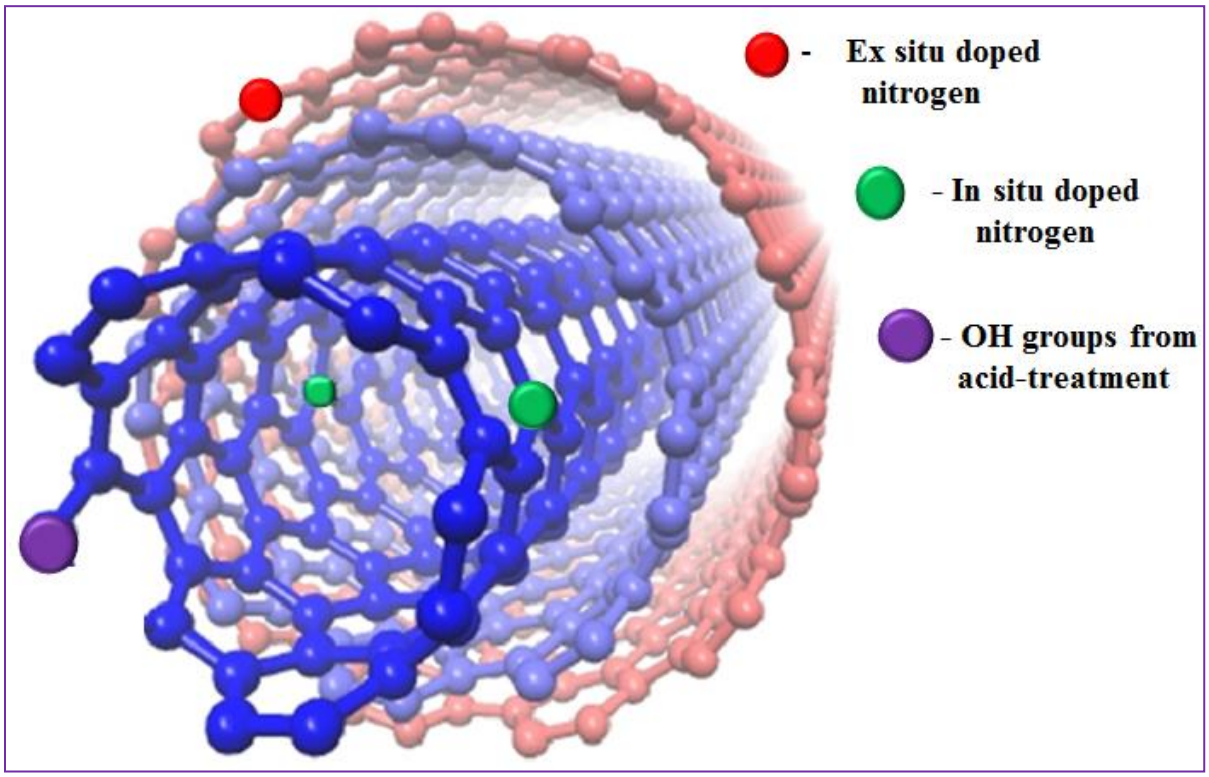

4.1 Overview

Multiwalled carbon nanotubes (MWCNTs) have now become an important industrial material [1]. Their intriguing properties (inclusive of high surface area, resistance to acidic/basic media, thermal stability and their versatility) justifies the multitude of work that is done on them [2], [3]. Recently, diverse research has been focused on tuning the electro-physical and adsorption properties of MWCNTs in order to meet specific needs [4]. Factors such as pore density, external surface area, purity, and functionalities determine the MWCNTs adsorption capacity [5]. Nonetheless, MWCNTs tend to aggregate due to van der Waals forces resulting in a decrease of the total surface area which is necessary for bulk pollutant adsorption [5]. Conversely, the aggregation of MWCNTs may create interstitial spaces between tubes that significantly increase the pore volume and grooves on the peripheral spaces of the MWCNTs bundles [5]. Thus, purification and functionalization of MWCNTs is a fundamental expedient to bring repulsion between the MWCNTs resulting in high affinity of the MWCNTs towards water pollutants [5].

Heteroatom doping of MWCNTs (with dopants such as: phosphorus, sulphur, nitrogen, and boron) is an effective way to create exotic physical and chemical functionalities that are useful for a multitude of novel applications [7]–[10]. In general, the dopants (p- or n-type) cause localization of 2pz electrons [10]. For instance; nitrogen dopants (n-type) induce a net positive charge on the carbon atoms due to their higher electronegativities than their neighboring carbons [11]. Consequently, the nitrogen doped multiwalled carbon nanotubes (N-MWCNTs) have a strong affinity to metals which makes them good metal-supports for application in catalysis [9], [12].Therefore, N-MWCNTs have been under rigorous scrutiny in oxygen reduction reactions [9], [13].

In TiO_2-based composites, the N-MWCNTs provide spatial confinement of TiO_2 and large supporting surface areas, leading to faster photocatalytic redox reactions. In this chapter, the adequate method of nitrogen doping to maximize the photocatalytic potential of TiO_2/MWCNTs was investigated. Their distinct properties were evaluated using Raman spectroscopy, thermogravimetric analysis (TGA) and transmission electron microscopy (TEM).

4.2 Results and Discussion

MWCNTs are explained as a sheet of graphene rolled up into a tube, hence ideal MWCNTs only consists of sp^2 graphitic carbons. However, functionalizing the MWCNTs creates defects in the carbon networks which consequently exhibit poor graphitic behavior.

4.2.1 Phase identification studies of the functionalized MWCNTs.

X-ray diffraction (XRD) was used to investigate the degree of graphitization of the functionalized MWCNTs. Figure 4.1 shows the XRD patterns of (i) *in situ* N-MWCNTs, (ii) *ex situ* N-MWCNTs (iii) fMWCNTs (iv) *in situ* fN-MWCNTs and (v) *ex situ* fN-MWCNTs. All XRD patterns exhibited common diffraction peaks at $2\Theta = \sim30^o$ and $2\Theta = \sim43^o$ (ICOD: 03-065-6212). The peaks in 29.6^o-31.4^o range were all characteristic of 002 line which corresponds to the hexagonal graphite that reflects the graphitic character of the nanotubes [22]. Thus, the 002 diffraction line was used to determine the interlayer spacing in order to estimate the graphitization degree of the functionalized MWCNTs. This was done using Bragg equation; $n\lambda = 2d\,sin\,\theta$, where n is a positive integer, λ is lambda, the wavelength of the X-ray used, and θ is theta, half of the Bragg angle (in radians) . This equation was used to determine the interlayer d(002) spacing and the results were then used in the Maire and Mering formula to calculate the graphitization degree (g) [23]. The deviation of the studied MWCNTs from the Marie and Mering's validity (validity range: $0 \leq g \geq 1$) was because the MWCNTs were functionalized which disorientated the carbon layers, thus reducing the graphitization properties. Thus the graphitization degree of the functionalized MWCNTs was reported with reference to the ideal graphite where g =1. Subsequently, the material with a graphitization degree closer to ideal graphite was regarded as more graphitic. The influence of different functionalization on the graphitization degree of the MWCNTs is shown in Table 4.1.

Maire and Mering formula : $d = 3.354 + 0.086(1 - g)$, where d is the interlayer spacing in angstroms (Å) and g is the graphitization degree.

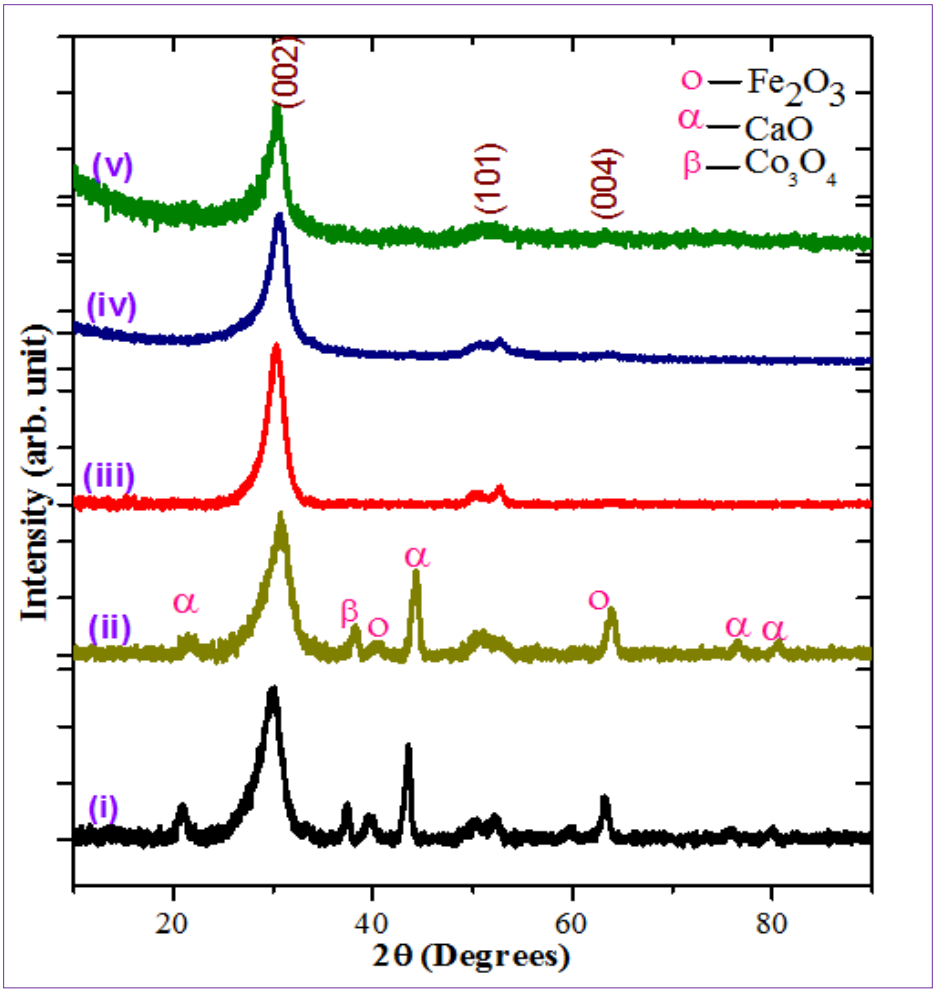

Figure 4.1: XRD pattern of functionalized MWCNTs (i) *in situ* doped N-MWCNTs, (ii) *ex situ* doped N-MWCNTs (iii) fMWCNTs (iv) *in situ* doped fN-MWCNTs (v) *ex situ* doped N-MWCNTs.

It was observed that *in situ* fN-MWCNTs exhibited low graphitic characteristic (g=6.92, further from ideal graphite). This was attributed to the defects that were created by nitrogen incorporation in the lattice. On the other hand, *ex situ* N-MWCNTs had relatively higher graphitization degree that was close to fMWCNTs. This is accounted by the fact that *ex situ* doping is done through annealing process which crystallizes the MWCNTs and only 0.15% of nitrogen was incorporated as reported in **Section 4.2.3**. However, all functionalized MWCNTs were not graphitized. It is noteworthy that the nitrogen doped MWCNTs exhibited 002 peaks at slightly higher angles relative to the fMWCNTs. This shift was attributed to nitrogen functionalities which created graphitic stacking and deformity in

the crystalline regularity by shorter C-N bonds [24]. Thus, high d(002) value corresponds to low graphitization degree.

Table 4.1: Parameters that were used to ascertain the quality of MWCNTs.

Sample name	2θ (degrees)	002 peak width	d_{002} (Å)	g (Å)
1. *Ex situ* N-MWCNTs	30.0	2.24	3.00	5.12
2. *In situ* N-MWCNTs	30.2	2.44	2.91	5.62
3. fMWCNTs	29.9	1.34	2.99	5.28
4. *Ex situ* fN-MWCNTs	30.6	1.26	2.96	6.07
5. *In situ* fN-MWCNTs	31.4	1.95	2.85	6.92

Furthermore, XRD was used to estimate to rank the purity of the MWCNTs. This was done using 002 peaks widths that were calculated using Origin Software and reported in Table 4.1 [23]–[25]. The purity of MWCNTs was investigated based on the fact that amorphous carbons are diffracted at angles close to the graphitic carbon [25]. As a result, high level of impurities are associated with broader 002 peaks [25], [26]. The *in situ* and *ex situ* N-MWCNTs exhibited broader 002 peak widths of 2.44 and 2.24 respectively, confirming the presence of amorphous carbon. On the contrary, Figure 4.1 shows an insignificant change in the 002 peak width of the fMWCNTs, *in situ* fN-MWCNTs and *ex situ* fN-MWCNTs. This is due to the acid functionalization which dissolved the amorphous carbon. However, *ex situ* fN-MWCNTs exhibited a sharper 002 peak which was evidence of a highly crystalline structure [9], [27]. The crystallinity of the *ex situ* fN- MWCNTs was accounted by the post thermal treatment which accounted as annealing by removing the impurities that were absorbed by the nanotubes from the atmosphere [28].

Notably, *in situ* N-MWCNTs and *ex situ* N-MWCNTs exhibited multiple peaks more than the other materials. The peaks at $2\Theta \approx 24.4^{o}$, 43.6^{o}, 76.1^{o} and 80.1^{o} (ICDD 01-077-2010), $2\Theta \approx 40.6^{o}$ and 63^{o} (ICDD 00-033-0664) and $2\Theta = 38.8^{o}$ (ICDD 01-089-8398) were assigned to calcium oxide, iron

oxide and cobalt oxide, respectively. These were from the catalyst used to synthesize the nanotubes. An additional peak at $2\Theta = 52^{o}$(C004 facets) was assigned to the weakly ordered graphitic structures [7]. The *in situ* fN-MWCNTs exhibited weaker 100 peaks showing high disordered carbon structures.

4.2.2 SEM and TEM of the functionalized MWCNTs

The electron microscopes (EM) were used to assess the morphology, purity, and the quality of the nanotubes. Figures 4.2(a) and 4.2(b) present the TEM and SEM micrographs of all the functionalized MWCNTs, respectively. Both EM analyses revealed that the nanotubes were randomly arranged with open ends. TEM confirmed that fMWCNTs, *ex situ* N-MWCNTs and *ex situ* fN-MWCNTs had a hollow inner surface with different average diameters. On the contrary, *in situ* doped N-MWCNTs formed a mixture of tubes with a 'membrane' and others with bamboo-like compartments inner surface. The bamboo-like structures have been widely identified as evidence of successful nitrogen incorporation [29]. The fMWCNTs, *in situ* N-MWCNTs, and *ex situ* N-MWCNTs exhibited a smooth outer surface as compared to the *in situ* fN-MWCNTs and *ex situ* fN-MWCNTs. The rough surface of the *in situ* fN-WMCTs was due to the high content of oxygen functional groups which could be readily anchored due to the net positive charge of the lattice that resulted from the nitrogen dopants. Nonetheless, the *ex situ* fN-MWCNTs showed a unique surface morphology. This observed morphology was attributed to the surface functionalization of nitrogen incorporation and acid treatment. It is noteworthy that the innermost tubes did not show any distortion.

Both TEM and SEM micrographs of N-MWCNTs (both *in situ* and *ex situ*) showed the presence of foreign particles which were attributed to the catalyst residue as affirmed by XRD. However, TGA analysis (**Section 4.2.3**) showed that *ex situ* N-MWCNTs had lower content of the catalyst residues compared to *in situ* N-MWCNTs. This insinuates that the catalyst residue further decomposed during *ex situ* doping, resulting to new carbon nanotubes where CH_3CN functioned as a carbon and nitrogen source [30]. As a result, there were a few nanotubes which showed branched-like structures. From SEM analysis, MWCNTs of smaller diameters were observed extending from other tubes which could be regarded as "secondary nanotubes", i.e. they were formed during the second heating process (*ex situ* doping).

Moreover, the catalyst residue could barely be observed from the *in situ* fN-MWCNTs. This confirmed that the catalyst was removed by acid treatment which simultaneously functionalized the materials. The nanotubes followed base-growth mechanism which suggests that there was a strong interaction between Co-Fe particles and the CaO [19]. This was abstracted from the fact that the catalyst residue was not observed on the open ends of the nanotubes [19]. As a result, the newly formed nanotubes only grew from the walls resulting in T-junction nanotubes. The average inner diameters of the nanotubes are reported in Table 4.2 below. The small average sizes of the *in situ* fN-MWCNTs was attributed to the high content of incorporated nitrogen [31].

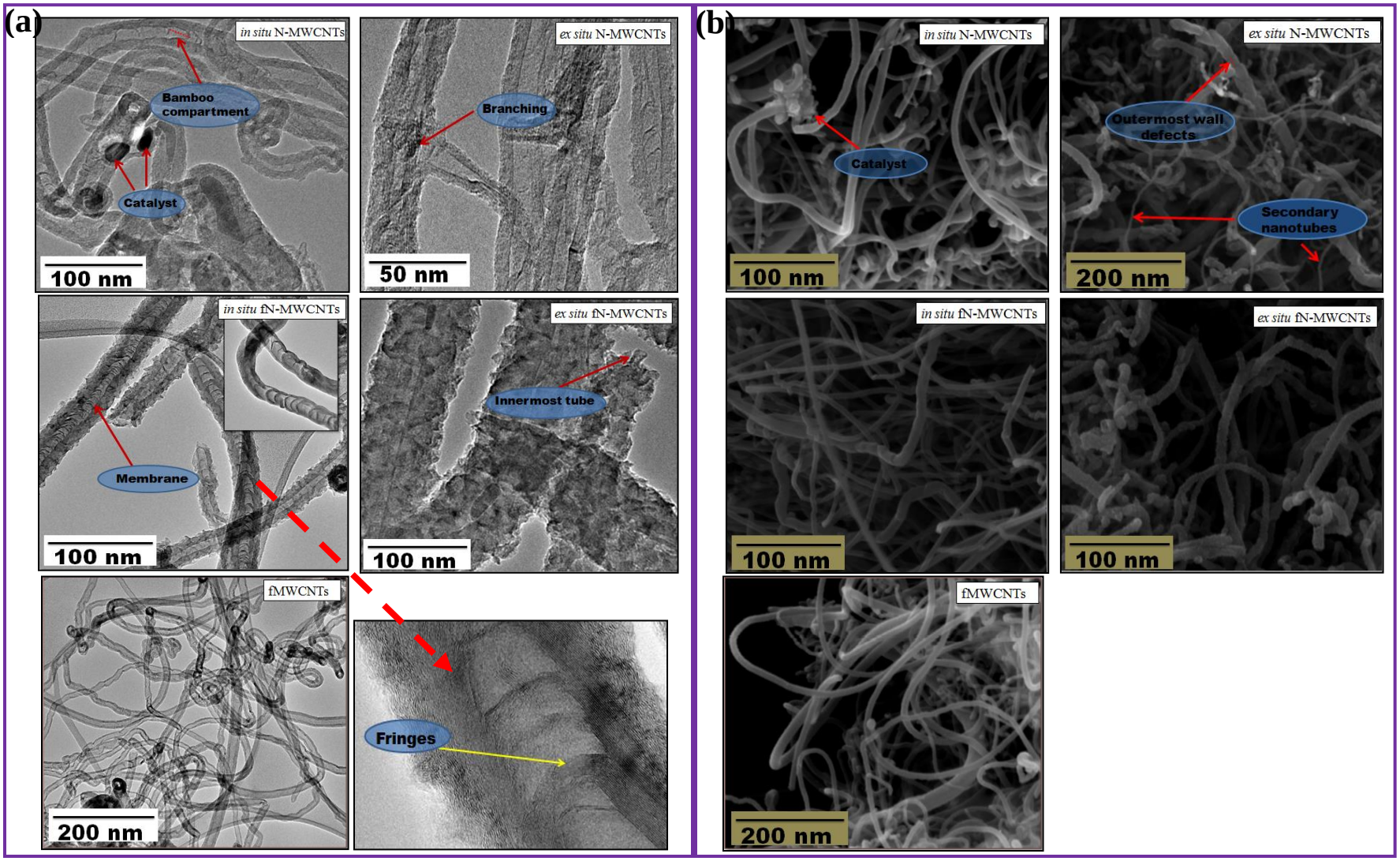

Figure 4.2: (a) TEM micrographs of the functionalized MWCNTs and (b) SEM micrographs of all the functionalized MWCNTs.

Table 4.2: Average sizes of the nanotubes extracted from the inner diameters size distribution plots

Sample name	Average inner diameter (nm)
fMWCNTs	9.8
in situ N-MWCNTs	6.8
ex situ N-MWCNTs	11.2
in situ fN-MWCNTs	10.9
ex situ fN-MWCNTs	12.3

4.2.3 Elemental analysis: (C and N) of the functionalized MWCNTs

CHNS analysis was performed to confirm the elemental constituents of each sample and quantify the nitrogen incorporated (Table 4.3). It was observed that *ex situ* N-MWCNTs contained very low %N content. This was justified by the highly crystalline MWCNTs which made distortion difficult for the N atoms to be incorporated in the lattice. Thus, the incorporation was highly limited. However, the incorporation was improved to 2.40% after acid functionalization. On the other hand, *in situ* N-MWCNTs contained N percentage of 2.90% which did not change after functionalization.

Table 4.3: C and N content in the N-doped MWCNTs

Sample name	% Carbon	% nitrogen
in situ N-MWCNTs	84	2.90
ex situ N-MWCNTs	96	0.15
in situ fN-MWCNTs	72	2.87
ex situ fN-MWCNTs	83	2.40

4.2.4 Energy-dispersive X-ray Spectroscopy analysis of the functionalized MWCNTs

Figure 4.3 (a-b) presents the EDX (energy-dispersive X-ray) spectra with affixed tables estimating the atomic% of the functionalized *in situ* N-MWCNTs and *ex situ* N-MWCNTs. The *in situ* N-MWCNTs exhibited a significant amount of Fe, Co, O, and Ca confirming the presence of the catalyst residue. This was in accord with the XRD results presented in Section 4.2.1. On the other hand, the *ex situ* N-MWCNTs showed only 1.82 atomic% of calcium from the catalyst residue. This confirmed the anticipation that the catalyst residue in the *ex situ* N-MWCNTs was used up during the doping process, resulting in branched CNTs. The slight difference in the carbon atomic% from the CHNS data was due to the foreign carbon from the carbon tape that was used during the SEM-EDX analysis.

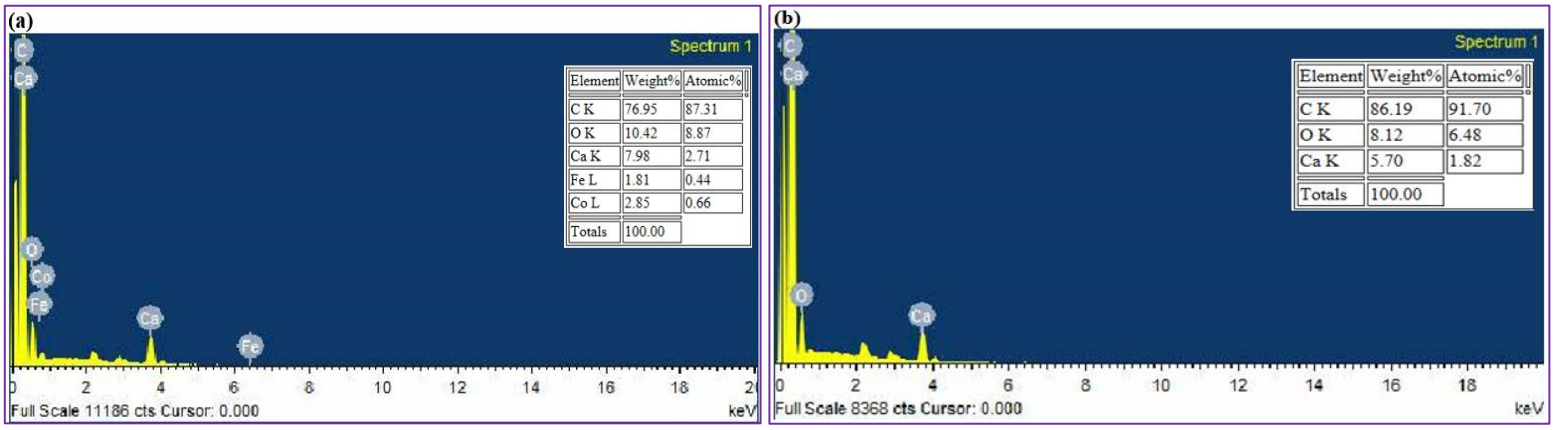

Figure 4.3: Energy dispersive spectra of (a) *in situ* N-MWCNTs (b) *ex situ* N-MWCNTs

Figure 4.3 (c-d) shows the EDX of the *in situ* fN-MWCNTs and *ex situ* fN-MWCNTs. Here it was observed that acid-treatment was also used to purify the MWCNTs. However, a very low amount of atoms from the catalyst were still observed. Moreover, Figure 4.3 (d) showed that the oxygen atomic% of the *ex situ* fN-MWCNTs was lower (2.64%) compared to the *in situ* fN-MWCNTs (10.22%). This could be due to the thermal treatment which has a potential to desorb these functional groups as observed from TGA under N_2 atmosphere (**Section 2.4.6**). The failure of EDX to determine the nitrogen content was due to its low sensitivity to light elements.

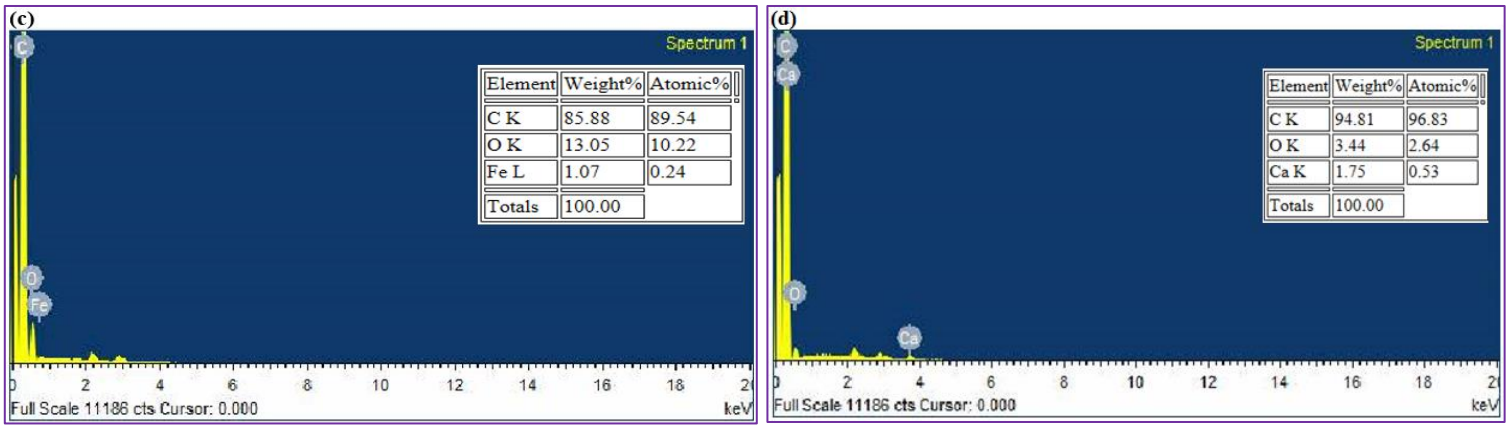

Figure 4.3: Energy-dispersive X-ray spectra of (c) *in situ* fN/MWCNTs (d) *ex situ* fN-MWCNTs.

4.2.5 Raman spectroscopy analysis of the functionalized MWCNTs

The structural and electronic properties of the functionalized carbon nanotubes were studied using Raman spectroscopy since it is a powerful technique for characterizing carbon materials [16]. Figure 4.3 shows the Raman spectra of (i) fMWCNTs (ii) *in situ* N-MWCNTs (iii) *ex situ* N-MWCNTs, (iv) *in situ* fN-MWCNTs and (v) *ex situ* fN-MWCNTs. It was inferred from the Raman spectra that the inner diameters of the functionalized MWCNTs were greater than 2 nm. This was depicted from the absence of the RBM's peaks which normally appear just above 200 cm^{-1} from the Raman spectrum of SWCNTs [32]. SWCNTs are used as reference because the Raman spectrum of MWCNTs is still not fully understood [32], [33].

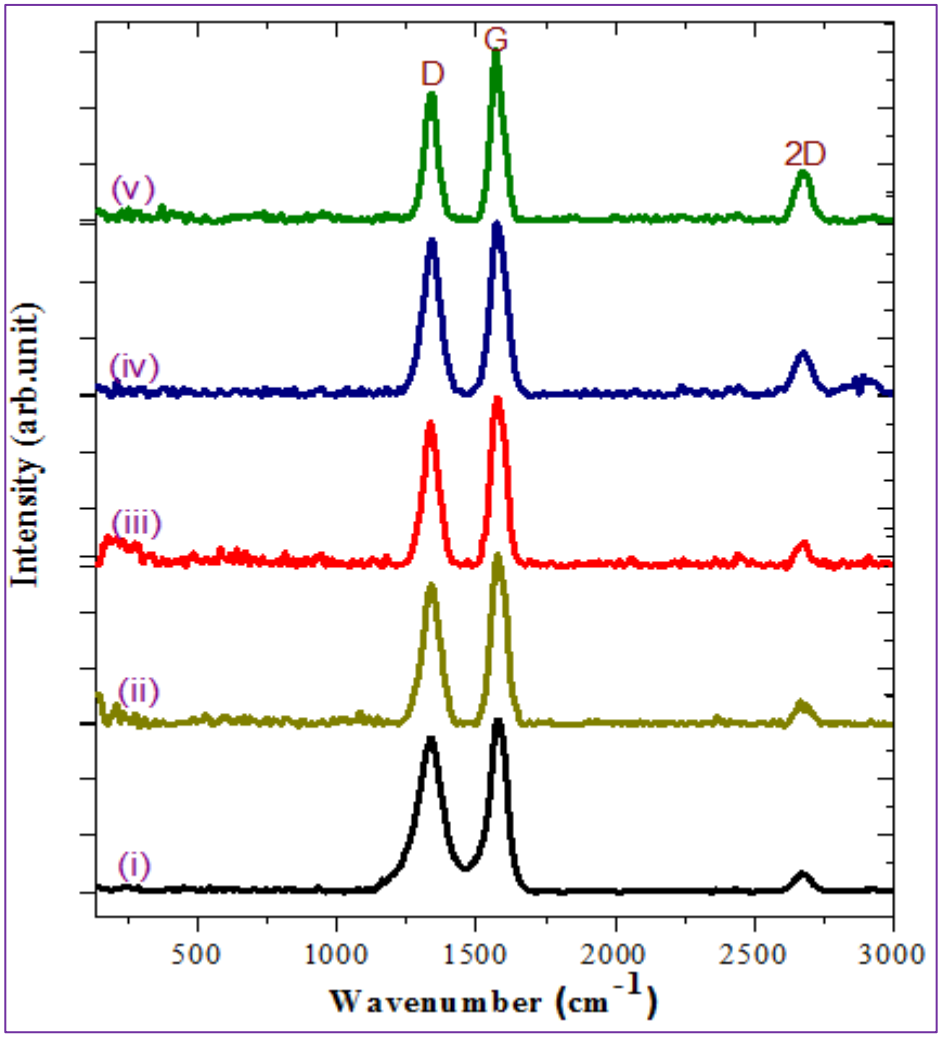

Figure 4.4: Raman spectra of (i) *in situ* N-MWCNTs (ii) *ex situ* N-MWCNTs (iii) fMWCNTs (iv) *in situ* fN-MWCNTs (v) *ex situ* fN-MWCNTs.

One of the disadvantages of Raman spectroscopy is its inability to detect impurities at low concentrations [20]. Thus, the impurities detected by XRD were not observed by Raman spectroscopy. However, it was successfully used to assess the defects of the functionalized MWCNTs using the intensity ratios of D (1300 cm^{-1}) to G (1500 cm^{-1}) bands [34]. The D band corresponds to the structural defects and disorder of carbon materials (i.e.: sp^3 and unstable sp^2 carbon) while the G band is associated with the tangential vibrations of stable sp^2 carbon atoms [16], [32], [35]. The concept is such that low ID/IG ratio (ID/IG <1) shows highly graphitic CNTs and the converse implies that there are higher defects in the lattice [36].

However, the intensity of the D band can be affected by the excitation wavelength of the laser and to some extent by the impurities [37]. On the contrary, 2D band responds from a two phonon process, thus its intensity is particularly sensitive to amorphous sp^2 carbons in the continuous benzene rings of the MWCNTs [38]. Thus, the intensity ratios of 2D band (2679 cm^{-1}) to G (1500 cm^{-1}) was also used to infer the defects of the nanotubes [37]. In this study, the ID/IG ratio and 2D/IG ratio were in agreement. The defects inferred are reported in Table 4.4 and they are attributed to the presence of nitrogen, and/or the oxygenated functionalities from acid treatment. This is particularly true for *in situ* N-MWCNTs and *in situ* fN-MWCNTs. The *ex situ* N-MWCNTs and *ex situ* fN-MWCNTs on the other hand could have gained more defects from the post thermal treatment, which could possibly create dangling bonds [17].

Table 4.4: Intensity ratios of the Raman bands used to determine the level of defects in the functionalized MWCNTs

Sample name	ID/IG	2D/IG
fMWCNTs	0.770	0.113
in situ N-MWCNTs	0.814	0.128
ex situ N-MWCNTs	0.645	0.068
in situ fN-MWCNTs	0.917	0.384
ex situ fN-MWCNTs	0.821	0.300

4.2.6 Thermogravimetric analysis (TGA) of the functionalized MWCNTs

Figures 4.4a and 4.4b show TGA and DTG data of the functionalized MWCNTs analyzed in air atmosphere respectively. TGA and DTG were used to evaluate the thermal stability of the functionalized MWCNTs and to characterize their level of purity. The thermal stability was identified at the oxidation temperature which is at the peak of the derivative weight loss [20], [38]. The crystallinity of the nanotubes structure, number of walls, presence of metal catalyst,

and the level of defects in the lattice play an important role in the thermal stability of the MWCNTs' overall structure [39]. Multiple peaks were observed from the DTG graphs of N-MWCNTs. These peaks were attributed to the decomposition of foreign materials that were present in the MWCNTs. The peaks observed at ~400 ^{o}C were attributed to the presence of amorphous carbon since it has been reported that they decompose at lower temperatures while the peaks at ~600 ^{o}C were attributed to the decomposition of the highly crystalline carbon [40], [41].

One of the unique advantages of *ex situ* nitrogen doping was the thermal annealing of the MWCNTs during the synthesis process. As a result, any impurities that might have been absorbed by the MWCNTs when it was exposed to air tend to be removed resulting in higher crystalline nanotubes [29]. Thus, the oxidation temperature of *ex situ* N-MWCNTs was higher than fMWCNTs. This could also be attributed to the lower defects of *ex situ* N-MWCNTs as compared to fMWCNTs as revealed by Raman spectroscopy results. In addition, XRD also revealed that *ex situ* N-MWCNTs were more graphitic relative to the other materials, which agrees with the observation from the TGA results. On the other hand, *in situ* N-MWCNTs had a lower thermal stability relative to fMWCNTs owing to their relatively high defects, impurities, and the fact that their method of functionalization was in exclusion of post thermal-treatment. The *in situ* synthesized fN-MWCNTs had the lowest thermal stability which was influenced by the high defects which resulted from acid treatment and nitrogen doping. TGA profiles also showed residual masses of ~19% and ~9% for the *in situ* and *ex situ* N-MWCNTs, respectively, while fMWCNTs and the fN-MWCNTs (both *in situ* and *ex situ*) showed insignificant residual masses. The residual masses observed from the N-MWCNTs samples were due to the metal catalyst that was used to fabricate the materials [7]. Although *ex situ* N-MWCNTs showed only 9% of residual catalyst, its derivative peak was wider with multiple peaks.

This could probably be the decomposition of the "secondary MWCNTs" which formed during *ex situ* doping process as observed from TEM and SEM images.

Furthermore, there were peaks exhibited at temperatures ~710 ^{o}C and ~785 ^{o}C, from DTG graphs of *in situ* and *ex situ* N-MWCNTs. These peaks are typically used to confirm that the

nanotubes are multiwalled [20]. The TGA profiles of *in situ* N-MWCNTs and *ex situ* N-MWCNTs also showed humps at temperatures ~620 ^{o}C and ~683 ^{o}C due to incomplete oxidation [40], [42]. Incomplete oxidation occurs when metal oxides provide oxygen required by the reaction and/or restrain the heat transfer creating localized hot spots, thus facilitating the oxidation of carbon resulting in incomplete oxidation as observed [39], [42], [43].

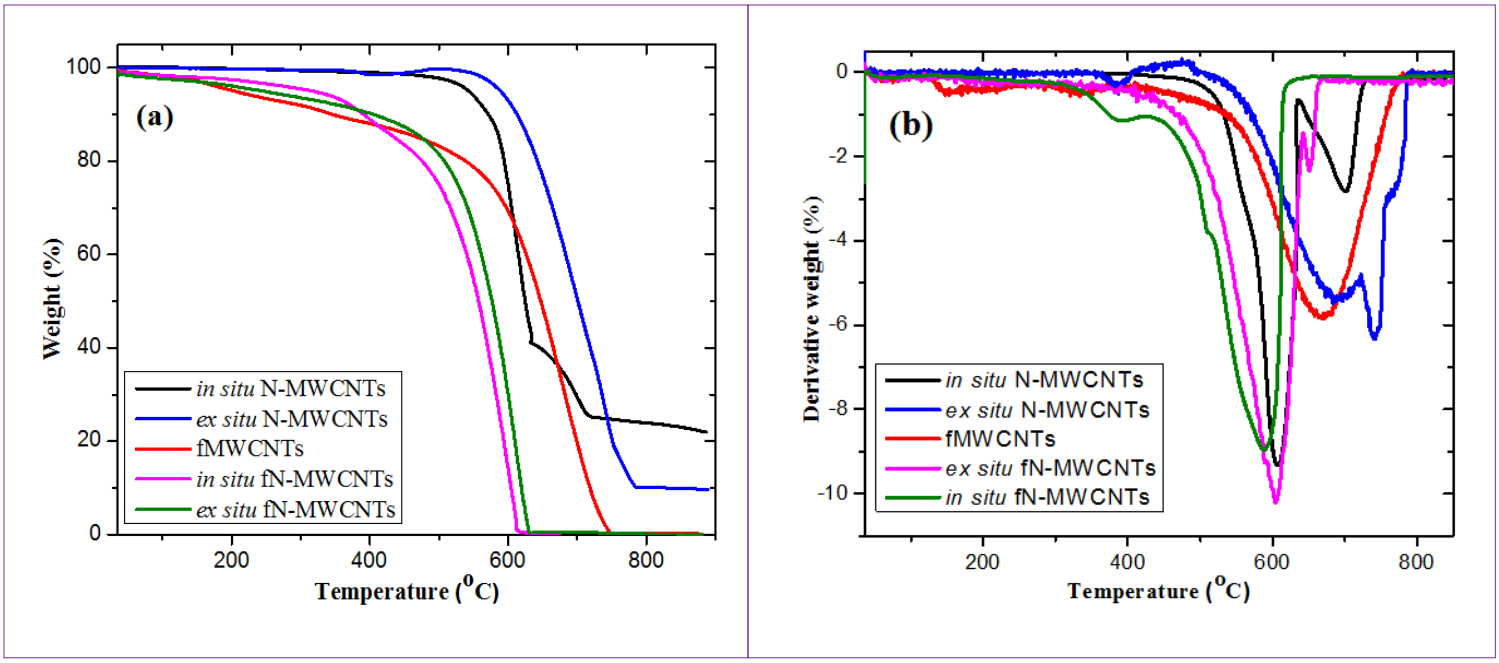

Figure 4.5: Thermal analysis plots of all the functionalized MWCNTs. (a) TGA profiles and (b) DTG profiles of obtained under air.

The TGA under N_2 atmosphere was performed to elucidate the temperature effect on the surface functionalities during *in situ* and *ex situ* doping methods. It has been reported that MWCNTs remain stable at higher temperatures under inert atmosphere because oxidation is hindered [20], [44]. However, *ex situ* fN-MWCNTs and *in situ* fN-MWCNTs in Figure 4.5 showed a weight loss at temperatures ~60, ~375, ~659 ^{o}C and ~779 ^{o}C. The weight loss observed around 60 ^{o}C was ascribed to the loss of H_2O, from the –OH functional groups [45]. Furthermore, the mass decrease observed at temperatures around 779 ^{o}C was attributed to the loss of oxygen atoms tightly bonded to the surface of the CNTs.

However, the *ex situ* fN-MWCNTs DTG profile exhibited no peak correlating to a loss of oxygen atoms. This insinuated that during *ex situ* doping of MWCNTs, a significant amount of oxygen atoms are desorbed. The loss of oxygen functional groups on *ex situ* fN-MWCNTs was further confirmed by SEM-EDS analysis (**Section 4.2.6**) which showed that the atomic% of oxygen in *ex situ* fN-MWCNTs was 6.48%, whilst *in situ* fN-MWCNTs contained 10.22% of oxygen atoms. Nevertheless, the peaks assigned to the formation of CO_2 (around 375 ^{o}C) as well as both CO and CO_2 generation (around 659 ^{o}C) were observed to be highly intense at low temperatures on the *ex situ* fN-MWCNTs profile compared to *in situ* fN-MWCNTs. The high intensities of these peaks (375 and 659 ^{o}C) suggests that the desorbed oxygen atoms during *ex situ* doping were further re-adsorbed after reacting with CH_3CN. On the other hand, the low temperatures of the peaks at 375 and 659 ^{o}C on *ex situ* fN-MWCNTs relative to *in situ* fN-MWCNTs revealed that the functional groups on *in situ* fN-MWCNTs lattice were more tightly bonded relative to *ex situ* fN-MWCNTs. This is due to the It is noteworthy that the residual weight percentages (assigned to stable carbon) from the TGA profiles below were an accession of the elemental carbon estimated by the carbon and nitrogen analysis (**Section 4.2.3**)

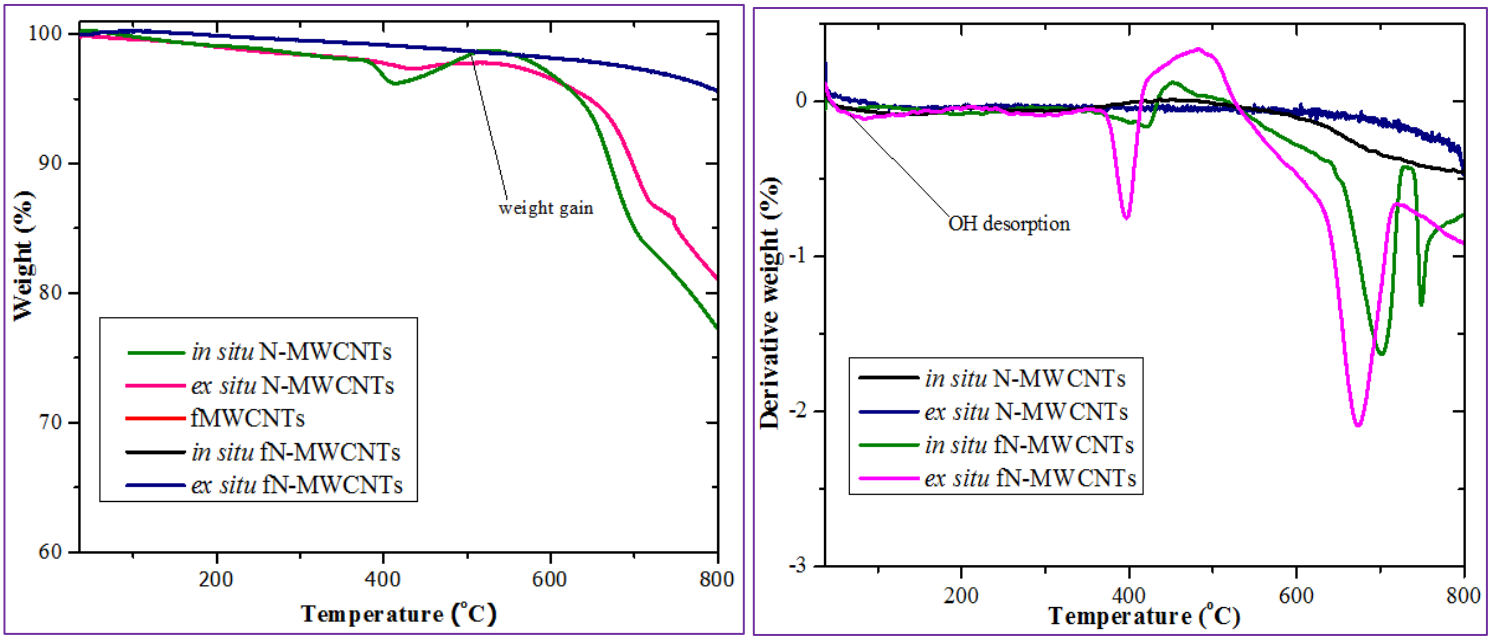

Figure 4.6: Thermal analysis plots of all the functionalized MWCNTs. (a) TGA profiles and (b) DTG profiles of obtained under N_2 atmosphere.

4.2.7 BET Surface area and pore volume analysis of the functionalized MWCNTs

The BET method is one of the important techniques in catalysis because it determines the surface areas of solids. The BET surface area of a material is proportional to the active sites, thus the adsorption rate of the studied materials may be predicted. Table 4.5 showed that the surface area of *in situ* doped and *ex situ* doped N-MWCNTs increased from 78.1 and 77.9 to 111.6 and 107.9 m^2/g after acid-treatment (fN-MWCNTs), respectively. This was attributed to the removal of amorphous carbon, black carbon, residue catalyst which opened inner cavities which can expose the internal surface area of the carbon materials [26]. In addition, the large surface area of the *in situ* fN-MWCNTs accord closely with the TGA and CHNS results which showed the presence of high functional groups in the lattice. These functionalities are responsible for the repulsion between the MWCNTs resulting in more exposed active sites. Furthermore, there was no difference in the pore volumes of the *ex situ* N-MWCNTs and *ex situ* fN-MWCNTs. This observation also confirmed that *ex situ* doping tends to remove the impurities through heat treatment and thus opens up the pores of the MWCNTs.

Table 4.5: Specific surface areas of all the functionalized MWCNTs determined from BET technique

Sample name	Surface area (m^2/g)	Pore volume (cm^3/g)
fMWCNTs	101. 6	15.8
in situ N-MWCNTs	78.1	12.1
ex situ N-MWCNTs	77.9	13.1
in situ fN-MWCNTs	111.6	15.9
ex situ fN-MWVNTs	107.9	13.1

4.3. Conclusion

This chapter summarized the effects of *in situ* versus *ex situ* nitrogen doping of MWCNTs. Besides the drawbacks of *ex situ* doping that have been referenced from literature, it has been discovered that during *ex situ* N-doping, branched MWCNTs may be obtained as by products. This can be avoided by using a non-carbon containing doping solvent, such as NH_3. However, this observation still requires thorough investigation to be confirmed. Nevertheless, MWCNTs were successfully doped with N atoms using both *in situ* and *ex situ* doping methods. The success of nitrogen doping was evinced by defects, narrower tubes, and low thermal stability and bamboo compartments. However, the bamboo compartments were only observed on *in situ* doped MWCNTs. The nitrogen doping content was quantified using C and N elemental analysis technique.

It was observed that a very low percentage (0.15%) of nitrogen was incorporated on *ex situ* N-MWCNTs from elemental analysis. Nonetheless, acid-treatment improved N anchoring sites on the *ex situ* N-MWCNTs, and removed the impurities from the *in situ* N-MWCNTs while simultaneously adding oxygen-containing functional groups. However, improving the anchoring sites on the *ex situ* N-MWCNTs was accompanied by a loss of oxygen functional groups. Based

on TGA analyses under N_2 atmosphere, the oxygenated functional groups were lost with increase in temperature in a form of H_2O and CO_2. Thus, the low % of oxygenated functional groups on *ex situ* fN-MWCNTs suggested that during ramping period of *ex situ* functionalization, the -OH and -COOH groups were lost, creating vacancies for N incorporation. Thus, it is crucial to consider whether the application of the *ex situ* fN-MWCNTs will require higher content of oxygenated functional groups or higher N contents. Based on this judgment, the *ex situ* doping can either be done by pre-functionalizing the MWCNTs prior to *ex situ* N doping or post-functionalization after *ex situ* N doping.

In comparison, *ex situ* N-MWCNTs paraded high by-products (impurities) from its broad DTG peak, with 10% less catalyst residue while *in situ* N-MWCNTs had a sharp DTG peak with high catalyst residue. This insinuates that the impurities on *ex situ* N-MWCNTs may be other carbon materials such as amorphous carbon, and the secondary MWCNTs. The inner diameter of fMWCNTs increased after *ex situ* doping from 9.8 to 12.3 nm. But the explanation for this observation remains unclear. On the other hand, there was a decrease in the inner diameter of *in situ* N-MWCNTs after acid-treatment (*in situ* fN-MWCNTs). The surface areas of the studied materials were in the following order: *in situ* fN-MWCNTs > *ex situ* fN-MWCNTs> fMWCNTs > *in situ* N-MWCNTs ~ *ex situ* N-MWCNTs. From the surface area data, it may be concluded that the *in situ* MWCNTs will be the best supporting material for TiO_2 due to the presence of more cavities to form a strong interphase with the TiO_2.

4.4 References

[1] J. H. Lehman, M. Terrones, E. Mansfield, K. E. Hurst, and V. Meunier, "Evaluating the characteristics of multiwall carbon nanotubes," *Carbon*, vol. 49, no. 8, pp. 2581–2602, 2011.

[2] L. Mabena, S. Sinha Ray, S. Mhlanga, and N. Coville, "Nitrogen-doped carbon nanotubes as a metal catalyst support," *Applied nanoscience*, vol. 1, no. 2, pp. 67–77, 2011.

[3] A. Ibhadon, and P. Fitzpatrick, "Heterogeneous photocatalysis: Recent advances and applications," *Catalysts*, vol. 3, no. 1, pp. 189–218, 2013.

[4] O. Y. Podyacheva and Z. R. Ismagilov, "Nitrogen-doped carbon nanomaterials: To the mechanism of growth, electrical conductivity and application in catalysis," *Catalysis today*, vol. 249, pp. 12–22, 2015.

[5] R. Das, S. B. A. Hamid, M. Ali, A. Ismail, S. Ramakrishna, "Multifunctional carbon nanotubes in water treatment: The present, past, and future," *Desalination*, vol. 354, no. 11, pp. 160-179, 2014.

[6] E. N. Nxumalo, P. J. Letsoalo, L. M. Cele, and N. J. Coville, "The influence of nitrogen sources on nitrogen doped multiwalled carbon nanotubes," *Journal of organometallic chemistry*, vol. 695, no. 24, pp. 2596–2602, 2010.

[7] M. Mamo, A. O. Sustaita, Z. N. Tetana, N. J. Coville, and I. Hümmelgen, "Nitrogen-doped, boron-doped and undoped multiwalled carbon nanotube/polymer composites in WORM memory devices.," *Nanotechnology*, vol. 24, no. 12, pp. 125–273, 2013.

[8] Z. N. Tetana, "Boron and nitrogen doped carbons for photochemical degradation reactions by," *Thesis*, pp. 1–235, 2013.

[9] L. Hlekelele, P. Tripathi, P. J. Franklyn, and S. H. Durbach, "Morphological and crystallinity differences in nitrogen- doped carbon nanotubes grown by chemical vapour deposition decomposition of melamine over coal fly ash.," *RSC Adv.*, vol. 6, pp. 76773–76779, 2016.

[10] P. K. Kahol, K. K. Satheesh Kumar, S. Geetha, and D. C. Trivedi, "Effect of dopants on

electron localization length in polyaniline," *Synthetic metals*, vol. 139, no. 2, pp. 191–200, 2003.

[11] D. R. Paul, W. J. Koros, R. Liu, Y. Hu, E. Baer, A. Hiltner, and H. D. Keith, "Nitrogen-Doped Carbon Nanotube," *Material and methods*, vol. 323, no. 6, PP. 1–19, 2009.

[12] C. Duong-Viet, B. Housseinou, T. Lai, L. Yuefeng , J. Tessonnier, J. Nhut, P. Granger, and C. Pham-Huu "Nitrogen-doped carbon composites as metal-free catalysts,"*Journal of materials and synthesis,* vol. 34, no. 3, pp. 234-267, 2017.

[13] A. Q. Zhao, J. Masa, and W. Xia, "Very low amount of TiO_2 on N-doped carbon nanotubes significantly improves oxygen reduction activity and stability of supported Pt nanoparticles," *Physical chemistry chemical physics*, vol. 17, no. 16, pp. 10767–10773, 2015.

[14] M. A. Kanygin, O. V. Sedelnikova, I. P. Asanov, L. G. Bulusheva, A. V. Okotrub, P. P. Kuzhir, A. O. Plyushch, S. A. Maksimenko, K. N. Lapko, A. A. Sokol, O. A. Ivashkevich, and P. Lambin, "Effect of nitrogen doping on the electromagnetic properties of carbon nanotube-based composites," *Journal of applied physics*, vol. 113, no. 14, pp. 1–9, 2013.

[15] Q. Wei, X. Tong, G. Zhang, J. Qiao, Q. Gong, and S. Sun, "Nitrogen-doped carbon nanotube and graphene materials for oxygen reduction reactions," *Catalysts*, vol. 5, no. 3, pp. 1574–1602, 2015.

[16] B. J. Matsoso, K. Ranganathan, B. K. Mutuma, T. Lerotholi, G. Jones, and N. J. Coville, "Time-dependent evolution of the nitrogen configurations in N-doped graphene films," *RSC Adv.*, vol. 6, no. 108, pp. 106914–106920, 2016.

[17] H. Cheng, C. Lua, J. Liua, Y. Yana, X. Hanb, H. Jina,Y. Wang, Y. Liu, C. Wu "Synchrotron radiation X-ray powder diffraction techniques applied in hydrogen storage materials - A review," *Progress in Natural Science: Materials international*, vol. 27, no. 1, pp. 66–73, 2017.

[18] S. D. Mhlanga, K. C. Mondal, R. Carter, M. J. Witcomb, and N. J. Coville, "The effect of synthesis parameters on the catalytic synthesis of multiwalled carbon nanotubes using Fe-

Co/$CaCO_3$ catalysts," *South African Journal of Chemicals*, vol. 62, pp. 67–76, 2009.

[19] N. Phao, E. N. Nxumalo, B. B. Mamba, and S. D. Mhlanga, "A nitrogen-doped carbon nanotube enhanced polyethersulfone membrane system for water treatment," *Physics and chemistry of the earth*, vol. 66, no. 1, pp. 148–156, 2013.

[20] M. A. M. Motchelaho, H. Xiong, M. Moyo, L. L. Jewell, and N. J. Coville, "Effect of acid treatment on the surface of multiwalled carbon nanotubes prepared from Fe-Co supported on $CaCO_3$: Correlation with Fischer-Tropsch catalyst activity," *Journal of molecular catalysis A: chemical*, vol. 335, no. 2, pp. 189–198, 2011.

[21] R. Lee, P. Nikolaev, H. Dai, P. Petit, J. Robert, C. Xu, Y. Lee, S. Kim, and S.G. Rinzler, "Crystalline Ropes of Metallic Carbon Nanotubes," *Science*, vol. 273, no. 5274, pp. 483–487, 1996.

[22] N. O. Ramoraswi and P. G. Ndungu, "Photo-catalytic properties of TiO_2 supported on MWCNTs, SBA-15 and Silica-Coated MWCNTs nanocomposites," *Nanoscale research letters*, vol. 10, no. 1, pp. 4–27, 2015.

[23] J. Majewska and B. Michalkiewicz, "Low temperature one-step synthesis of cobalt nanowires encapsulated in carbon," pp. 1013–1016, 2013.

[24] A. N. Suboch, S. V. Cherepanova, L. S. Kibis, D. A. Svintsitskiy, O. A. Stonkus, A. I. Boronin, V. Chesnokov, A. I. Romanenko, Z. R. Ismagilov, "Observation of the superstructural diffraction peak in the nitrogen doped carbon nanotubes: simulation of the structure," *Fullerenes, nanotubes and carbon nanostructures*, vol. 24, no. 8, pp. 1–26, 2016.

[25] N. Chiwaye, L. L. Jewell, D. G. Billing, D. Naidoo, M. Ncube, and N. J. Coville, "*In situ* powder XRD and Mössbauer study of Fe-Co supported on $CaCO_3$," *Materials research bulletin*, vol. 56, no. 2, pp. 98–106, 2015.

[26] B. Gao, G. Z. Chen, and G. Li Puma, "Carbon nanotubes/titanium dioxide (CNTs/TiO_2) nanocomposites prepared by conventional and novel surfactant wrapping sol-gel methods exhibiting enhanced photocatalytic activity," *Applied catalysis B: Environmental*, vol. 89, no. 4, pp. 503–509, 2009.

[27] Y. Xiong, Z. Li, Q. Guo, and Y. Xie, "Synthesis of Multiwalled and bamboo-like Well-crystalline CNx," *Society*, vol. 44, no. 19, pp. 6506–6508, 2005.

[28] R. Jin, Z.X. Zhoua, and D. Mandrus, "The effect of annealing on the electrical and thermal transport properties of macroscopic bundles of long multi-wall carbon nanotubes," *Physica B: Condensed matter*, vol. 388, no. 2, pp. 326–330, 2007.

[29] F. Ghaemi, L. C. Abdullah, and Paridah Tahir, "Core/Shell structure of Ni/NiO encapsulated in carbon nanosphere coated with few- and multi-layered graphene: Synthesis, Mechanism and Application," *Polymers*, vol. 123, no. 4, 2016.

[30] S. Darbari, Y. Abdi, F. Haghighi, S. Mohajerzadeh, and N. Haghighi, "Investigating the antifungal activity of TiO_2 nanoparticles deposited on branched carbon nanotube arrays," *Journal of Physics D: Applied physics*, vol. 44, no. 24, p. 245401, 2011.

[31] E. N. Nxumalo and N. J. Coville, "Nitrogen doped carbon nanotubes from organometallic compounds: A review," *Materials*, vol. 3, no. 3, pp. 2141–2171, 2010.

[32] M. S. Dresselhaus, G. Dresselhaus, R. Saito, and A. Jorio, "Raman spectroscopy of carbon nanotubes," *Physics reports*, vol. 409, no. 2, p. 47, 2005.

[33] H. Jantoljak, J. P. Salvetat, L. Forr, and C. Thomsen, "Low-energy Raman-active phonons of multiwalled carbon nanotubes," *Applied physics A: Materials science & processing*, vol. 67, no. 1, pp. 113–116, 1998.

[34] D. Christofilos, J. Arvanitidis, E. Efthimiopoulos, X.Zhao, "High pressure Raman studies of carbon nanotube materials," *Journal of Physics: Conference series*, vol. 121, no. 16, p. 162–193, 2008.

[35] S. D. Mhlanga, E. N. Nxumalo, N. J. Coville, and V. V. Srinivasu, "Nitrogen doping of CVD multiwalled carbon nanotubes: Observation of a large g-factor shift," *Materials chemistry and physics*, vol. 130, no. 3, pp. 1182–1186, 2011.

[36] B. K. Mutuma, B. Matsoso, K. Ranganathan, D. Wamwangi, and N. J. Coville, "Generation of open-ended, worm-like and graphene-like structures from layered spherical carbon materials," *RSC Adv.*, vol. 6, no. 24, pp. 20399–20408, 2016.

[37] R. A. DiLeo, B. J. Landi, and P. Raffaelle, "Purity assessment of multiwalled carbo nanotubes by Raman spectroscopy, "*AIP Journal of Applied Physics*, vol 101, no. 6, pp. 64–307, 2007.

[38] Y. C. Choi, K. Min, and M. S. Jeong, "Novel method of evaluating the purity of multiwalled carbon nanotubes using Raman spectroscopy. *Journal of Nanomaterials*, vol. 10, no. 115, pp. 1–6, 2013.

[39] T. N. Phaahlamohlaka, "Synthesis of carbon nanofibers and their subsequent use as catalyst supports for Fischer- Tropsch synthesis ," *Thesis*, pp 1–289, 2013.

[40] G. Widmann, "Interpreting TGA curves," *UserCom*, pp. 1–20, 2001.

[41] M. A. M. Motchelaho, "Iron and Cobalt Catalysts Supported on Carbon Nanotubes for Use in the Fischer-Tropsch Synthesis," 2011.

[42] A. R. Harutyunyan, B. K. Pradhan, J. Chang, G. Chen, P. C. Eklund, "Purification of single walled carbon nanotubes by selective microwave heating of catalystparticles," *Journal of physical chemistry B*, vol. 106 no. 33, pp. 86–71 (2002)

[43] X. Su, Y. Shuai, Z. Guo, and Y. Feng, "Functionalization of multi-walled carbon nanotubes with thermo-responsive azide-terminated poly(N-isopropylacrylamide) via click reactions," *Molecules*, vol. 18, no. 4, pp. 4599–4612, 2013.

[44] P. Y. Du, H. Li, X. Fu, W. Gu, and X. Liu, "A 1D anionic lanthanide coordination polymer as an adsorbent material for the selective uptake of cationic dyes from aqueous solutions," *RCS Dalton Transaction home*, vol. 44, no. 30, pp. 13752–13759, 2015.

[45] N. A. Mansor, J. Tessonnier, M. G. Kutty, R. Schlögl, and S. B. A. Hamid, "Chemically Modified Carbon Nanotubes (CNTs) with Oxygen and Sulfur Containing Functional Groups for Adsorption of Mercury," *Material science*, vol. 20, pp. 66–70, 2011.

5

Chapter five

Study of TiO_2-based composites

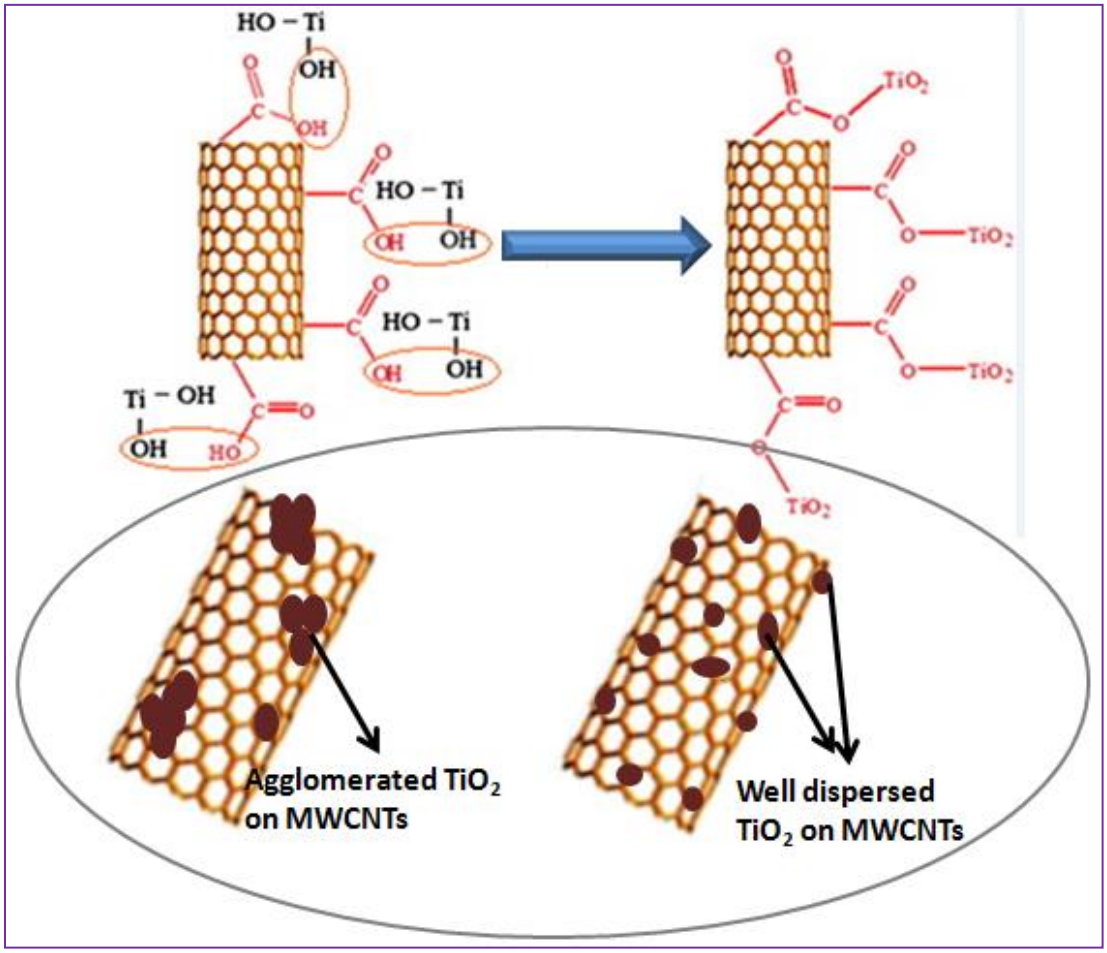

5.1 Overview

Considerable efforts have been devoted to the design of ideal photocatalysts for many reactions. Various semiconductors have been explored in a wide range of photocatalytic applications to alleviate the steadily worsening environmental issues and energy crisis [1]. However, the established photocatalysts require further examination to improve their overall efficiency in photocatalysis. For instance, titanium dioxide (TiO_2) has been fervently researched due to its high refractive index, long-term stability, high reactivity, reduced toxicity, and UV absorption [2], [3]. However, its quantum efficiency is limited by drawbacks inclusive of (i) sintering (ii) low affinity to organic pollutants which result in high mass transfer limitation; and (iii) electron-hole recombination which causes low quantum yield of excitons [4]–[6]. Thus there is a need for more research in controlling its particle size, phase composition, and chemical composition in order to achieve its maximized quantum efficiency.

Previous work reported that supporting TiO_2 on moderate amount of functionalized multiwalled carbon nanotubes (MWCNTs) enhances its quantum efficiency for sensor devices, hydrogen evolution and photocatalysis, to name a few [7]. The addition of MWCNTs form a lower Fermi level leaving an excess of valence band holes in the TiO_2 to migrate to the surface and initiate the photocatalysis reaction [8], [9]. Furthermore, MWCNTs can be tailored by doping them with nitrogen (N-MWCNTs) to improve the formation of semiconductor-metal junction where electrons flow from the material with a higher Fermi level to lower Fermi level, hence achieving charge separation. In addition, nitrogen doped multiwalled carbon nanotubes (N-MWCNTs) accelerate electron transfer in the photocatalysis system, enhance the binding energy of TiO_2 to the carbon which may reduce the TiO_2 particle size, and create new adsorption sites minimizing mass transfer limitation [10]. Certainly, the enhancement of TiO_2's photocatalytic activity relies on the surface, charge kinetics, and energy band engineering.

Thus, this chapter is aimed at exploiting the dispersion degree of TiO_2 on MWCNTs, and synergistic benefits of combining the two [7], [11]. Ideally, TiO_2 particles should be homogenously dispersed on the MWCNTs for them to harvest light evenly [12]. The output of

the composite structure is controlled by surface functionalization of the MWCNTs (studied in chapter 4), method of synthesis, and the amount of TiO_2 added on the MWCNTs [11]. In this study, convenient sol-gel method was used to add 80% of TiO_2 on functionalized MWCNTs. The nanocomposites were named based on the type of functionalization that was done on the MWCNTs. Thus, the composites studied in this chapter are referred to as TiO_2/fMWCNTs, *in situ* TiO_2/N-MWCNTs, *in situ* TiO_2/fN-MWCNTs, *ex situ* TiO_2/N-MWCNTs, and *ex situ* TiO_2/fN-MWCNTs.

5.2 Results and Discussion

TiO_2 possesses vital properties that largely influence its photocatalytic activity: crystal phase, surface area, exposed crystal facets, uncoordinated surface sites, defects in the lattice, and degree of crystallinity. These properties can be effectively controlled by tuning its morphology via synthesis of composite materials.

5.2.1 Phase identification studies of the TiO_2-based composites

Figure 5.1 displays the XRD profiles of commercial TiO_2 and various samples of supported TiO_2 catalysts. All the XRD patterns showed characteristic peaks for TiO_2 in the anatase phase. These patterns were in accord with the anatase characteristic peaks (ICOD 00-021-1272). Although the anatase peak (101) is usually observed at $2\Theta = 26^{\circ}$, the shift of this peak in this study was primarily attributed to the large crystallite size of the TiO_2 which could be due to m probably due to the peaks interference effect [13]. In addition, many other factors such as the structure, lattice and the pH may contribute to the shift of the peak position [13]. Furthermore, the (101) peak is typically used to determine the crystallite sizes [13], [14]. However, the same peak cannot be used for the supported TiO_2 since it overlaps with the graphitic carbon peak (002) which is reflected in the same region [15]. In lieu, the peak at $2\Theta = 56.5^{\circ}$ which is characteristic of pure anatase TiO_2 in all the analyzed samples was used. With the aid of Scherrer equation, the crystallite size of commercial TiO_2 was determined to be 63.5 nm, whilst the TiO_2 on *in situ* fN-MWCNTs had the crystallite size of 5.64 nm. In addition, the high intensity peak of the

commercial TiO_2 relative to the *in situ* TiO_2/fN-MWCNTs ratified the estimated crystallite sizes. This was reckoned by the fact that *in situ* fN-MCNTs has a strong affinity for TiO_2 due to the net positive charge on the carbons atoms, resulting to smaller particle sizes of TiO_2 [16].

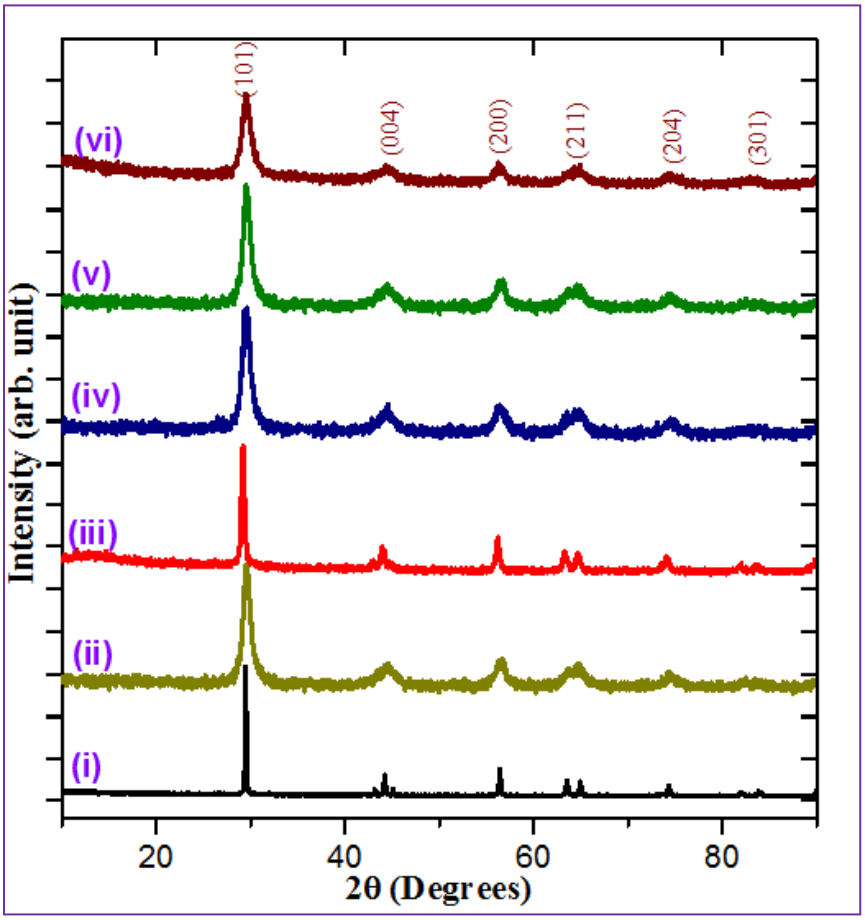

Figure 5.1: XRD diffractograms of TiO_2-based composites (i) TiO_2 (ii) *in situ* TiO_2/N-MWCNTs (iii) *ex situ* TiO_2/N-MWCNTs (iv) TiO_2/fMWCNTs (v)*in situ* TiO_2/fN-MWCNTs (vi) *ex situ* TiO_2/fN-MWCNTs.

Moreover, the width of the (211) peak increased from *ex situ* TiO_2/N-MWCNTs < *in situ* TiO_2/N-MWCNTs< TiO_2/fMWCNTs < *ex situ* TiO_2/fN-MWCNTs< *in situ* TiO_2/fN-MWCNTs. This observation correlates with the decrease in TiO_2 crystallite size in the composites. The interplanar spacing between atoms was also calculated by using the Bragg's law. The obtained

results are reported in Table 5.1 below. It is likely that TiO_2 particles with small crystallite experience high strain which causes coulumbic repulsion between the particles [17]. Consequently, the interplanar spacing increased with decrease of TiO_2 crystallite sizes.

The specific surface areas (SSA) of the samples were also determined using the following formula: $S = \frac{6 \times 10^3}{D_P \rho}$, where D_p is the crystallite size and ρ is the density of TiO_2, such that ρ= 4.23 $g.cm^{-3}$ [18]. Notably, this formula was used with the assumption that the TiO_2 particles were homogeneously spherical [18]. The specific surface area (SSA) for TiO_2 was found to be 22.3 m^2/g. The difference of this SSA from the BET surface area was due to the inaccurate estimation of TiO_2 crystallite size.

Table 5.1: The properties of self-supported and MWCNTs supported TiO_2 that were determined from the XRD peaks.

Sample name	Crystallite sizes (nm)	D spacing (Å)
TiO_2	63.5	3.49
TiO_2/fMWCNTs	8.03	1.8941
in situ TiO_2/N-MWCNTs	10.23	1.9027
ex situ TiO_2/N-MWCNTs	23.6	1.9578
in situ TiO_2/fN-MWCNTs	5.64	1.8865
ex situ TiO_2/fN-MWCNTs	7.8	1.8913

5.2.2. Structural analysis of MWCNTs

The particle size, crystallinity and morphology of the TiO_2 were further examined using transmission electron microscope (TEM). Commercial TiO_2 (anatase) particles were at an average of 145 nm in size. There was an overlap of TiO_2 particles which could be an indication of its aggregation tendencies [19]. The micrographs of supported TiO_2 showed that the dispersion of TiO_2 can be largely improved by the inclusion of MWCNTs. However, the TiO_2 dispersion was affected by the type of functionalization of the MWCNTs. Notably, fMWCNTs

(acid-treated) exhibited better TiO_2 coverage than N-MWCNTs (both *in situ* and *ex situ*). Thus nitrogen doping independently, is not sufficient enough to prevent the sintering drawback of TiO_2. However, with the aid of acid-functionalization, *in situ* fN-MWCNTs and *ex situ* fN-MWCNTs showed a clear interaction between the TiO_2 and carbon. This could be due to the presence of –COOH groups in the acid-treated MWCNTs which readily formed Ti-O-C bonds with the titania. As a result, functionalization by both acid-treatment and nitrogen doping creates more active sites. Nevertheless, *ex situ* TiO_2/fN-MWCNTs were more of random composites rather that a clear coating of TiO_2. This was attributed to the agglomeration of *ex situ* fN-MWCNTs as observed in Chapter 4.

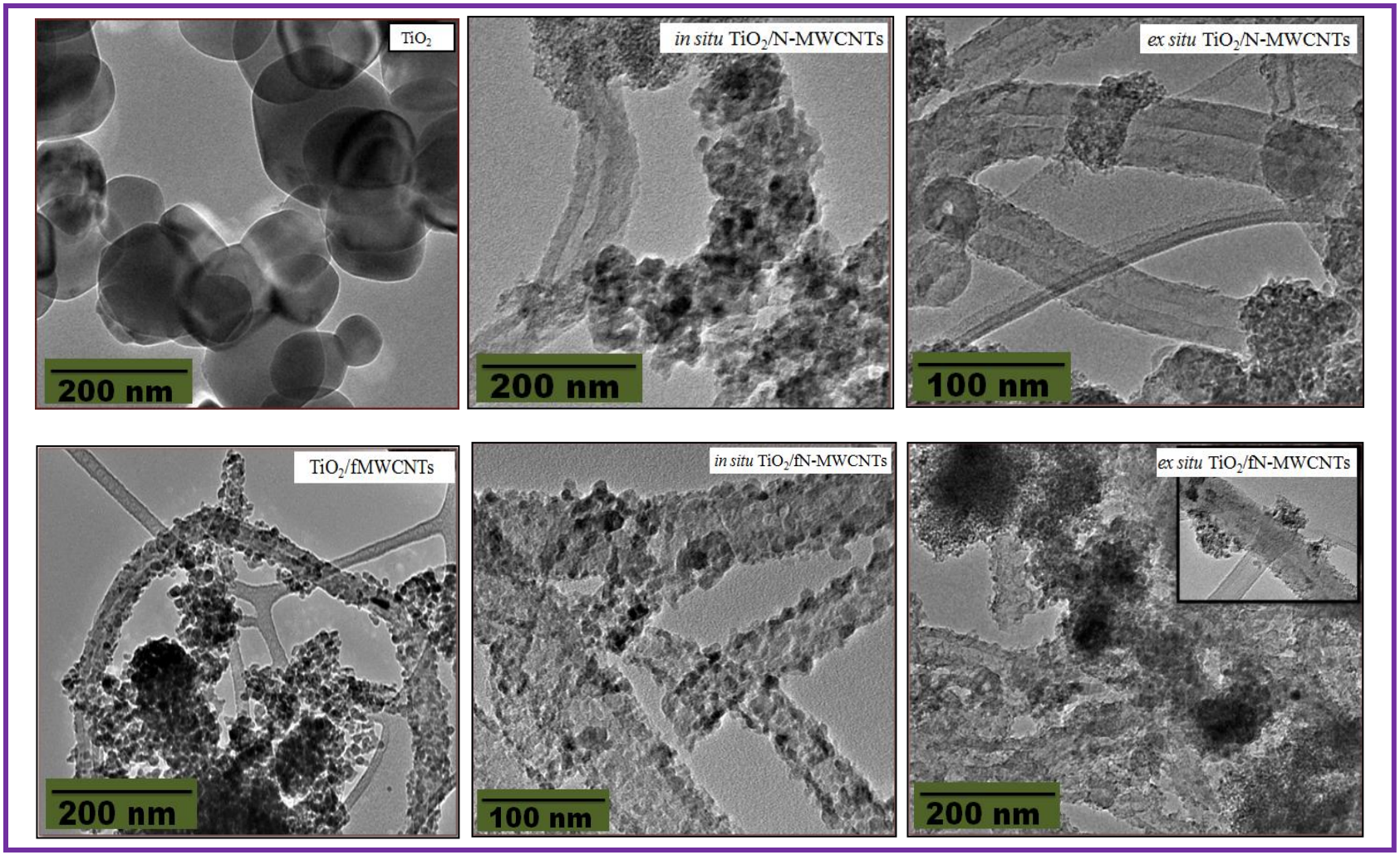

Figure 5.2: TEM micrographs of the commercial anatase TiO_2 and sol-gel TiO_2 on MWCNTs with different functionalization

5.2.3 Optical properties of the TiO_2/MWCNTs composites

TiO_2 is admired for its photostability and high redox potential [14], [19]. However, the wide band gap of TiO_2 restricts the use of the natural and abundant source of light, sun. The sun contains of 95% of visible light which makes it impossible to harness exitons from the TiO_2 photocatalyst [19]. Thus there is a need to modulate the properties of TiO_2 as means of making it a visible light-responsive photocatalyst. Figure 5.3 presents the UV-Vis spectra of the catalysts. The excitation wavelengths of the composites were at around 326 nm, which was slightly higher than the TiO_2's excitation wavelength observed at 322 nm. This could have been due to the conjugation of the double bonds in the MWCNTs lattice which allows л-electrons to readily transition from one state to another in the system.

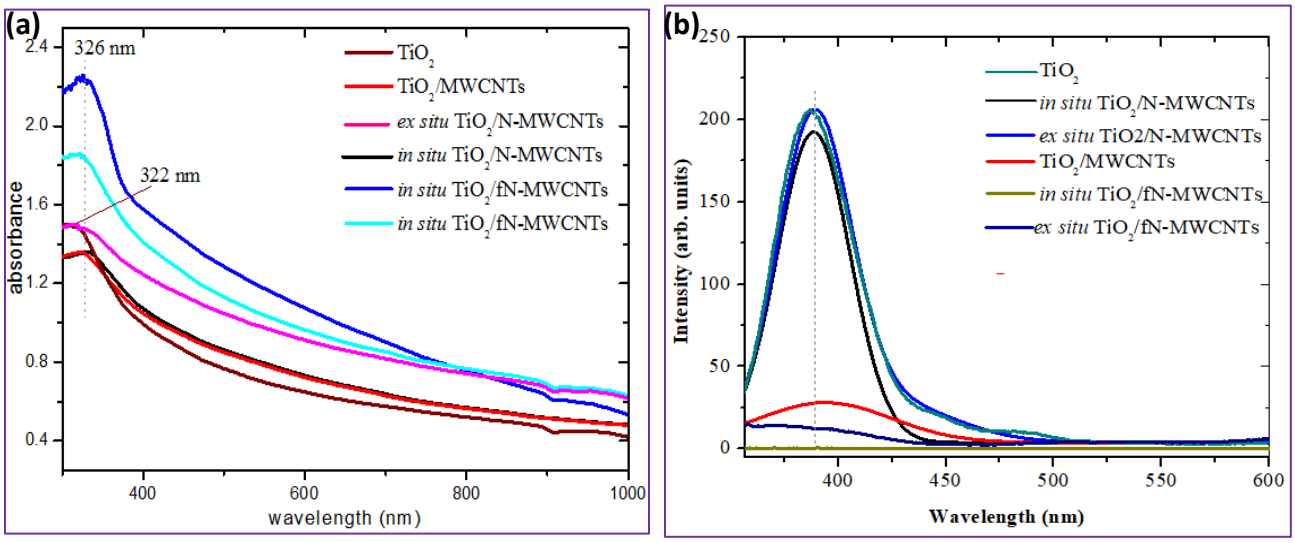

Figure 5.3: (a) PL and (b) UV-Vis spectra of the TiO_2/MWCNTs composites

In addition, the photoluminescence spectrophotometry was used to ascertain the emission peaks of the catalysts. This analysis gives an insight about the electron/hole charge recombination in the catalysts which fundamentally inhibits the photocatalysis process. Figure 5.4(b) revealed a reduction in the emission peaks on the carbon supported TiO_2. This was an indication that the MWCNTs could prevent the charge recombination. The TiO_2/N-MWCNTs spectra exhibited

poor capability to prevent the charge recombination. This was observed from the small reduction in the emission peak of TiO_2/N-MWCNTs compared to TiO_2/fN-MWCNTs.

5.2.4. Raman spectroscopy

Figure 5.3 shows the Raman spectra characteristics of all the TiO_2-based composites. The Raman spectrum of TiO_2 exhibited the typical vibrational bands of anatase at 400, 521 and 644 cm^{-1}. These bands corresponds to the Raman active modes E_g, B_{1g}, B_{1g} overlapping with A_{1g}, and E_g symmetry, respectively [13], [20]. This analysis confirms the identified anatase phase of TO_2 from the XRD pattern [20]. Similar Raman bands were also observed on the spectra of TiO_2 supported on functionalized MWCNTs. However, these bands were slightly shifted to higher frequencies, broadened and less intense. This was attributed to the fact that the TiO_2 on the MWCNTs had small particles and it was highly dispersed relative to the commercial TiO_2 [13]. In particular, the frequency shift of the E_g mode of composites was due to phonon confinement caused by a decrease in the size of anatase. Hence, as it was predicted from the crystallite size obtained from the XRD data, the E_g band of *in situ* TiO_2/fN-MWCNTs shifted comparatively higher indicating smaller TiO_2 crystal size of anatase. This observation shows that the kinetics of Ti-O-C formation were greater than the aggregation of the TiO_2 [4], [12].

Furthermore, the composites also exhibited the characteristic peaks corresponding to the MWCNTs at 1350 and 1600 cm^{-1} which are associated with the D and G bands, respectively [21], [22]. The Raman profiles portraying the D and G bands are presented in Figure 5.3(b) below. These Raman bands were suppressed by the strong intensity of TiO_2 bands as Figure 5.3(a) presented. However, the D and G bands of *ex situ* N-MWCNTs and *in situ* N-MWCNTs were relatively stronger, and could be observed. This was attributed to the uncoated areas of the carbon materials by TiO_2 as observed from TEM results [20]. Thus, it could be depicted that *in situ* fN-MWCNTs and *ex situ* fN-MWCNTs were fully covered with TiO_2 from the weak D and G bands relative to the anatase band.

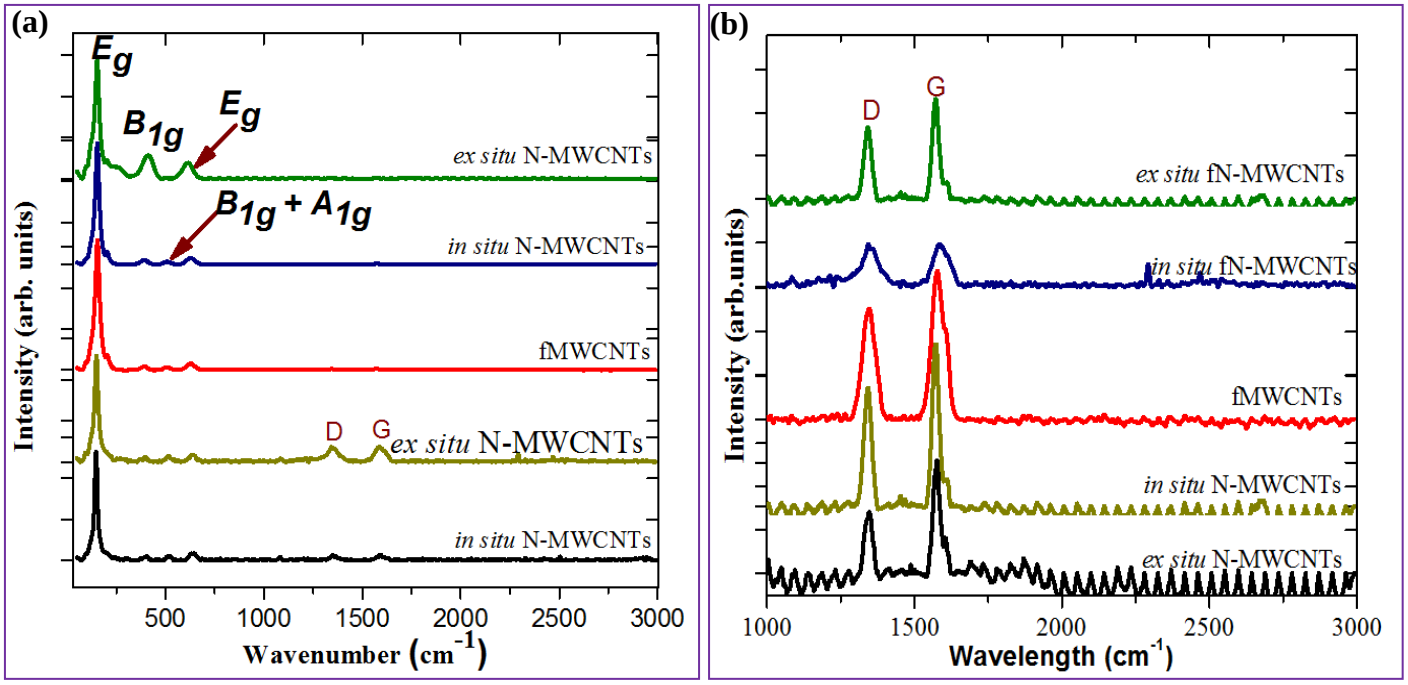

Figure 5.4: (a) Raman spectra of TiO_2-carbon composites (b) band characteristics of the carbon materials in the composites.

5.2.5 Thermal analysis of the TiO_2/MWCNTs composites

The thermal stabilities of the TiO_2/C composites were evaluated using TGA technique under an oxidizing atmosphere. This technique was used to monitor the temperature at which oxidation ($C + O_2 \rightarrow CO_2$) occurs on the catalysts, as well as to ascertain the weight% of TiO_2 in the composites [23]. Figure 5.5 (a) and 5.5 (b) presents the TGA and DTG profiles of the composites, respectively. Here it was observed that the oxidation temperature of the MWCNTs decreased from 631 ^oC observed on the *in situ* TiO_2/N-MWCNTs to 589 ^oC recorded for *in situ* TiO_2/fN-MWCNTs. Thus, it can be seen that the acid treated samples oxidize more readily than the TiO_2/N-MWCNTs. Furthermore, the TGA profiles of the composites exhibited a gradual weight decrease from intermediate temperatures. This was attributed to the presence of the metal particles which have the potential to catalyze carbon oxidation [23].

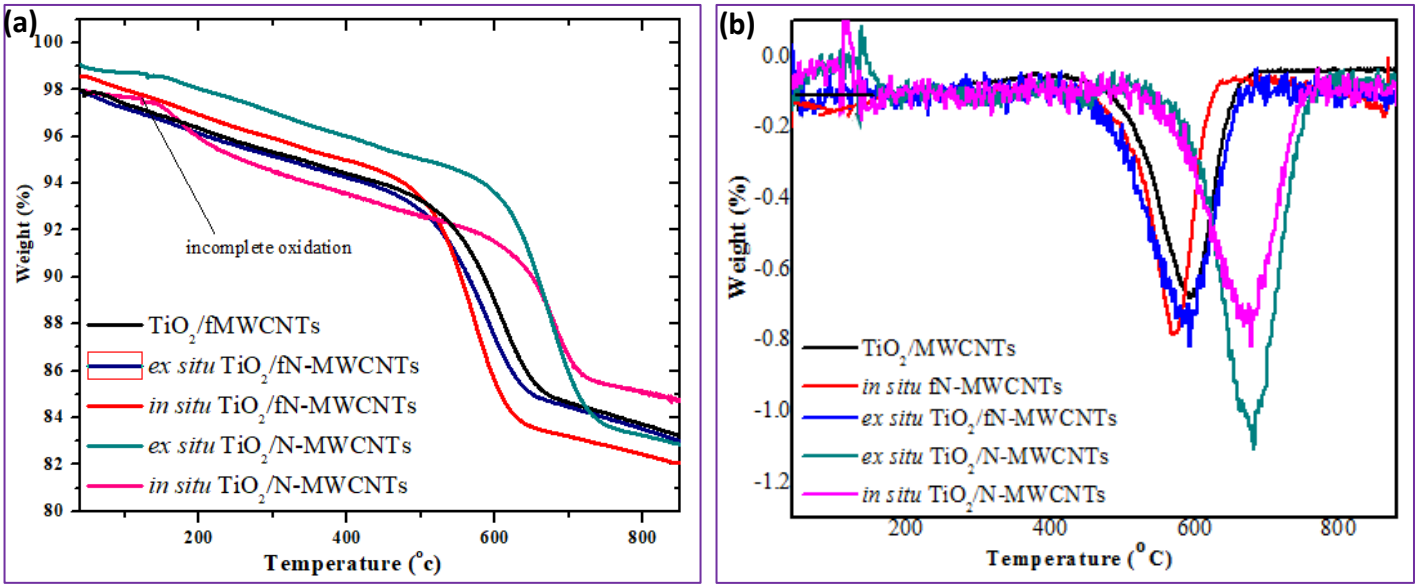

Figure 5.5: Thermal analysis plots of all TiO_2/MWCNTs composites. (a) TGA profiles and (b) DTG profiles of obtained under air.

Figure 5.5 showed the residual weights observed from the TGA profiles at 900 ^oC. The high residual weight observed from the *in situ* fN-MWCNTs could be due to the presence of both the catalyst as revealed in Chapter 4, and the TiO_2. However, the *ex situ* TiO_2/N-MWCNTs exhibited a residual weight equal to those of the acid-treated samples showing the absence of impurities. The purity of the *ex situ* TiO_2/N-MWCNTs was also verified by the sharp derivative peak as compared to the *in situ* TiO_2/N-MWCNTs [24].

5.2.6 BET Surface area and pore volume analysis of TiO_2-based composites

The presented data in Table 5.2 shows the surface properties of the TiO_2-based composite obtained from the N_2 adsorption-desorption isotherms. As predicted by XRD analysis, MWCNTs in the composite hinders the crystal growth of TiO_2, hence allowing more active sites of the TiO_2 to be exposed. Consequently, there was a significant increase in the surface area of self-supported TiO_2 after including the MWCNTs. Conversely, surface areas of the composites were lower than the functionalized MWCNTs. The reduction in the MWCNTs surface area was

accounted by the fact that TiO_2 particles occupy the pores of the MWCNTs, thus prevents the contribution of the bare MWCNTs to the total surface area of the composites [14].

Table 5.2: BET surface areas and pore sizes of all the TiO_2-based nanocomposites and bare TiO_2.

Sample name	Surface area (m^2/g)	Pore size (cm^3/g)
TiO_2	50.6	4.7
in situ TiO_2/N-MWCNTs	76.24	10.4
ex situ TiO_2/N-MWCNTs	59.33	9.9
TiO_2/fMWCNTs	92.06	11.3
in situ TiO_2/fN-MWCNTs	100.72	12.1
ex situ TiO_2/fN-MWCNTs	92.15	8.9

5.3 Conclusions

In this chapter, the role of functionalized MWCNTs as supporting materials of TiO_2 has been established. Raman spectroscopy and XRD both showed that the TiO_2 used in this study was purely anatase. Morphological studies showed that the composites' geographical properties were mostly influenced by the type of functionalization of the MWCNTs. TiO_2/N-MWCNTs (*both in situ* and *ex situ*) showed large areas of uncovered nanotubes with TiO_2 agglomerates distributed in the composites. The failure of obtaining full coverage on these materials was an indication that nitrogen doping solely could not create enough binding sites for TiO_2. Conversely, composites that contained acid-treated MWCNTs (fMWCNTs, *in situ* fN-MWCNTs and *ex situ* fN-MWCNTs) showed full coverage of TiO_2. Consequently, the crystallite size of TiO_2 was reduced from 63.5 nm to 8.03, 7.8 and 5.64 nm after introducing fMWCNTs, *ex situ* fN-MWCNTs and *in situ* fN-MWCNTs, respectively.

This shows that the presence of functionalized MWCNTs hindered the rapid crystal growth of TiO_2 during sol-gel synthesis by generating TiO_2-C bonds. The small TiO_2 particles resulted in an increase in the BET surface area of TiO_2. The surface area of TiO_2 was also estimated from its XRD pattern which deviated from the BET surface area due to limitations of Scherrer equation on non-spherical shapes. Thus Scherrer equation can only give a rough estimate of the crystallite size and not the exact crystallite size. However, TEM average size calculations tend to be accurate. Furthermore, the size increase was proportional to the interplanar spacing between the materials. In summary, to obtain catalyst-free, high surface area and small crystallite size composite with full coverage of TiO_2 on the MWCNTs support, *in situ* doping method is recommended over *ex situ* doping.

5.4 References

[1] The wolfon foundation, "TiO_2: Uses of titanium dioxide," *RSC: Advancing the Chemical Science*, no. 207890.

[2] A. Ajmal, I. Majeed, R. N. Malik, H. Idriss, and M. A. Nadeem, "Principles and mechanisms of photocatalytic dye degradation on TiO_2-based photocatalysts: a comparative overview," *RSC Advances*, vol. 4, no. 70, pp. 37003–37026, 2014.

[3] L. T. S. Thao, T. T. T. Dang, W. Khanitchaidecha, D. Channei, and A. Nakaruk, "Photocatalytic degradation of organic dye under UV-A irradiation using TiO_2-vetiver multifunctional nano particles," *Materials*, vol. 10, no. 2, pp. 1–12, 2017.

[4] Y. Yao, G. Li, S. Ciston, R. M. Lueptow, and K. Gray, "Photoreactive TiO_2 /carbon nanotube composites: Synthesis and reactivity," *Environmental science & technology*, vol. 42, no. 13, pp. 4952–4957, 2008.

[5] H. Wang, H. Li, J. Wang, J. Wu, D. Li, M. Liu, and P. S. Key "Nitrogen-doped TiO_2 nanoparticles better TiO_2 nanotube array photo-anodes for dye sensitized solar cells," *Electrochimica Acta*, vol. 137, no. 13, pp. 744–750, 2014.

[6] K. M. Reza, A. S. W. Kurny, and F. Gulshan, "Parameters affecting the photocatalytic degradation of dyes using TiO_2: a review," *Applied water science*, vol. 10, no. 7, pp. 1–10, 2015.

[7] A. Q. Zhao, J. Masa, and W. Xia, "Very low amount of TiO_2 on N-doped carbon nanotubes significantly improves oxygen reduction activity and stability of supported Pt nanoparticles," *Physical chemistry and chemical physics*, vol. 17, no. 16, pp. 10767–10773, 2015.

[8] M. J. Uddin, F. Cesano, S. Bertarione, F. Bonino, S. Bordiga, D. Scarano, and A. Zecchina "Tailoring the activity of Ti-based photocatalysts by playing with surface morphology and silver doping," vol. 196, pp. 165–173, 2008.

[9] R. Su, N. Dimitratos, J. Liu, E. Carter, S. Althahban, X. Wang, Y. Shen, S. Wendt, X. Wen, J. W. Niemantsverdriet, B. Iversen, C. Kiely, G. J. Hutchings, and F. Besenbacher, "Mechanistic insight into the interaction between a Titanium Dioxide photocatalyst and Pd co-catalyst for improved photocatalytic performance," *ACS Catalysis*, vol. 6, no. 7, pp. 4239–4247, 2016.

[10] L. Wang, L. Shen, Y. Li, L. Zhu, J. Shen, and L. Wang, "Enhancement of photocatalytic activity on TiO_2-nitrogen-doped carbon nanotubes nanocomposites," *International Journal of Photoenergy*, vol. 20, no. 341, pp. 1–7, 2013.

[11] K. Ouyang, S. Xie, and X. Ma, "Photocatalytic activity of TiO_2 supported on multiwalled carbon nanotubes under simulated solar irradiation," *Ceramics international*, vol. 39, no. 7, pp. 7531–7536, 2013.

[12] H. Dong, "An overview on limitations of TiO_2-based particles for photocatalytic degradation of organic pollutants and the corresponding countermeasures," *Water research*, vol. 79, pp. 128–146, 2015.

[13] A. V. Vorontsov, and S. V. Tsybulya, "Influence of Nanoparticles Size on XRD Patterns for Small Monodisperse Nanoparticles of Cu^0 and TiO_2 Anatase, " *Industrial and engineering chemistry research*, vol. 57, no. 9, pp. 2526−2536, 2018.

[14] N. O. Ramoraswi, and P. G. Ndungu, "Photocatalytic properties of TiO_2 supported on MWCNTs, SBA-15 and silica-coated MWCNTs nanocomposites," *Nanoscale research letters*, vol. 10, no. 1, p. 4–27, 2015.

[14] B. Gao, G. Z. Chen, and G. Li Puma, "Carbon nanotubes/titanium dioxide ($CNTs/TiO_2$) nanocomposites prepared by conventional and novel surfactant wrapping sol-gel methods exhibiting enhanced photocatalytic activity," *Applied catalysis B: Environmental*, vol. 89, no. 3–4, pp. 503–509, 2009.

[15] K. Woan, G. Pyrgiotakis, and W. Sigmund, "Photocatalytic carbon nanotube-TiO_2 composites," *Advanced materials*, vol. 21, no. 1, pp. 2233–2239, 2009.

[16] L. Hlekelele, P. Tripathi, P. J. Franklyn, and S. H. Durbach, "Morphological and

crystallinity differences in nitrogen- doped carbon nanotubes grown by chemical vapour deposition decomposition of melamine over coal fly ash.," *RSC Advances*, vol. 6, no. 1, pp. 76773–76779, 2016.

[17] J. Majewska and B. Michalkiewicz, "Low temperature one-step synthesis of cobalt nanowires encapsulated in carbon," vol. 111, no. 10, pp. 1013–1016, 2013.

[18] T. Theivasanthi and M. Alagar, "Titanium dioxide (TiO_2) Nanoparticles - XRD Analyses – An Insight." *Research in Physics*, vol. 66, no. 5, pp. 1–10, 2013

[19] S. Bagheri, N. Muhd Julkapli, and S. Bee Abd Hamid, "Titanium dioxide as a catalyst support in heterogeneous catalysis," *Scientific World Journal*, vol. 2014, p. 727496, 2014.

[20] Z. N. Tetana, "Boron and nitrogen doped carbons for photochemical degradation reactions by," *Thesis*, pp. 1–235, 2013.

[21] B. K. Mutuma, B. Matsoso, K. Ranganathan, D. Wamwangi, and N. J. Coville, "Generation of open-ended, worm-like and graphene-like structures from layered spherical carbon materials," *RSC Advances*, vol. 6, no. 24, pp. 20399–20408, 2016.

[22] B. J. Matsoso, K. Ranganathan, B. K. Mutuma, T. Lerotholi, G. Jones, and N. J. Coville, "Time-dependent evolution of the nitrogen configurations in N-doped graphene films," *RSC Advaces*, vol. 6, no. 108, pp. 106914–106920, 2016.

[23] M. W. Dlamini, "Spherical carbons as model supports for Fe, Co, and Fe-CoFischer-Tropsch catalysts,"*Thesis*, pp. 1-208, 2016.

24. B. K. Mutuma, "Synthesis and characterization of solid, hollow, core-shell, and worm-like carbon nanostructures for applications in organic photovoltaic devices and chemical sensors," *Thesis*, pp. 1-269, 2016

6

Chapter six

Photocatalytic degradation of methyl violet

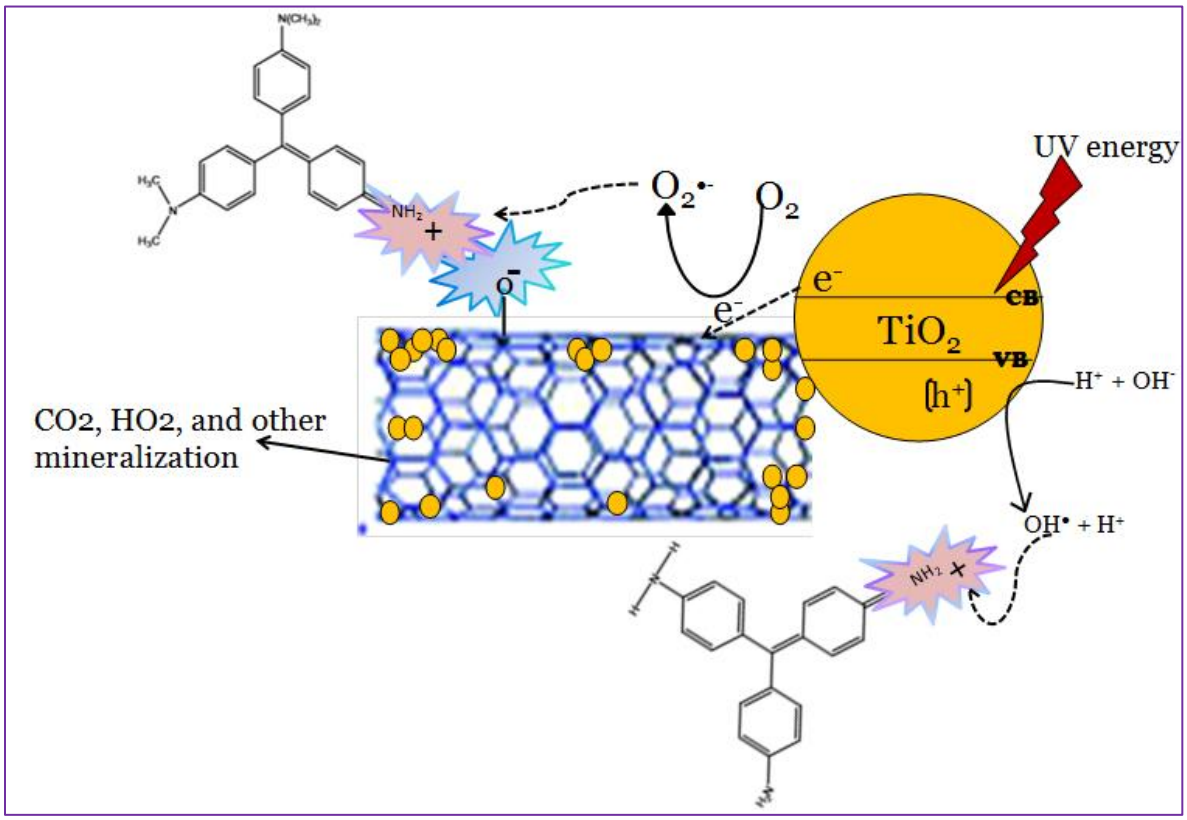

6.1 Overview

The growth in human population is proportional to the increase in demand of colored cloths, food, paper, and many other matters that require high usage of dyes. Consequently, large amounts of organic dyes effluents are discharged into the environment from time to time during the dyeing process in attempt to meet these demands [1]. Therefore concerns exist regarding the environmental impacts of these dyes [2]. These dyes are toxic, and can form dangerous by-products through oxidation, hydrolysis, or other chemical reactions taking place in the wastewater phase [2]. Methyl violet (MV 6B) is a mutagen and mitotic poison that is used in vast for textile and paper dyeing. Because of its tinctorial strength and complex structure, it cannot be easily removed it from wastewater by conventional methods [3]. In addition, MV 6B is carcinogenic, non-biodegradable and has a very bright color [3]. As a result, it stays on the water beds showing an unpleasant color even at very low concentrations, while it also hinders sunlight and oxygen into the depth of the water [3]. The suggested solution to this tragedy is to find a low-cost and effective method that can recycle the industrial wastewater and prevent the release of the dye-contaminated wastewater into the environment [4]. Considering the global water crisis, photocatalytic degradation may be of great help because it can minimize the volumes of fresh water used by the dye-industries, and simultaneously prevent the dye contamination of rivers, lakes and dams.

TiO_2-based heterogeneous photocatalysis is considered as a potential solution because it is cost-effective and highly oxidative such that complete mineralization of methyl violet and many other organic pollutants may be achieved [5]. TiO_2 and many other photocatalysts have a great potential of converting photon energy to chemical energy [6], [7]. In general, the photocatalytic degradation involves several steps such as adsorption-desorption, electron-hole pair production, recombination of electron pair, and chemical reaction [8]. Although it has been widely studied, the research in photocatalysis still continues in attempt to minimize the recombination of electron pair, and to increase the catalyst's activity and turnover number. This is because billions of dollars in industries go to catalyst replacement and process shut down every year. Thus there is a vital need of developing a deactivation-resistant catalyst with high activity. The photocatalytic degradation experiments were carried out using a solar simulator as a UV-light

source at room temperature. The parameters that may affect the photocatalytic rate were optimized for economical and environmental safety purposes. The selectivity of the prepared photocatalyst was also investigated by studying two different dyes; methyl violet and methyl orange. These dyes are commonly available in the market and have complete different structures as presented in Figure 6.1 below. Methyl violet is a basic (cationic) dye while methyl orange is an acidic (anionic) azo dye. The selectivity to the two structures may be influenced by the number of rings in the structure, functional groups, or the ionic nature of the dye molecule. The study of catalyst recyclability was highly essential to discover the influence of the functionalized MWCNTs on the turnover number of TiO_2. In this chapter, the photocatalytic degradation of TiO_2/N-MWCNTs (i.e.: both *in situ* and *ex situ* synthesized) were not included because they contained high amount of Fe, Co, CaO (Chapter 5) which could lead to secondary water pollution. Thus, the catalysts studied were TiO_2, TiO_2/fMWCNTs, *in situ* TiO_2/fN-MWCNTs and *ex situ* TiO_2/fN-MWCNTs.

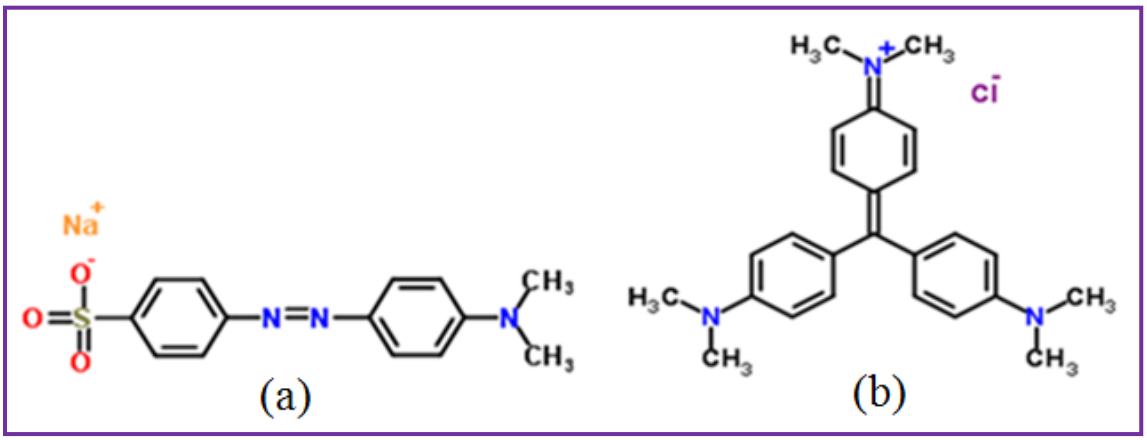

Figure 6.1: Chemical structures of (a) Methyl orange (b) Methyl violet.

6.2 Results and Discussion

Photocatalytic treatment of MV 6B-containing water assisted by TiO_2-based nanocomposites depends on several experimental parameters. Some of the fundamental parameters were varied to optimize the film fabrication process. However, other parameters were all fixed throughout the studies, i.e.: TiO_2 percentage was kept at 80%, pH at neutral, intensity at 180 W, stirring rate at

100 rpm, distance between the light source and the solution was 18 cm, and all reactions were done at room temperature (25 ^{o}C). The solutions used in all experiments were prepared using fresh tap water which was only contaminated with solid dye to a desired concentration. The standard UV-Vis spectrum of methyl violet has been shown by Figure 6.2. The photocatalytic degradation efficiency was calculated using the following equation:

Photocatalytic degradation efficiency: $\mathbf{(\eta) = \frac{Co-Ct}{Co} X\ 100,}$ where Co refers to the initial dye concentration and Ct is the dye concentration over time.

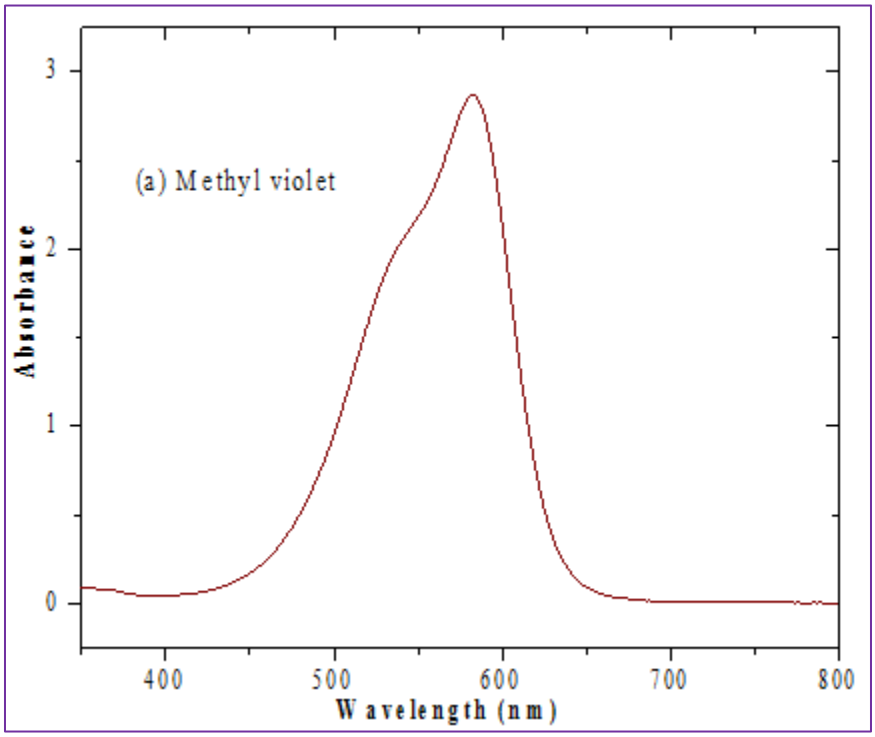

Figure 6.2: UV-Vis absorption spectrum of methyl violet

6.2.1 Adsorption effect

Photocatalytic degradation process occurs on the surface of a photocatalyst; hence adsorption should be its commencement step to prevent mass transfer limitation [9]. Figure 6.2 shows the adsorption capacities of (i) TiO_2, (ii) TiO_2/fMWCNTs, (iii) *ex situ* TiO_2/fN-MWCNTs, (iv) *in situ* TiO_2/fN-MWCNTs, (v) fMWCNTs, (vi) *ex situ* fN-MWCNTs, and (vii) *in situ* fN-MWCNTs. This study was done by stirring 100 ml of MV solution (20 ppm) containing 150 mg

of the catalyst of interest in the dark for 120 minutes. The adsorption of MV by TiO_2 was the lowest compared to the all other materials. This was ascribed to its low affinity towards organic pollutants, and its low surface area and porosity [10]. Notably, the adsorption capacity of TiO_2 improved from 18% to 31%, 35%, and 41%, after being supported on fMWCNTs, *ex situ* fN-MWCNTs and *in situ* fN-MWCNTs, respectively. This was attributed to the pore size distribution, surface functional groups (-OH, -COOH), and the high surface active site to volume ratio of the functionalized MWCNTs which gives them high adsorption[11].

In addition, the higher adsorption efficiency of *in situ* TiO_2/fN-MWCNTs was proportional to its larger surface area of 100.72 m^2/g relative to that of TiO_2 (50.6 m^2/g), *ex situ* TiO_2/fN-MWCNTs (92.2 m^2/g), and TiO_2/fMWCNTs (92.1 m^2/g). Conclusively, the trend of the increasing adsorption capacities of the studied materials was in correlation to their increasing surface area. It is noteworthy that materials with higher adsorption capacities may result in rapid diffusion of the dye molecules from solution to the surface of the catalyst leading to higher photocatalytic degradation efficiency. However, adsorption process only depends on the surface area and porosity of the material while photocatalysis also depends on the optical properties of the material [12]. Thus, regardless of the low adsorption capacity of TiO_2 due to its low surface area compared to the functionalized MWCNTs, its photocatalytic efficiency was higher (see section 6.2.2) owing to its higher charge-carrier mobility and its wide and direct band gap (3.2 eV) which provides high redox potential [13]. Furthermore, negligible change in the concentration of MV was observed after 60 min. This was attributed to the unavailability of the active sites on the materials, indicating that adsorption-desorption equilibrium was reached [14]. Thus, to eliminate the probability of adsorption contribution in the photocatalytic improvement, the mixture was stirred in the dark for 60 min prior to photocatalysis studies.

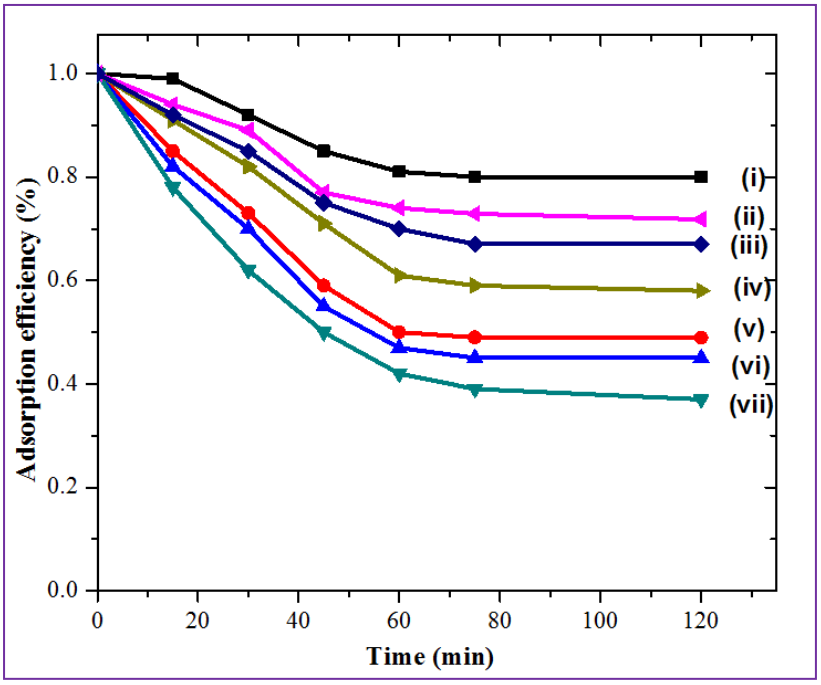

Figure 6.3: Adsorption effect of MWCNTs-supported catalysts: (i) TiO_2 (ii) TiO_2/fMWCNT (iii) *ex situ* TiO_2/N-MWCNTS (iv) *in situ* TiO_2/N-MWCNTs (v) TiO_2/fMWCNTs (vi) *ex situ* fN-MWCNTs (vii) *in situ* fN-MWCNTs

6.2.2 Photodegradation: Effect of time

This study was performed to investigate the role of light, TiO_2, and functionalized MWCNTs in the photocatalytic degradation of MV in a period of 2 hours. Seven sets of experiments were performed using 100 mg of catalyst, in a 100 ml solution of 20 ppm MV. The stirring rate was kept at 100 rpm at room temperature and neutral pH and the data were reported in Figure 5.6. In the first experiment, the MV solution showed no decolourization effect in the absence of light and catalyst. Thereafter, the solution was exposed to UV light only. It was observed that light alone could not rapidly decompose the organic dye. However, an amount of 0.62% of dye was removed [15]. This alludes that methyl violet would require a couple of years to degrade in water if it is exposed to light and oxygen [16]. Thus the degradation process of methyl violet in this study was accelerated by adding a catalyst. The photocatalytic degradation of methyl violet was tested using fMWCNTs, followed by *in situ* fN-MWCNTs and then *ex situ* fN-MWCNTs under UV illumination. Their photocatalytic degradation efficiency was in this order: *in situ* fN-

MWCNTs> *ex situ* fN-MWCNTs> fMWCNTs. The higher degradation capability of *in situ* fN-MWCNTs was attributed to the modified electronic band structure of the MWCNTs through the acid-treatment and the homogeneous incorporation of nitrogen atoms in the lattice [11]. Because the band gap of MWCNTs is determined by the circumferential quantum confinement, acid-treatment and nitrogen doping may adjust its band bap [11], [19]. The modified band gap coupled with the defects on the walls of the host material may lead to enhanced photocatalytic efficiency [16].

After adding TiO_2 in the system, the degradation rate of methyl violet was enhanced enormously. However, due to the rapid recombination of photogenerated electrons and holes and other limitations, it could not degrade the dye completely in 2 hours [17]. Subsequently, the effect of TiO_2/fMWCNTs, *in situ* TiO_2/fN-MWCNTs, and *ex situ* TiO_2/fN-MWCNTs in degrading methyl violet was investigated. The results showed that the photocatalytic degradation efficiency of TiO_2 was greatly improved. The *in situ* TiO_2/fN-MWCNTs exhibited high photocatalytic degradation efficiency on account of the better TiO_2 dispersion, smaller TiO_2 particles, and larger surface area. This substantiates that *in situ* nitrogen doping tunes the MWCNTs into better supports for photocatalysis compared to *ex situ* doping [18].

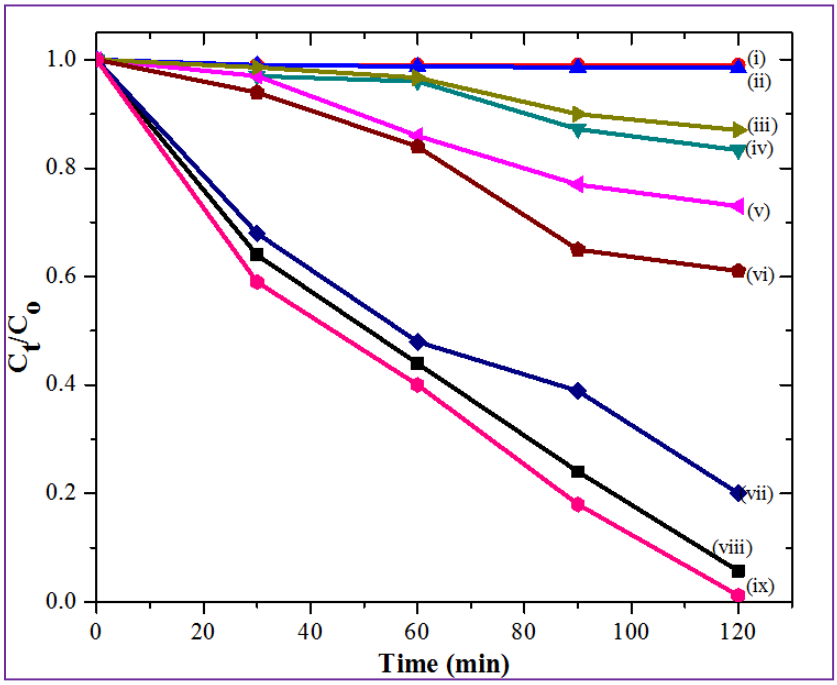

Figure 6.4: Time effect: (i) Blank, (ii) UV illumination (iii) fMWCNTs (iv) *ex situ* fN-MWCNTs (v) *in situ* fN-MWCNTs (vi) TiO_2 (vii) TiO_2/fMWCNTs (viii) *ex situ* TiO_2/fN-MWCNTs (ix) *in situ* TiO_2/fN-MWCNTs.

6.2.3 Effect of catalyst dosage

The amount of catalyst feasible to degrade 20 ppm of 100 mL MV solution was investigated by conducting photodegradation experiments under UV light using 50-200 mg of the catalyst loadings. This study was essential to determine the economic value of the photocatalytic process [20]. These studies were done within exposure time of 1h30, 20 ppm of MV, neutral pH, at room temperature. As observed in figure 6.4, the degradation of MV increases with increasing amount of catalyst loaded. This is due to the increase of the number of active sites on the photocatalyst surface [21]. As a result, a higher uptake of dye occurs at a shorter period of time. Furthermore, the number of •OH radicals which are required in actual discoloration of dye solution tends to increase, hence degradation occurs at a faster rate. However, beyond 150 mg of photocatalyst, the solution was supersaturated such that most of the catalyst was suspended. This

resulted into failure of UV radiation from penetrating and a light screening effect that led to the reduction of the surface area exposed to irradiation [22]. As a result, the percentage of dye degraded tended to decrease after 150 mg. Thus 150 mg was discerned as the optimum catalyst dosage. This was observed in all the catalysts studied.

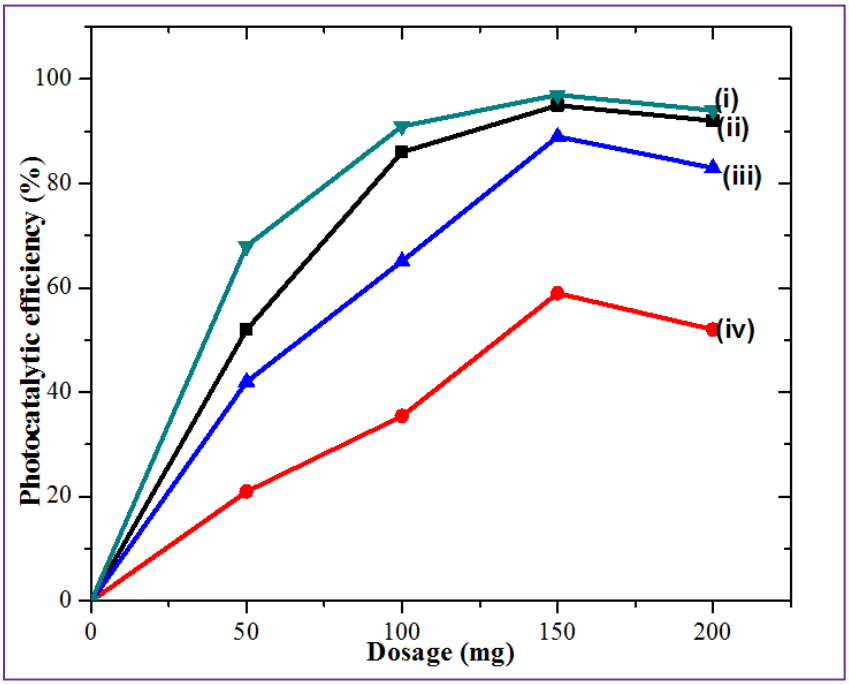

Figure 6.5: Catalyst dosage: (i) *in situ* TiO_2/fN-MWCNTs (ii) *ex situ* TiO_2/fN-MWCNTs (iii) TiO_2/fMWCNTs (iv) TiO_2.

6.2.4 Effect of dye initial concentration

This study was conducted by varying the organic dye initial concentration from 5 to 25 ppm at a fixed optimum dosage of catalyst (150 mg), 100 mL dye solution and 50 minutes exposure time at room temperature. The pollutant concentration study showed a decrease in the rate of degradation as the dye concentration was increased. This observation can be explained by various reasons: (1) Increasing the initial MV concentration increases the competition for attachment to each active site of catalyst resulting in a lot of excess dye in the solution which persist in solution until earlier attached molecules are degraded. The suspended dye prevents

light from penetrating through to the catalyst by adsorbing significant amount of UV [22]. Consequently, adsorption of photons by the catalyst surface may decrease resulting in the reduction of superoxide ions and hydroxyl radicals' formation; (2) High initial concentration of MV means that high amount of MV is adsorbed on the catalyst surface. Thus, the adsorbed MV may inhibit the reaction by occupying the catalyst active sites resulting in the reduction of positive holes or hydroxyl radicals' generation. However, a few other studies found results contrary to these findings. For instance, Saquib and Muneer reported that the degradation rate increased with increasing substrate concentration up to a certain limit and then declined. The difference of these findings was attributed to the difference in experimental conditions. Notably, the degradation rate of MV 6B was fast with *in situ* TiO_2/fN-MWCNTs than *ex situ* TiO_2/fN-MWCNTs. This was due to its high potential to prohibit the electron/hole recombination, the homogeneous coating of TiO_2, and its large surface area and pore density.

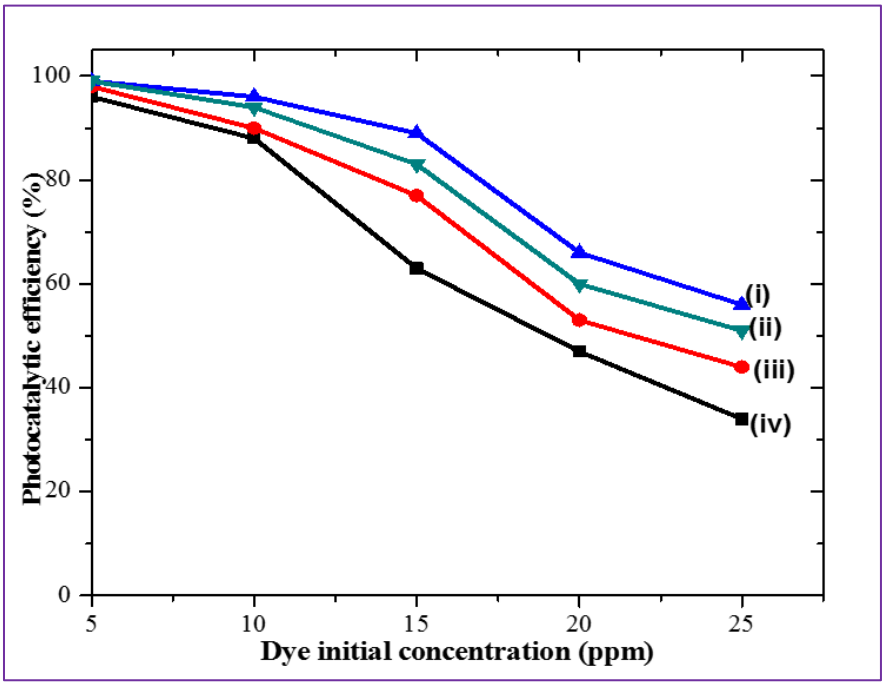

Figure 6.6: MV initial concentration (i) *in situ* TiO_2/fN-MWCNTs (ii) *ex situ* TiO_2/fN-MWCNTs (iii) TiO_2/fMWCNTs (iv) TiO_2.

6.2.5 Recyclability studies

Catalyst deactivation is one of the main challenges in industries such that billions of dollars are spent yearly on catalyst replacement [23]. Thus the study of catalyst reusability is vital. In the case of TiO_2 catalyst, the typical deactivation that may be faced is thermal degradation and sintering [24]. As reported in literature, TiO_2 undergoes anatase to rutile phase transition at temperatures above 450 ^oC, resulting in the reduction of photocatalytic activity [25]. In addition, TiO_2 may lose its catalytic surface area due to crystallite growth (sintering). Thus, this study aims to investigate the role of functionalized MWCNTs in prevention of TiO_2 deactivation over time.

Using the optimum catalyst dosage in 20 ppm of MV solution, the photocatalytic stability of TiO_2 was examined within 1h30 exposure time. The experiments were conducted for three cycles, where the catalyst was filtered out after use, washed with ethanol, and dried in an oven for 12 hours. The recovered catalyst was then annealed under N_2 atmosphere for 2 hours at 300 ^oC, characterized with TEM and BET, and then reused in photocatalytic degradation experiments. These experiments were all conducted under similar conditions and the results obtained were depicted in Table 6.1.

Table 6.1: Photocatalytic efficiency of recycled catalysts for 3 cycles.

Catalyst name	Original	1st recycled	2nd recycled
TiO_2	70%	48%	32%
TiO_2/fMWCNTs	87%	58%	50%
in situ TiO_2/fN-MWCNTs	98%	95%	94%
ex situ TiO_2/fN-MWCNTs	93%	89%	83%

The photocatalytic degradation efficiency of MV decreased with the recycling runs. This was attributed to the loss of active sites after each cycle. According to Figure 6.6, TEM showed that

TiO_2 particles were more aggregated after use. The aggregation of the particles blocks the reactive sites resulting in slower degradation rate of MV. These results were corresponding with the BET surface area of the catalysts which also decreased with the recycling runs as shown in Figure 6.7. Due to the imbalanced mass ratios of TiO_2 to MWCNTs, there were TiO_2 particles that were suspended in the slurry (not bonded to MWCNTs), thus the excess TiO_2 tend to agglomerate with the bonded TiO_2 particles as observed from TEM resulting in lower surface area [26].

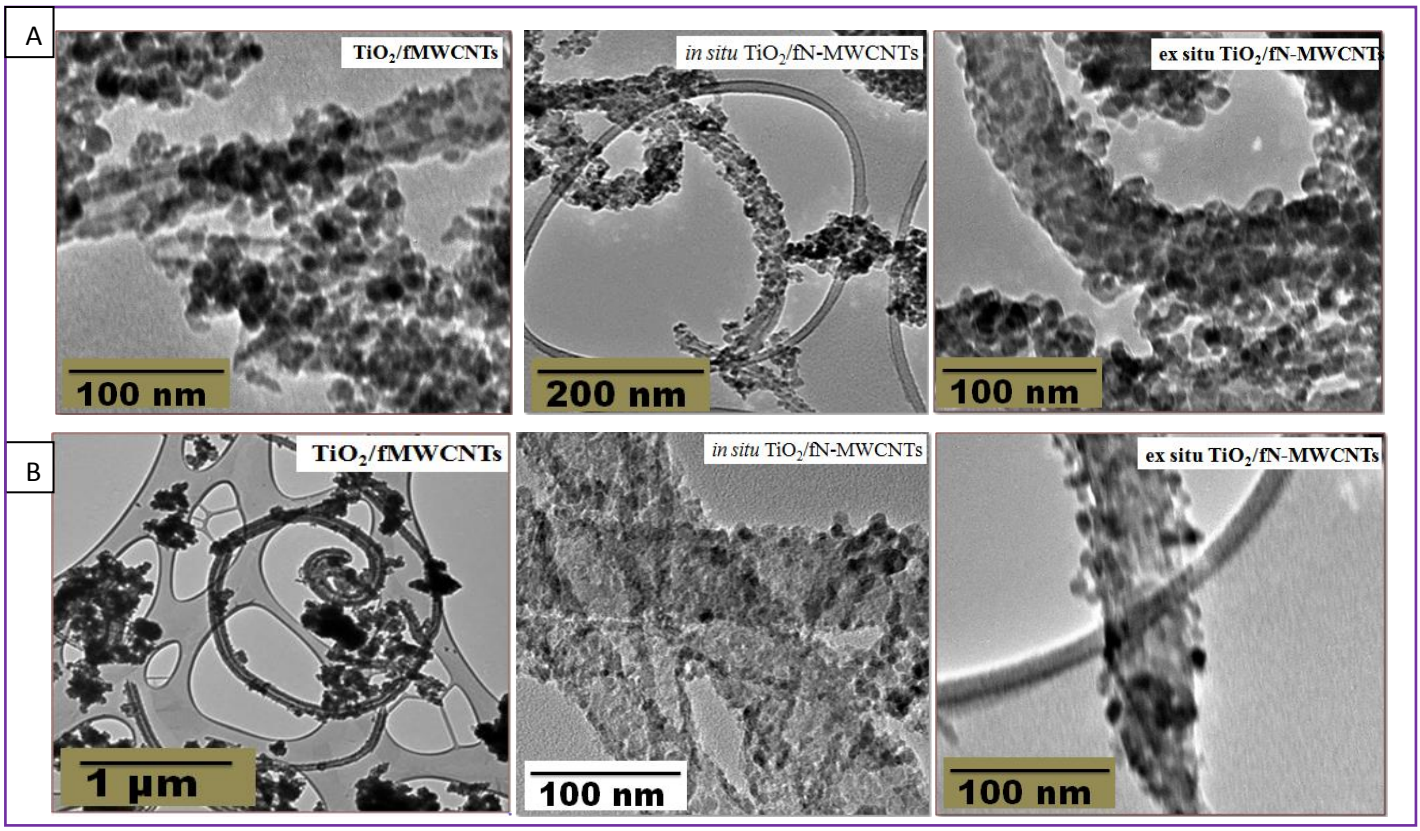

Figure 6.7: TEM micrographs of recycled catalyst for three trials. Row A: presents the catalysts used for 2 cycles, and Row B: presentments catalysts from the third cycle.

However, as reported in the previous chapters, *in situ* fN-MWCNTs were homogeneously functionalized which led to most of the particles being bonded to its surface. Hence, less agglomeration was observed on the *in situ* TiO_2/fN-MWCNTs. After the 2nd cycle, the surface areas of TiO_2, TiO_2/fMWCNTs, *in situ* TiO_2/fN-MWCNTs, and *ex situ* TiO_2/fN-MWCNTs

reduced to 41.2, 55, 99 and 82 m^2/g, respectively. These results indicate that homogeneously coating of TiO_2 on MWCNTs does not only improve the degradation rate, but also prevents catalytic deactivation. This is attributed to the strong interphase (Ti-O-C) that forms in dispersing the TiO_2 onto the MWCNTs.

6.2.5.1 Morphological and Surface area studies of the recycled photocatalysts

The BET surface areas (Table 6.2) of the photocatalysts gradually decreased after each cycle. The degree by which the surface areas decreased corresponds to the morphologies of the catalysts as observed in Figure 6.6. It is noteworthy that the losses of the photocatalysts' active sites were caused by mainly crystal growth formation and incomplete removal of the dye molecules. The morphologies of the MWCNTs supports remained unchanged for all three cycles.

Table 6.2 BET surface areas of recycled catalyst for three cycles.

Sample name	**BET surface area (m^2/g)**		
	Original	1st recycled	2nd recycled
TiO_2	50.6	50	41.2
TiO_2/fMWCNTs	68	62	55
in situ TiO_2/fN-MWCNTs	100.8	100.1	99.3
ex situ TiO_2/fN-MWCNTs	92.2	88	81.6

6.2.6 Selectivity studies

Figure 6.7 shows the photocatalytic degradation of methyl violet (azine cationic dye) and methyl orange (an azo anionic dye). The two dyes were degraded under identical experimental conditions of 20 ppm MV 6B initial concentration, 150 mg of catalyst dosage in 100 mL of the dye solution. However, methyl orange was degraded at a slower rate compared to methyl violet. This was explained by the different routes of mineralization followed by the two dyes with

regards to their distinct structures [27]. Photodegradation of methyl orange starts with a generation of SO_4^{2-} from attack of the sulfonyl group by the photo-induced OH radical [27]. This reaction can be expressed by $C_{14}H_{14}N_3Na\text{-}SO_3^- + OH\bullet \rightarrow C_{14}H_{14}N_3Na\text{-}OH + SO_3\bullet^-$, followed by $SO_3\bullet^- + OH^- \rightarrow SO_4^{2-} + H\bullet$. The induced SO_4^{2-} tends to adhere on the catalyst surface, and consequently inhibit the reaction by blocking the reactive sites of the photocatalyst [27], [28]. This process is known as poisoning. Conversely, methyl violet's mineralization generates NO_3 ions which tend to accelerate the photodegradation by forming hydroxyl radicals [29], [30]. This resulted in faster kinetics of methyl violet degradation as compared to methyl orange. Nevertheless, the poisoning that was experienced in methyl orange degradation was reversible [27]. Thus, the process was only comparatively slower, but still acceptable.

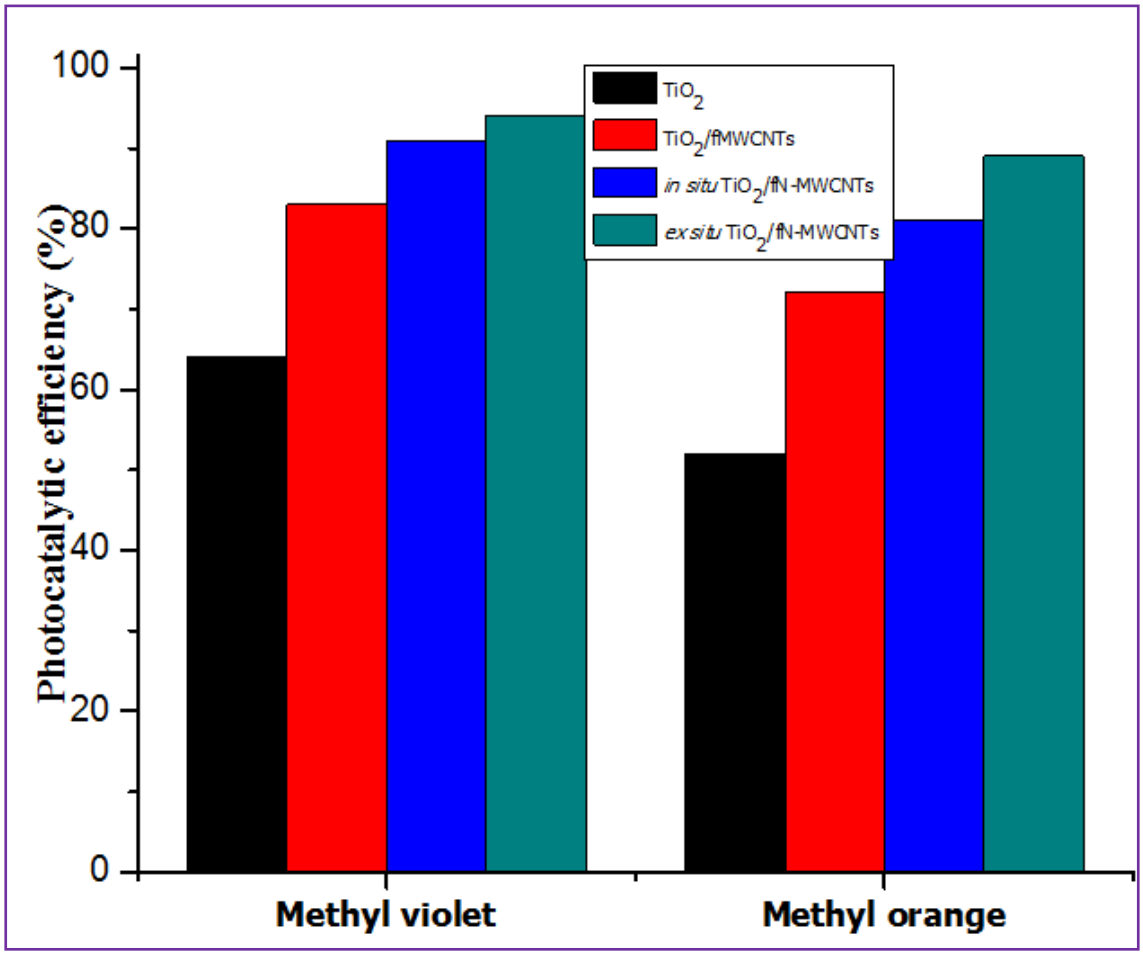

Figure 6.8: Selectivity study by comparison between the degradation rate of Methyl orange and methyl violet under identical conditions.

6.3 Conclusion

The efficiency of supported TiO_2 in the degradation of methyl violet was evaluated. 150 mg of the TiO_2-carbon based catalyst was required to obtain maximum efficiency in the degradation of 20 ppm methyl violet. This was explored by optimizing dye concentration and catalyst dosage, where every other parameter was kept constant in each optimization. The method of functionalization plays a major role in the activity and stability of the catalyst. Basically, nitrogen doping enhanced the catalyst's activity with a greater capacity relative to fMWCNTs. Nonetheless, *in situ* TiO_2/fN-MWCNTs exhibited a fast degradation rate of methyl violet relative to *ex situ* TiO_2/fN-MWCNTs. This was attributed to the fact that *ex situ* TiO_2/fN-MWCNTs was a random composite which was prone to aggregation of TiO_2 as compared to *in situ* TiO_2/fN-MWCNTs.

Consequently, nanoparticles that were closer to the UV light source tended to block those that are further from the light source. Furthermore, the reusability studies were done by running experiments for three cycles under similar conditions. The photocatalytic activity of *in situ* TiO_2/fN-MWCNTs decreased by only 4% after the third cycle while *ex situ* TiO_2/fN-MWCNTs decreased by 10%. This was justified by the decrease of their surface areas. Thus to obtain higher degradation rate, and stable catalyst over time, *in situ* doping method is recommended. This is attributed to the high defects of *in situ* fN-MWCNTs (see Chapter 4), which created more sites with higher coordination number. The selectivity of the catalysts was also studied by comparing the degradation rates of methyl violet and methyl orange. Methyl orange was degraded at a slower rate compared to methyl violet due to the release of sulphate ions which partially inhibits the degradation process. It is worth to note that the photocatalytic degradation of organic dyes is strongly affected by the substituents in the dye structure.

6.4 References

[1] C. J. Ogugbue and T. Sawidis, "Bioremediation and detoxification of synthetic wastewater containing triarylmethane dyes by aeromonas hydrophila isolated from industrial effluent.," *Biotechnology research international*, vol. 2, no. 17, pp. 927–985, 2011.

[2] A. L. Ahamd, W. A. Harris, Syafiee, and O. B. Seng, "Removal of dye from wastewater of textile industry using membrane technology," *Jurnal teknologi*, vol. 36, no. 6, pp. 31–44, 2007.

[3] K. Saeed, I. Khan, T. Gul, and M. Sadiq, "Efficient photodegradation of methyl violet dye using TiO_2/Pt and TiO_2/Pd photocatalysts," *Applied water science*, vol. 6, no. 1, pp. 8–24, 2017.

[4] R. Raliya, C. Avery, S. Chakrabarti, and P. Biswas, "Photocatalytic degradation of methyl orange dye by pristine titanium dioxide , zinc oxide , and graphene oxide nanostructures and their composites under visible light irradiation," *Applied nanoscience*, vol. 7, no. 5, pp. 253–259, 2017.

[5] S. Ortelli, M. Blosi, S. Albonetti, A. Vaccari, M. Dondi, and A. L. Costa, "TiO_2-based nano-photocatalysis immobilized on cellulose substrates," *"Journal of photochemistry & photobiology, A: Chemistry,"* vol. 276, no. 1, pp. 58–64, 2014.

[6] N. Jafari, R. Kasra-Kermanshahi, M. R. Soudi, A. H. Mahvi, and S. Gharavi, "Degradation of a textile reactive azo dye by a combined biological-photocatalytic process: Candida tropicalis Jks2 -TiO_2/UV," *Iranian Journal of Environmental Health Science & Engineering*, vol. 9, no. 1, p. 1–33, 2012.

[7] T. L. Hathway, "Titanium dioxide photocatalysis : studies of the degradation of organic molecules and characterization of photocatalysts using mechanistic organic chemistry," *Thesis*, pp. 1–1642009.

[8] N. Daneshvar, D. Salari, and A. R. Khataee, "Photocatalytic degradation of azo dye acid red 14 in water on ZnO as an alternative catalyst to TiO_2," *Journal of photochemistry and Photobiology A: Chemistry*, vol. 162, no. 3, pp. 317–322, 2004.

[9] M. Umar and H. A. Aziz, "Photocatalytic degradation of organic pollutants in water," *Environmental risk and treatment*, pp. 195–208, 2013.

[10] H. Dong, G. Zeng, L. Tang, C. Fan , C. Zhang, X. He, and Y. He "An overview on limitations of TiO_2-based particles for photocatalytic degradation of organic pollutants and the corresponding countermeasures," *Water research*, vol. 79, pp. 128–146, 2015.

[11] K. Ouyang, S. Xie, and X. Ma, "Photocatalytic activity of TiO_2 supported on multiwalled carbon nanotubes under simulated solar irradiation," *Ceramics international*, vol. 39, no. 7, pp. 7531–7536, 2013.

[12] O. Y. Podyacheva and Z. R. Ismagilov, "Nitrogen-doped carbon nanomaterials: To the mechanism of growth, electrical conductivity and application in catalysis," *Catalysis today*, vol. 249, pp. 12–22, 2015.

[13] R. Su, N. Dimitratos, J. Liu, E. Carter, S. Althahban, X. Wang, Y. Shen, S. Wendt, X. Wen, J. W. Niemantsverdriet, B. Iversen, C. J. Kiely, G. Hutchings, and F. Besenbacher, "Mechanistic insight into the interaction between a Titanium Dioxide photocatalyst and Pd co-catalyst for improved photocatalytic performance," *ACS Catalysis*, vol. 6, no. 7, pp. 4239–4247, 2016.

[14] N. Bt, A. Mansor, J. Tessonnier, M. G. Kutty, R. Schlögl, and S. B. A. Hamid, "Chemically modified carbon nanotubes (CNTs) with oxygen and sulfur containing functional groups for adsorption of mercury," *RSC Advances*, vol. 20, pp. 66–70, 2011.

[15] A. Ajmal, I. Majeed, R. N. Malik, H. Idriss, and M. A. Nadeem, "Principles and mechanisms of photocatalytic dye degradation on TiO_2 based photocatalysts: a comparative overview," *RSC Advances*, vol. 4, no. 70, pp. 37003–37026, 2014.

[16] M. Doğan and M. Alkan, "Removal of methyl violet from aqueous solution by perlite," *Journal of colloid and interface science*, vol. 267, no. 1, pp. 32–41, 2003.

[17] L. T. S. Thao, T. Dang, W. Khanitchaidecha, D. Channei, and A. Nakaruk, "Photocatalytic degradation of organic dye under UV-A irradiation using TiO_2-vetiver multifunctional nano particles," *Materials*, vol. 10, no. 2, pp. 1–12, 2017.

[18] H. Cheng, C. Lua, J. Liua, Y. Yana, X. Han, H. Jina, Y. Wang, Y. Liu, and C. Wu, "Synchrotron radiation X-ray powder diffraction techniques applied in hydrogen storage materials - A review," *Progress in natural Science: materials international*, vol. 27, no. 1, pp. 66–73, 2017.

[19] C. Lamprecht, A. Ebner, F. Kienberger, P. Hinterdorfer, R. Klingeler, R. B. Sim, and E. Berlin, "Exploring Carbon nanotubes and their interaction with cells using Atomic Force Microscopy," *Biomedical science*, vol. 881, no. 59, pp. 1–16, 2011.

[20] A. Q. Zhao, J. Masa, and W. Xia, "Very low amount of TiO_2 on N-doped carbon nanotubes significantly improves oxygen reduction activity and stability of supported Pt nanoparticles," *Physical chemistry chemical physics*, vol. 17, no. 16, pp. 10767–10773, 2015.

[21] M. H. Habibi, A. Hassanzadeh, and S. Mahdavi, "The effect of operational parameters on the photocatalytic degradation of three textile azo dyes in aqueous TiO_2 suspensions," vol. 172, no. 3, pp. 89–96, 2005.

[22] A. Gnanaprakasam, V. M. Sivakumar, and M. Thirumarimurugan, "Influencing Parameters in the Photocatalytic Degradation of Organic Effluent via Nanometal Oxide Catalyst : A Review," *Indian journal of materials science*, vol. 2015, pp. 1–16, 2015.

[23] T. S. Wu, K. X. Wang, G. D. Li, S. Y. Sun, J. Sun, and J. S. Chen, "Montmorillonite-Supported Ag/TiO_2 nanoparticles: An efficient visible-Light bacteria photodegradation material," *ACS Applied materials and interfaces*, vol. 2, no. 2, pp. 544–550, 2010.

[24] K. M. Reza, A. S. W. Kurny, and F. Gulshan, "Parameters affecting the photocatalytic degradation of dyes using TiO_2: A Review," *Applied water science*, pp. 1–10, 2015.

[25] T. Luttrell, S. Halpegamage, J. Tao, A. Kramer, E. Sutter, and M. Batzill, "Why is anatase a better photocatalyst than rutile?-Model studies on epitaxial TiO_2 films.," *Scientific Reports*, vol. 4, no. 2, pp. 4–43, 2014.

[26] Y. Yao, G. Li, S. Ciston, R. M. Lueptow, and K. Gray, "Photoreactive TiO_2/carbon nanotube composites: Synthesis and Reactivity," *Environmental science & technology*, vol. 42, no. 13, pp. 4952–4957, 2008.

[27] H. Lachheb, E. Puzenata, A. Houasb, M. Ksibib, E. Elaloui, C. Guillard, and J. Herrmanna, "Photocatalytic degradation of various types of dyes (Alizarin S, Crocein Orange G, Methyl Red, Congo Red, Methylene Blue) in water by UV-irradiated titania," *Applied catalysis B: Environmental*, vol. 39, no. 1, pp. 75–90, 2002.

[28] S. Da Dalt, A. K. Alves, and C. P. Bergmann, "Photocatalytic degradation of methyl orange dye in water solutions in the presence of MWCNT/TiO_2 composites," *Materials research bulletin*, vol. 48, no. 5, pp. 1845–1850, 2013.

[29] G. Favaro, D. Confortin, P. Pastore, and M. Brustolon, "Application of LC-MS and LC-MS-MS to the analysis of photo-decomposed crystal violet in the investigation of cultural heritage materials aging," *Journal of mass spectrometry*, vol. 47, no. 12, pp. 1660–1670, 2012.

[30] N. Kazmierczak and D. A. Van der Griend, "Improving student results in the crystal violet chemical kinetics experiment," *Journal of chemical education*, vol. 94, no. 1, pp. 61–66, 2017.

7

Chapter seven

Study of TiO_2/cellulose-N-MWCNTs

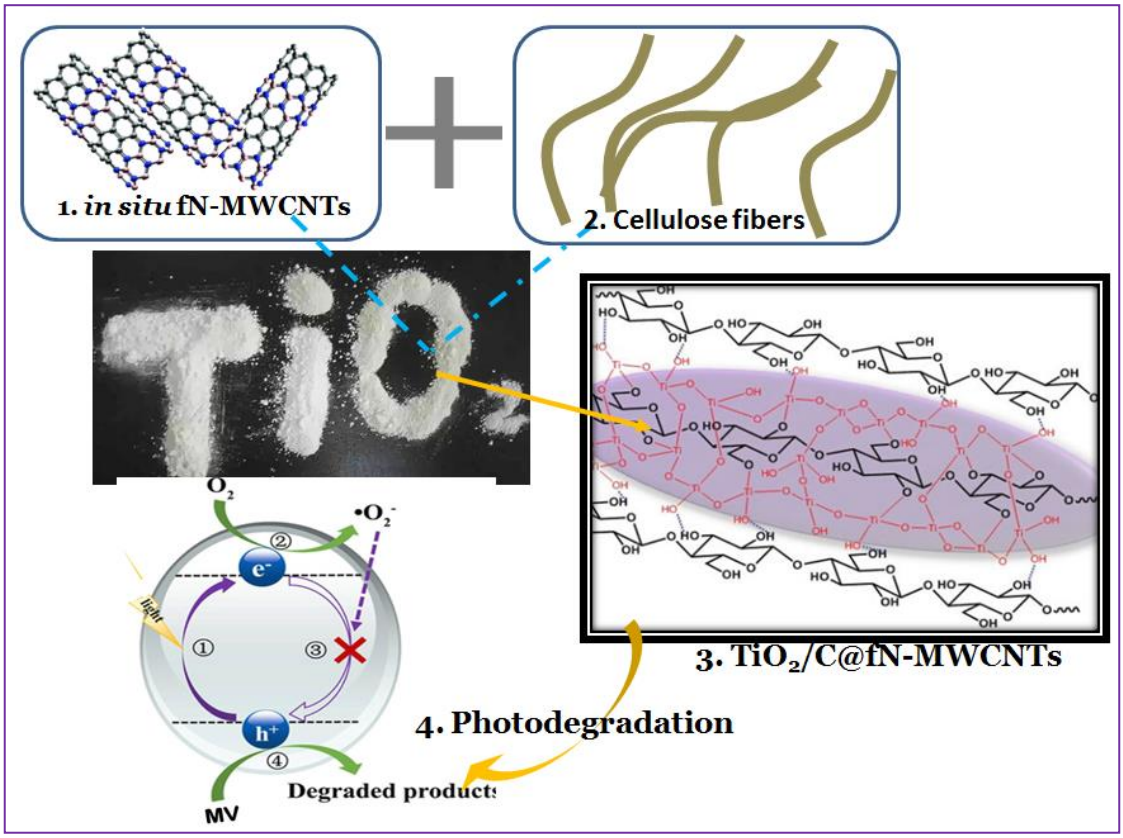

7.1 Overview

Carbon nanotube (CNT) filled polymer composites are increasingly gaining attention in various fields such as telecommunications, pH sensors and paper making [1]. This is because of their lightweight, and significantly improved thermal, mechanical and electrical properties. The development of these polymeric composites was prompted by anticipating that CNTs can significantly improve the physical, thermal and electrical characteristics of polymers [1]. In addition, multiwalled carbon nanotubes (MWCNTs) make ideal fillers in these composites owing to their high aspect ratio which aids in fiber bridging and enhance mass fraction [2]. However, the fabrication of these composites remains a challenge due to a lack of reliable and cost-effective fabrication method [2]. Electrospinning is a simple and versatile technique that has the potential to fabricate ultrafine fibers [3]. The diameter, alignment, and purity of the fibers can be varied based on the processing conditions which include the electrostatic potential and electrospinning distance (distance between tip of nozzle and collector device) [4], [5]. Nevertheless, there are still drawbacks of aggregates formation of the composites which result in low mass fraction tolerance, and the inability to achieve CNT-polymer interfacial bonding [6].

Various methods have been explored to attenuate these drawbacks. The methods include etching, polymer wrapping, controlled oxidation and chemical treatments [7], [8]. Chemical treatments are mostly preferred because they provide stable functionalization which leads to effective load transfer through covalent bonding [7]. Thus, different chemical modifications of MWCNTs have been explored in chapter 4 of this work. The MWCNTs were functionalized by HNO_3 treatment (fMWCNTs), *in situ* nitrogen doping (*in situ* N-MWCNTs), *ex situ* nitrogen doping (*ex situ* N-MWCNTs), and both HNO_3 treatment and nitrogen doping (fN-MWCNTs). It is believed the carboxylic and hydroxyl groups are the binding points to the polymers [9]. Among many other polymers, cellulose polymer has been barely studied in the composites due to its low solubility in many solvents [10]. However, this study focused on cellulose polymer considering its compatibility with the MWCNTs due to their low density, high aspect ratio, high stiffness, extremely high strength and high surface areas [10], [11]. To overcome the solubility obstacle, cellulose acetate solution was used in electrospinning to fabricate the cellulose fibrils. It was

hypothesized that MWCNTs with cellulose fibrils will have adsorption synergistic effect which can enhance the overall efficiency of a photocatalytic process. Thus the functionalized MWCNTs that exhibited high adsorption capacity were used in this study. The competence of *in situ* fN-MWCNTs as supporting material for TiO_2 has been ratified in chapter 5. We herein report on the application of fN-MWCNTs reinforced on cellulose (C@fN-MWCNTs) electrospun fibers as support of TiO_2 in the photocatalytic degradation of methyl violet in water. The feasible parameters for a satisfactory photocatalytic degradation of methyl violet in water have been optimized in chapter 6. Thus, the reported optimal conditions will be used to ascertain the photocatalytic degradation efficiency of TiO_2/C@fN-MWCNTs. Similar studies have been conducted by Seongcheol Mun *et al.* where cellulose-TiO_2-MWCNTs hybrid was studied for use as NH_3 gas sensor at room temperature [9]. However, there are no research works where cellulose-N-MWCNTs composite has been studied as TiO_2 support in photocatalytic degradation of organic dyes in water.

7.2 Results and Discussion

In an attempt to manufacture ultrafine cellulose fibers, researchers have reported that cellulose acetate in its primary form can be easily processed by spinning in solution form. Thus a process of deacetylation is required to convert cellulose acetate into cellulose. Hence, characterization by special techniques such as FTIR spectroscopy is required to confirm the surface chemical structure of the electrospun fibers.

7.2.1 Fourier transform infrared spectroscopy (FTIR) analysis of cellulosic materials

Figure 7.1 presents the FTIR patterns of cellulose acetate fibers, cellulose fibers, TiO_2/cellulose, C@fN-MWCNTs fibers and TiO_2/C@fN-MWCNTs composite. The fibers were electrospun from cellulose acetate solution, followed by deacetylation to obtain cellulose fibers. FTIR was then used to affirm the changes in the chemical structures of the cellulose acetate and cellulose. The cellulose acetate fibers exhibited characteristic adsorption peaks at 1745 cm^{-1} (υC=O) and 1234 cm^{-1} (υC–O–C) which diminished after deacetylation. This was a confirmation that the conversion of cellulose acetate to cellulose fibers was successful [12]. The peaks observed at

~2899 cm^{-1} and 1428 cm^{-1} were assigned to C-H stretching of CH_2 and CH_2 symmetric bending modes, respectively. Both cellulose fibers and C@fN-MWCNTs exhibited a broad band at ~3344 cm^{-1}, which was derived from inter- and intra-chain OH–groups [5]. However, this peak was reduced in the FTIR spectrum of C@fN-MWCNTs showing that the hydroxyl groups participated in the anchoring of the cellulose with the fN-MWCNTs. This observation also concurred with the enhancement of the C-O-C peak at 13180 cm^{-1} in the C@fN-MWCNTs spectrum [6]. The TiO_2-based composites also exhibited their characteristic peaks at 539 cm^{-1} corresponding to the frequency of anatase particles [13]. Nevertheless, the cellulosic peaks observed at 1650 cm^{-1} remained unchanged, showing that the chemical structure of the cellulose after electrospinning and reinforcing them with the fN-MWCNTs is not altered.

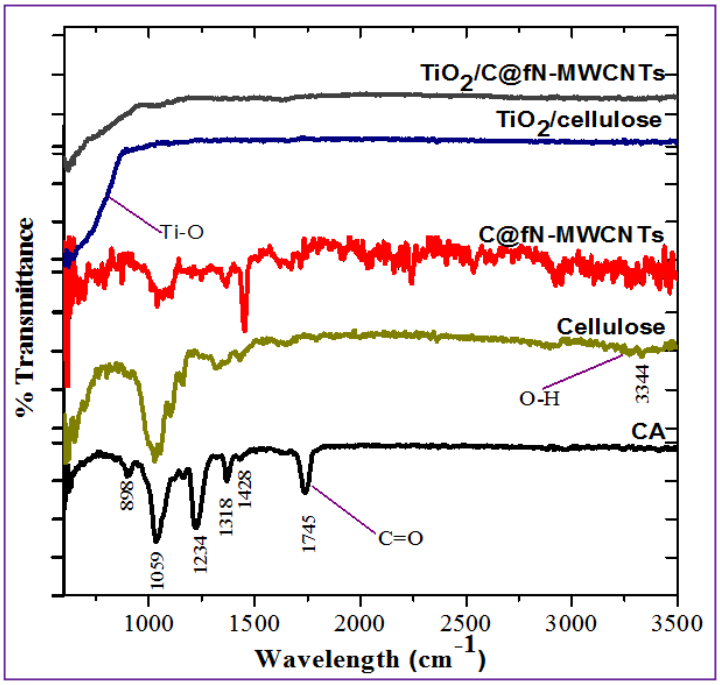

Figure 7.1: FTIR spectra of cellulose acetate (CA), cellulose fibrils, C@fN-MWCNTs, TiO_2/cellulose, and TiO_2/C@fN-MWCNTs.

7.2.2 Phase Identification the catalysts.

X-ray diffraction (XRD) analysis was use to investigate the crystalline sizes, crystallinity index (CI) and for phase identification. The XRD diffractograms of the electrospun fibers are presented

in Figure 7.2. The broad peaks at 2Θ ≈ 14.5°–15.3°, 15.7°–16.30°, and 21.62°–22.90° reflections were attributed to (110), (200), and (002) crystallographic plane, respectively. Whilst the peak at 2Θ = 18.30°–18.40° reflection was assigned to the amorphous phase of cellulose [12]. As observed from the XRD patterns, cellulose fibers exhibited the presence of amorphous carbon. However, the degree of cellulose crystallinity was improved after the inclusion of fN-MWCNTs. The estimated crystalline indices, crystallite sizes and interplanar spacing are presented in Table 7.1. This was affirmed by (110) peak which became more intense after the addition of fN-MWCNTs. The crystalline indices were calculated using the Segal methods (Equation 7.1) [14].

Amorphous subtraction method: $\%C.I = \frac{I200-Iam}{Iam} x\ 100$ eq. (7.1)

Where C.I is the crystalline index, I_{002} is the intensity attributed to the (002) peak at lattice diffraction of ~22°, and I_{am} is the intensity of diffraction peak assigned to amorphous cellulose.

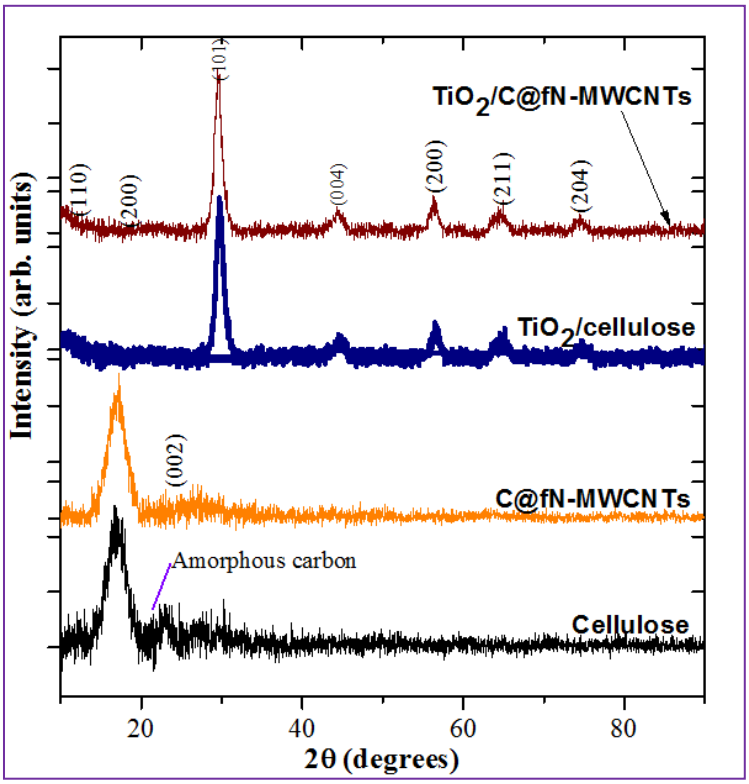

Figure 7.2: XRD diffractograms of bare supported TiO_2 by carbonaceous materials.

The crystalline index of cellulose fibers increased from 79.22% to 97.0%, after being reinforced with the fN-MWCNTs. This was attributed to the graphitic contribution of fN-MWCNTs (studied in Chapter 4). However, the crystalline and amorphous material in the fibers could not be quantified because there are many other parameters inclusive but not limited to peak width variation and other peaks positions that may contribute to the crystallinity have been neglected [12], [15]. Moreover, crystalline sizes of TiO_2 in the composite fibers were estimated using Bragg's equation on the (101) peak. It was discovered that the TiO_2 crystalline size in TiO_2/cellulose decreased drastically after the inclusion of *in situ* fN-MWCNTs. On the other hand, the crystalline size of cellulose fibers decreased with an increase of crystalline index after the *in situ* fN-MWCNTs were reinforced.

Table 7.1: Crystallinity properties of the cellulosic materials estimated using XRD diffractograms.

Sample name	d-spacing (Å)	Crystalline size (nm)	Crystalline index (%)
Cellulose fibers	5.3	38.1	69
C@fN-MWCNTs	2.0	23.4	87
TiO_2/cellulose	2.1	31.9	-
TiO_2/C@fN-MWCNTs	1.9	10.5	-

7.2.3 Surface morphology analysis

Scanning electron microscopy (SEM) was used to analyze geometric properties of the fibers. The morphology micrographs are presented below (Figure 7.3). Cellulose fibers were in a form of long, interconnected uniform fibers with minimal beads observed. On the other hand, C@fN-MWCNTs composites were beaded fibrils with randomly dispersed fN-MWCNTs. Although the fibers were not orderly aligned, minimal aggregation was observed on the C@fN-MWCNTs fibers. The surface morphology and the estimated diameter of the fN-MWCNTs remained

unchanged after electrospinning. However, they were shortened due to the chemical modification which made them vulnerable during electrospinning [7]. This observation corresponds to what was predicted by Fujigaya *et al.* [7]. Furthermore, a noticeable distance between the cellulose fibrils and fN-MWCNTs was observed. This indicates that there was columbic repulsion between the two materials with negative charges [16], [17]. Thus the desired interfacial adhesion of the cellulose with the *in situ* fN-MWCNTs could not be achieved. The large amounts of OH-functional groups on the surface tend to block the pores of the materials, resulting in low surface area (section 7.5) [18].

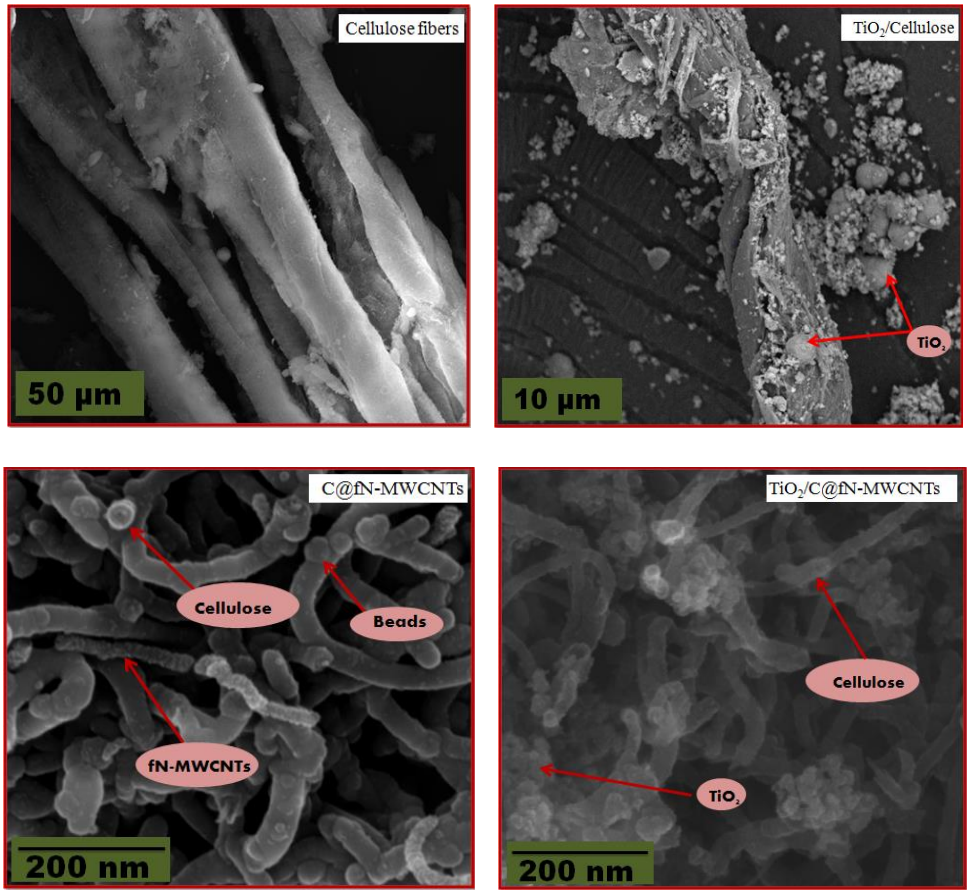

Figure 7.3: SEM micrographs of the Cellulose, C@fN-MWCNTs, and TiO_2-based composites.

The average diameter of cellulose fibers was found to be 16.27 µm whilst for C@fN-MWCNTs it was only 29.87 nm. It was hypothesized that this was due to the different solubilities between

the cellulose acetate and fN-MWCNTs. However, the cause to the size reduction of the cellulose fibrils after including fN-MWCNTs is still unclear. Notably, there are several factors that may have affected the fibers diameter, which are polymer concentration, the different solubilities between cellulose acetate and fN-MWCNTs, and the voltage used just to name a few [4], [19]. TiO_2/cellulose composite barely showed interaction between TiO_2 and cellulose. Lumps of TiO_2 were observed indicating a rapid hydrolysis of the titanium precursor before the reaction products adhere on the cellulose surface support [20]. On the contrary, TiO_2/C@fN-MWCNTs composite contained TiO_2 agglomerates randomly arranged. The small particles of TiO_2 in these composites revealed that there was an interaction between TiO_2 and C@fN-MWCNTs.

7.2.4 Optical studies

According to XRD and SEM (section 7.2.1 &7.2.3), the crystallite size of TiO_2 in TiO_2/C@fN-MWCNTs composite was impressively small. However, these particles barely covered the surface of C@fN-MWCNTs. Thus optical properties of the composites were investigated by UV-Vis absorption and photoluminescence (PL) spectrometer to confirm the electron flow in the composites as presented in Figure 7.4 (a and b). Figure 7.4(a) shows the UV-Vis spectra where the excitation wavelengths of the catalysts were observed at the peak maxima. The TiO_2/cellulose showed a better capacity to absorb radiation at longer wavelength compared to TiO_2/C@fN-MWCNTs. The excitation peak shift observed on the TiO_2/cellulose could be due to the large molecular framework of the cellulose. In addition, SEM micrograph of the TiO_2/cellulose has showed poor interaction between the TiO_2 and the cellulose fibers, thus the unshared electrons on the surface functional groups (-OH) of cellulose could have increased the length of the л-system through resonance and shifted the absorption bands to longer wavelengths.

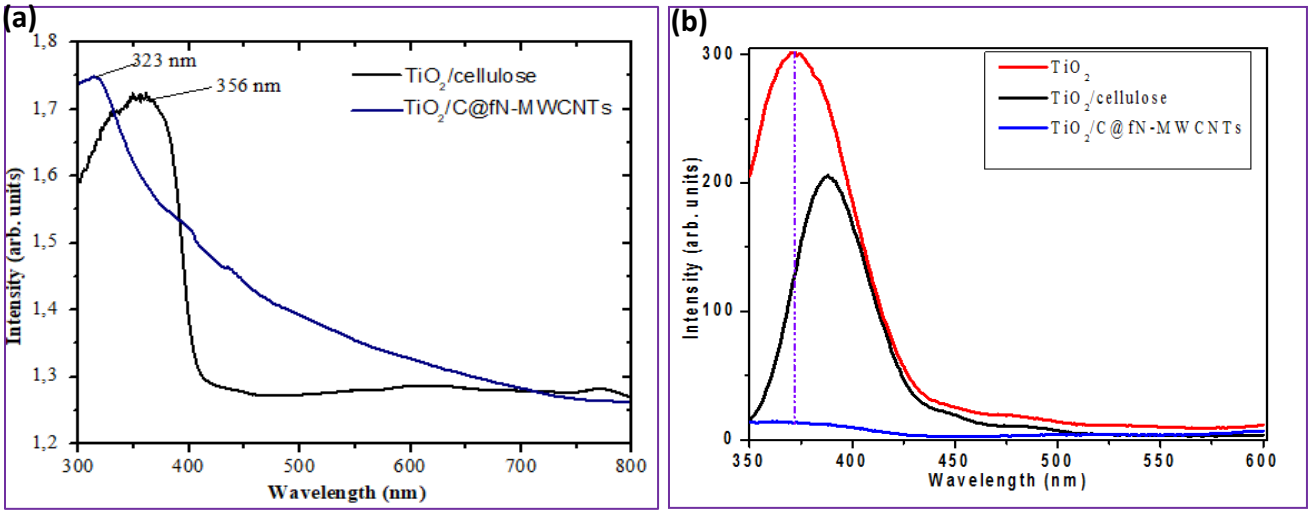

Figure 7.4: (a) UV-Vis and (b) PL spectra of bare and supported TiO_2 on carbonaceous materials.

The PL peak intensities are reported in Table 7.2. Furthermore, there was a significant red shift of the TiO_2 peak after being supported on the cellulose polymer confirming the observations on UV-Vis spectra. The decrease of measured PL intensity was associated with the suppression of the recombination of exitons (electron-hole recombination) by the carbonaceous materials [22]. Thus, C@fN-MWCNTs hybrid showed a great potential of preventing the electron/hole recombination as compared to cellulose.

Table 7.2: Emission peak intensities of TiO_2-cellulose based catalysts.

Sample name	PL peak intensity
TiO_2	292
TiO_2/cellulose	188
TiO_2/C@fN-MWCNTs	12.37

7.2.5 BET Surface area and pore size analysis of cellulose fibers, C@fN-MWCNTs and their respective catalysts

Surface analysis of catalysts is highly crucial because catalysis process takes place on the surface of the materials. Thus, the surface area and porosity of the prepared catalysts was investigated using Bruanner Emmett Teller (BET) technique. These two parameters are essential in understanding the adsorption capacity of the prepared materials which is the fundamental step of the photocatalytic degradation. The BET results are presented in Table 7.3 below. The observed surface areas in ascending order were 33.8, 47.1, 58.4, and 65.3 m^2/g for C@fN-MWCNTs, TiO_2/cellulose, TiO_2/C@fN-MWCNTs and cellulose, respectively. It was low surface area of C@fN-MWCNTs was probably due to the beads that were observed from its SEM micrographs which blocked the active sites of the sample. In addition, the overcrowding of OH-groups on the two materials could have blocked the pores, hence hindering the interaction with N_2 gas during BET measurements [24]. Consequently, adding TiO_2 on C@fN-MWCNTs increased the surface area. On the contrary, cellulose surface area decreased due to the sticky aggregates of TiO_2 that formed during sol-gel synthesis of the composite [25].

Table 7.3: BET measurements of the cellulosic materials with their TiO2-based composites.

Sample name	BET surface area (m^2/g)	Pore size (nm)
Cellulose	65.3	16.33
C@fN-MWCNTs	33.8	3.95
TiO_2/cellulose	47.1	7.14
TiO_2/C@fN-MWCNTs	60.4	13.20

7.3 Photocatalytic degradation of methyl violet using cellulosic materials as TiO_2 supports

The applicability of the prepared catalysts in photocatalytic degradation of methyl violet was investigated. The experimental conditions that are feasible for this process have been established

in Chapter 6 of this study. Thus, 150 mg of catalyst (100 mL) was added in a 20 ppm dye solution under UV irradiation for 2 hours.

7.3.1 Adsorption effect

The adsorption capacities of the prepared catalysts were investigated to determine the equilibrium concentration (Ceq) of methyl violet. These experiments were done in the absence of light under the same experimental conditions reported above. The results obtained from this study are presented in Figure 7.5. The adsorption capacities of the catalysts increased with increasing surface area and porosity. This makes it clear that the adsorption of methyl violet on the surface of the catalyst predominantly depends on the availability of pores and functional groups on the surface of the catalyst. Thus, there was a rapid uptake of organic dye between time 0 and 60 minutes for all the studied catalysts. After 60 minutes, only insignificant amount of methyl violet was adsorbed indicating a full coverage of the catalysts' surfaces [26]. The concentrations of methyl violet at the adsorption-desorption (Ceq) point were 18.7, 17.4, 17.65, and 17.58 ppm for C@fN-MWCNTs, cellulose, TiO_2/cellulose, and TiO_2/C@fN-MWCNTs, respectively.

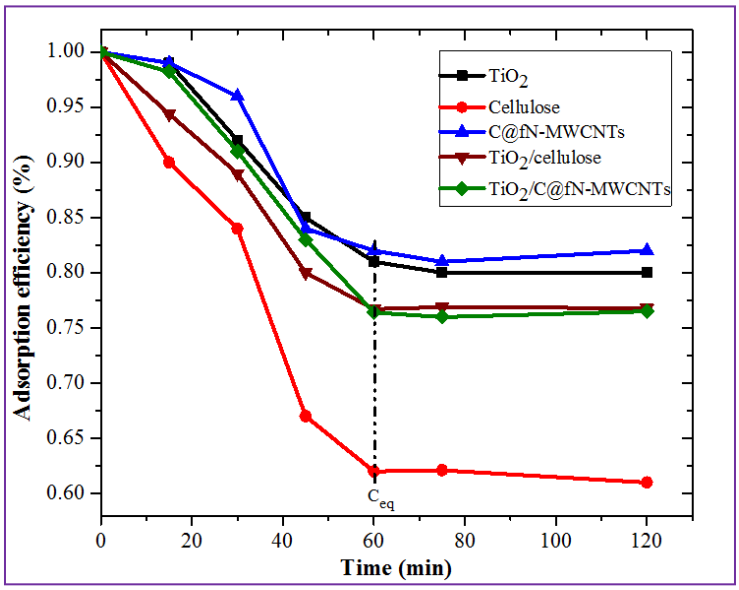

Figure 7.5: Effect of adsorption on photocatalytic degradation of methyl violet using the cellulosic supported catalyst.

7.3.2 Photocatalytic degradation of methyl violet

Figure 7.6 shows the photocatalytic degradation experiments that were conducted under UV light irradiation at room temperature. In each of these experiments, the optimal parameters that have been reported in Chapter 6 were used (i.e. catalyst dosage=150, dye concentration= 20 ppm and exposure time= 90 minutes). To eliminate the adsorption contribution, the catalyst-containing dye solutions were first stirred in the dark for 60 minutes where Ceq was obtained. The intensity was kept at 180 W, while stirring the solution at 100 rpm. Only 12.4% and 34% of dye was degraded in the presence of cellulose and C@fN-MWCNTs, respectively. Nevertheless, these materials fulfilled their supporting role on the photocatalytic degradation process. The photocatalytic degradation efficiency of bare TiO_2 improved from 59.4% to 63.1% and 65.0% after being supported on cellulose and C@fN-MWCNTs, respectively. Comparatively, TiO_2/C@fN-MWCNTs exhibited high photocatalytic degradation activity than TiO_2/cellulose. This was attributed to its high surface area, and the small particle size of TiO_2.

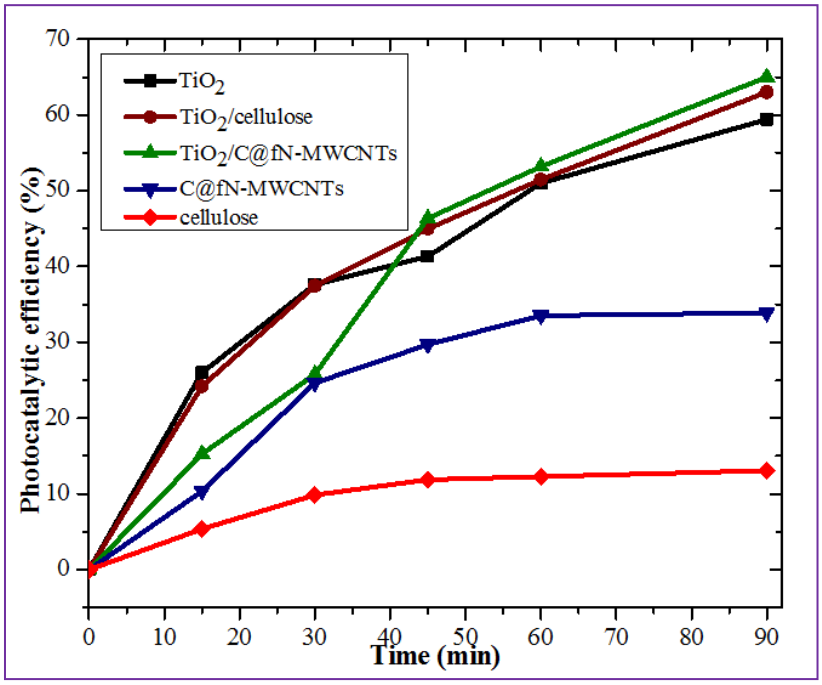

Figure 7.6: Photocatalytic degradation of methyl violet, using the prepared catalysts

7.4 Conclusions

This chapter has established the properties of cellulose-N-MWCNTs (C@fN-MWCNTs) composite material and its application in the removal of organic dyes in water. The fabrication of this composite using electrospinning was successful with minimal agglomeration of the fibers. However, SEM showed that there was no interaction between the MWCNTs and cellulose fibrils. This is a major drawback for most studies in the polymer-MWCNTs composites. The observed gap between the two materials was attributed to columbic repulsion from the negative charges on the surface of the materials. Nonetheless, FTIR showed a reduction of the 3344 cm^{-1} band which indicated that some of the OH-groups were part of the interaction of the cellulose and the *in situ* fN-MWCNTs. Moreover, the crystalline index of the cellulose was increased by 17.78%.

The electrospun cellulose fibrils were smooth, interconnected fibers in the micron range. However, the average size of the fibrils reduced to 29.87 nm after an introduction of *in situ* fN-MWCNTs. As a result, more OH-groups from both materials in the composites were exposed. This led to a dramatically decrease in the surface area of cellulose from 65.3 to 33.8 m^3/g. On the other hand, the presence of the OH-groups improved TiO_2 incorporation on the composite material. This was confirmed by the decrease in the crystallite size of TiO_2 in the TiO_2/C@fN-MWCNTs composite. The PL spectra, also confirmed that a strong TiO-C interphase was formed, more prominently on the TiO_2/C@fN-MWCNTs composite. Thus, one of the major drawbacks of TiO_2 of the recombination of photogenerated electron-hole was hindered. Notably, the photocatalytic degradation activity of TiO_2/C@fN-MWCNTs was high despite the low surface area of its support. Although the photoactivity of TiO_2/cellulose was improved, the *in situ* TiO_2/fN-MWCNTs showed the best photocatalysis results. This was because of the beaded nature of the C@fN-MWCNTs which resulted to a low adsorption capacity. On the other hand, there was poor interaction of materials in the TiO_2/cellulose composites. Thus there is still a need to improve the interfacial bonding between the cellulose polymer and *in situ* fN-MWCNTs in order to enhance the composite's adsorption capacity.

7.5 References

[1] S. Yun, and J. Kim, "Multi-walled carbon nanotubes-cellulose paper for a chemical vapor sensor," *Sensors and actuators, B: Chemical*, vol. 150, no. 1, pp. 308–313, 2010.

[2] N. E. Badawi, A. R. Ramadan, A. M. K. Esawi, and M. El-Morsi, "Novel carbon nanotube-cellulose acetate nanocomposite membranes for water filtration applications," *Desalination*, vol. 344, pp. 79–85, 2014.

[3] H. Q. Liu and C. Y. Tang, "Electrospinning of cellulose acetate in solvent mixture N,N-dimethylacetamide (DMAc)/acetone," *Polymer journal*, vol. 39, no. 1, pp. 65–72, 2007.

[4] M. Phiriyawirut and T. Phachamud, "Suitable electrospinning condition for gallic acid-loaded cellulose acetate fiber," *Research Journal of pharmaceutical, biological and chemical sciences*, vol. 2, no. 3, pp. 210–220, 2011.

[5] K. Ohkawa, S. Hayashi, N. H. Yamamoto, and J. Ducreux, "Preparation of pure cellulose nanofiber via electrospinning," *Textile research journal*, vol. 79, no. 15, pp. 1396–1401, 2009.

[6] A. C. Ritts, Q. Yu, H. Li, S. J. Lombardo, X. Han, Z. Xia, and J. Lian, "Plasma treated multiwalled carbon nanotubes (MWCNTs) for epoxy nanocomposites," vol. 4 4, no. 3, pp. 2142–2155, 2011.

[7] T. Fujigaya and N. Nakashima, "Non-covalent polymer wrapping of carbon nanotubes and the role of wrapped polymers as functional dispersants." Polymer, vol. 193, no. 4, pp. 1–19, 2014.

[8] M. S. Maubane, M. A. Mamo, E. N. Nxumalo, W. A. L. Van Otterlo, and N. J. Coville, "Tubular shaped composites made from polythiophene covalently linked to Prato functionalized N-doped carbon nanotubes," *Synthetic Metals*, vol. 162, no. 24, pp. 2307–2315, 2012.

[9] S. Mun, Y. Chen, and J. Kim, "Cellulose-titanium dioxide-multiwalled carbon nanotube hybrid nanocomposite and its ammonia gas sensing properties at room temperature," *Sensors and Actuators, B: Chemical*, vol. 171, no. 72, pp. 1186–1191, 2012.

[10] C. Li, Q. Liu, S. Shu, Y. Xie, Y. Zhao, and B. Chen, "Preparation and characterization of regenerated cellulose / TiO_2/ZnO nanocomposites and its photocatalytic activity," *Materials letters*, vol. 117, no. 1, pp. 234–236, 2014.

[11] C. Lamprecht, A. Ebner, F. Kienberger, and P. Hinterdorfer, R. Klingeler and R. B. Sim, B. Heidelberg,"Exploring carbon nanotubes and their interaction with cells using Atomic Force Microscopy," *Biomedical Science*, 2011, pp. 1–16.

[12] C. W. Kim, D. S. Kim, S. Y. Kang, M. Marquez, and Y. L. Joo, "Structural studies of electrospun cellulose nanofibers," *Polymer*, vol. 47, no. 14, pp. 5097–5107, 2006.

[13] Z. N. Tetana, "Boron and nitrogen doped carbons for photochemical degradation reactions by," *Thesis*, pp. 1–235, 2013.

[14] K. Lefatshe, C. M. Muiva, and L. P. Kebaabetswe, "Extraction of nanocellulose and in-situ casting of ZnO/cellulose nanocomposite with enhanced photocatalytic and antibacterial activity," *Carbohydrate polymers*, vol. 164, no. 345,pp. 301–308, 2017.

[15] S. H. Wu, X. H. Qin, and M. X. Li, "The structure and properties of cellulose acetate materials: A comparative study on electrospun membranes and casted films," *Journal of industrial textiles*, vol. 44, no. 1, pp. 85–98, 2014.

[16] M. a Mamo, A. O. Sustaita, Z. N. Tetana, N. J. Coville, and I. a Hümmelgen, "Nitrogen-doped, boron-doped and undoped multiwalled carbon nanotube/polymer composites in WORM memory devices.," *Nanotechnology*, vol. 24, no. 12, p. 125–203, 2013.

[17] J. Yin and B. Deng, "Polymer-matrix nanocomposite membranes for water treatment," *Journal of membrane science*, vol. 479, no. 19, pp. 256–275, 2015.

[18] S. Bhoware, M. S. Maubane, T. Phaahlamohlaka, A. Shaikjee, and N. J. Coville, "Cu grown carbon nanofibers - Variation of their chemical and physical properties," *Chemical Physics letters*, vol. 577, no. 1, pp. 71–75, 2013.

[19] B. Ghorani, S. J. Russell, and P. Goswami, "Controlled morphology and mechanical characterisation of electrospun cellulose acetate fibre webs," *International Journal of Polymer science*, vol. 54, no. 12, pp. 1–16, 2013.

[20] S. Ortelli, M. Blosi, S. Albonetti, A. Vaccari, M. Dondi, and A. L. Costa, "Chemistry TiO_2 based nano-photocatalysis immobilized on cellulose substrates," *"Journal of photochemistry & photobiology, A: Chemistry,"* vol. 276, pp. 58–64, 2014.

[21] L. Wang, L. Shen, Y. Li, L. Zhu, J. Shen, and L. Wang, "Enhancement of photocatalytic activity on TiO_2-nitrogen-doped carbon nanotubes nanocomposites enhancement of photocatalytic activity on TiO_2-nitrogen-doped carbon nanotubes nanocomposites," *International journal of photoenergy*, vol. 13, no. 9, pp. 1–7, 2013.

[22] L. T. S. Thao, T. T. T. Dang, W. Khanitchaidecha, D. Channei, and A. Nakaruk, "Photocatalytic degradation of organic dye under UV-A irradiation using TiO_2-vetiver multifunctional nano particles," *Materials*, vol. 10, no. 2, pp. 1–12, 2017.

[23] K. Woan, G. Pyrgiotakis, and W. Sigmund, "Photocatalytic carbon nanotube-TiO_2 Composites," *Advanced materials*, vol. 21, no. 1, pp. 2233–2239, 2009.

[24] T. N. Phaahlamohlaka, "Synthesis of carbon nanofibers and their subsequent use as catalyst supports for Fischer- Tropsch synthesis " *Thesis*, 2013.

[25] A. Snyder, Z. Bo, R. Moon, J. Rochet, and L. Stanciu, "Reusable photocatalytic titanium dioxide – cellulose nanofiber films," *Journal of colloid and interface science*, vol. 399, no. 55, pp. 92–98, 2013.

[26] A. N. Rao, B. Sivasankar, and V. Sadasivam, "Chemical kinetic studies on the photocatalytic degradation of direct yellow 12 in the presence of ZnO catalyst," *Journal of molecular catalysis*, vol. 306, no. 1, pp. 77–81, 2009.

8

Chapter eight

General Conclusions and Recommendations

8.1: General Conclusions

Previous studies in literature have demonstrated that cellulose-MWCNTs composite have exceptional thermal, mechanical, and physical properties. However, the dispersion of MWCNTs in the cellulose polymer and the formation of strong adhesion between the two materials remains a challenge. In this study, we have explored different kinds of chemical modifications of MWCNTs that may attenuate these challenges. Thereafter, the most adequate functionalized MWCNTs were used in the C@fN-MWCNTs composite material.

CVD method was successfully used to synthesize the MWCNTs using C_2H_2 over a 10% Fe-Co/$CaCO_3$ catalyst. The synthesized MWCNTs were chemically modified by refluxing in 55% HNO_3 and/or nitrogen doping using *in situ* and *ex situ* methods where CH_3CN was used as a nitrogen and carbon source. The modified support materials were then characterized using TEM, SEM, TGA, BET, XRD, Raman spectroscopy, and CHNS techniques. TEM and SEM analyses showed high impurities present in the *in situ* N-MWCNTs which were identified by XRD analysis as Fe, Co, Ca residue from the catalyst. This was also concurred by TG analysis which revealed that the catalyst residue was at most 19%. However, DTG peak disclosed that *ex situ* N-MWCNTs were highly impure relative to *in situ* MWCNTs. Even so, the catalyst residue observed from TGA curve was only 9%. Thus the impurities in *ex situ* N-MWCNTs were attributed to the presence of amorphous carbon and SWCNTs. CHNS confirmed successful nitrogen doping with 0.15% and 2.9% for *ex situ* N-MWCNTs and *in situ* N-MWCNTs, respectively. Acid treatment was successfully used to remove the impurities, add functional groups on the surface of the support materials, and improve nitrogen incorporation on *ex situ* N-MWCNTs.

The catalysts respective to all the characterized support materials were then studied. TEM showed that *in situ* fN-MWCNTs led to homogeneous coverage of TiO_2. Whist *ex situ* fN-MWCNTs showed a random composite. The TiO_2 crystallite sizes in the composites were estimated using Scherrer equation. The crystallite size of TiO_2 was drastically decreased from 63.5 nm to 8.03, 7.8 and 5.64 nm after introducing fMWCNTs, *ex situ* fN-MWCNTs and *in situ*

fN-MWCNTs, respectively. The small crystallite size of TiO_2 on *in situ* accounted for its ability to accelerate electron transfer in the photocatalysis system, enhance the binding energy of TiO_2. Raman spectroscopy and TiO_2 revealed that the TiO_2 that was used was purely anatase. XRD and TEM revealed that TiO_2/N-MWCNTs (both *in situ* and *ex situ*) exhibited high impurities with minimal interaction between the N-MWCNTs and the TiO_2. Thus, these materials were not examined in the photocatalytic degradation. The experimental parameters for photocatalytic degradation were optimized. The optimal conditions were found to be 150 mg of catalyst, in 20 ppm of dye solution and the time frame was 1 hour and 30 minutes. The recyclability of the catalysts was also examined. Bare TiO_2 lost its catalytic activity faster than the supported TiO_2. The *in situ* TiO_2/fN-MWCNTs successfully degraded 20 ppm of methyl violet in a period of 90 minutes.

The *in situ* fN-MWCNTs were used in the fabrication of C@fN-MWCNTs composites material owing to their outstanding aforementioned properties. SEM showed that there was a dramatically decrease in the diameter of the cellulose after an introduction of *in situ* fN-MWCNTs. Nevertheless, the C@fN-MWCNTs exhibited a low surface area due to its beaded structure and also probably due the overcrowding of OH-groups from both carbonaceous materials. Conversely, TiO_2/C@fN-MWCNTs exhibited small crystallite size estimated from Scherrer equation. This indicated that the presence of C@fN-MWCNTs could prevent the rapid hydrolysis of TiO_2 precursor by instantly forming TiO-C bonds. This was confirmed by photoluminescence, which also showed that the photogenerated electron-hole recombination was prevented more effectively on the TiO_2/C@fN-MWCNTs. Consequently, the photocatalytic degradation of TiO_2/cellulose was improved by 2% after incorporating *in situ* fN-MWCNTs into the polymer. In conclusion, *in situ* nitrogen doping is a feasible method to achieve adequate catalytic activity.

The inclusion of *in situ* fN-MWCNTs successfully enhanced the cellulose's crystallinity, and the TiO-C interaction. Thus, polymeric composite (C@fN-MWCNTs) improved the capability of cellulose polymer as a support material of TiO_2. Nevertheless, the total performance of C@fN-

MWCNTs as TiO_2 support in photocatalytic degradation of the organic dye was not satisfactory as it could not exceed that of individual *in situ* fN-MWCNTs. This may be due to the following reasons: (1) the reduction in the surface area, which resulted in low adsorption capacity and thus lowers degradation efficiency. (2) The high degree of structural defects of the *in situ* fN-MWCNTs from its bamboo-like morphology which resulted in high reactivity. (3) The *in situ* TiO_2/fN-MWCNTs showed a clear TiO_2 coating on the MWCNTs which resulted in more TiO_2 particles harvesting light, unlike in the TiO_2/C@fN-MWCNTs which was a random composite. (4) The individual *in situ* fN-MWCNTs showed high purity from the acid treatment, which contributed to its adsorption capacity whereas C@fN-MWCNTs showed the presence of beads on the surface.

8.2 Recommendation

C@fN-MWCNTs composite exhibited a great potential as catalyst support. However, the electrospun composite fibers exhibited non-uniform, randomly arranged fibers with beads, resulting in low surface area. Thus further research for the development of novel C@fN-MWCNTs, perhaps by optimizing the experimental parameters such as the mass fraction, voltage, and the CA solution concentration is necessary.

The properties of the TiO_2-carbon composites can be evaluated by performing the density functional theory (DFT) calculations in order to infer the interfacial electronic structures and electron transfer between the carbonaceous materials and the TiO_2. In addition, powerful techniques such as XPS can be used to investigate the role of nitrogen configuration in the TiO_2-carbon composites. Electron paramagnetic resonance (EPR) and *in situ* TEM techniques can be used to explore the electronic effects, such as the band gap variation of MWCNTs in the TiO_2-carbon composites.